The future of cross-border capacity management in Europe

Emily Little

université PARIS-SACLAY

The Future of Cross-border Capacity Management in Europe

L'avenir de la gestion de la capacité d'interconnexion transfrontalière en Europe

Thèse de doctorat de l'université Paris-Saclay

École doctorale n° 573, Interfaces : matériaux, systèmes, usages (INTERFACES)
Spécialité de doctorat : Ingéniérie des systèmes complexes
Graduate School : Sciences de l'ingénierie et des systèmes
Référent : CentraleSupélec

Thèse préparée dans l'unité de recherche Laboratoire Génie Industriel (Université Paris-Saclay, CentraleSupélec) sous la direction de Pascal DA COSTA, Professeur à CentraleSupélec, la co-direction de Yannick PEREZ, Professeur à CentraleSupélec

Thèse soutenue à Paris-Saclay, le 25 novembre 2022, par

Emily LITTLE

Composition du jury

Membres du jury avec voix délibérative

Marija JANKOVIC Professeur, CentraleSupélec	Présidente
Cédric CLASTRES Professeur des universités, Université Grenoble Alpes	Rapporteur & Examinateur
Carine STAROPOLI Professeur, Paris School of Economics Maître de Conférences HDR, l'Université Paris 1-Panthéon Sorbonne	Rapporteur & Examinatrice
Hung-po CHAO President & CEO, Energy Trading Analytics, LLC.	Examinateur
Pierre HENNEAUX Chercheur, Université Libre de Bruxelles	Examinateur

THESE DE DOCTORAT
NNT : 2022UPAST154

université PARIS-SACLAY | ÉCOLE DOCTORALE Interfaces: matériaux, systèmes, usages

Titre: L'avenir de la gestion de la capacité d'interconnexion transfrontalière en Europe

Mots clés: Flow-based, Réseau, Marché, Interconnections, Electricité

Résumé: L'ouverture du marché européen de l'électricité a renforcé l'enjeu des échanges transfrontaliers. Les méthodes de calcul et allocation de la capacité du réseau sont au coeur de cette question. La méthode flow-based se rapproche de la réalité physique du réseau en intégrant les dépendances de flux entre différentes zones, et offre, à niveau de risque donné, une capacité supérieure à la méthode Net Transfer Capacity utilisée auparavant. Le contexte de la transition énergétique met en lumière de nouveaux problèmes ; par exemple, l'erreur de prévision croissante entre les transactions à long terme, le marché à court terme et la répartition en temps réel. De plus, un modèle de production, plus éloigné des centres de charge et un peu plus largement distribué que les centrales conventionnelles, menace de pousser le réseau existant à ses limites. Si l'investissement dans le réseau est bien sûr un élément important de la solution, il deviendra également encore plus nécessaire d'utiliser le réseau existant aussi efficacement que possible.

Les principales contributions de cette thèse sont de trois types. Tout d'abord, elle montre que l'intérêt économique des flexibilités du réseau croit avec la pénétration des énergies renouvelables intermittentes. Ensuite, elle propose une description minutieuse et actualisée de la méthodologie flow-based opérationelle. Les travaux se distinguent de la littérature existante en donnant une vision plus complète et plus précise des aspects théoriques et opérationnels de cette méthodologie. Enfin, une évolution du flow-based est proposée qui permet de mieux intégrer les flexibilités du réseau dans l'algorithme opérationnel de couplage des marchés.

Title: The Future of Cross-border Capacity Management in Europe

Keywords: Flow-based, Grid, Interconnections, Market, Electricity

Abstract: The liberalization of the European electricity market reinforced the need for efficient, market-driven cross-border congestion management. The methods to calculate and allocate the capacity of transmission networks are at the heart of this discussion. The flow-based method integrates the flow dependencies between market zones to more accurately model the physical constraints of the grid, providing a higher cross-border capacity available to the market without increasing the risk, compared to the Net Transfer Capacity method. The context of the energy transition brings into light new issues; for one, the increasing forecast error between the long term transactions, the day ahead market and the real time dispatch. Additionally, a pattern of generation farther from load centers and more widely distributed than conventional plants threatens to push the existing network to its limits. While network investment is of course a large piece of the solution, it will also become more important to utilize the existing network as efficiently as possible.

The main assets of this thesis are three-fold. First, the increasing value of transmission-level grid flexibility is shown in a system with high levels of variable renewable energy sources. Second, with the ultimate aim of presenting an updated form of the European capacity calculation, the existing flow-based method is presented in detail. This goes beyond the work in the existing literature to provide a comprehensive look at the theoretical and operational aspects in extended detail. Thirdly, an updated version of the existing capacity calculation is proposed, allowing for improved integration of grid flexibility options and considering the operational complexities and existing market clearing algorithm.

Acknowledgements

I would like to begin by expressing my profound thanks to all the jury members–Marija Jankovic, Cédric Clastres, Carine Staropoli, Hung-po Chao and Pierre Henneaux–for the time they spent reading my dissertation and analyzing and assessing my research. The discussions following my defense rekindled my interest in the subject and have definitely inspired me to continue work on the topic in the next years.

I'd next like to thank the many supervisors that I had along the way who had such a huge impact on my work. The subject of my PhD is such that it touches on many distinct disciplines and I was lucky to be able to have in depth discussions with experts across all the relevant fields.

To Pascal and Yannick. Thank you for making yourself available whenever I had questions and for helping me to understand economic concepts that are somewhat less intuitive for my engineering-tilted brain.

To Efthymios. Your help on the more technical aspects of network modeling and security constraints was indispensable. Thank you so much for all the time you spent helping me to understand these concepts and the interesting discussions we had (and of course your recommendations for travels in Greece).

To Jean-Yves. I distinctly remember the first time we discussed the flow-based method in Versailles. At that point, just following my *stage de fin d'études*, I thought I understood the concept quite well. Little did I know, I was simply at a very small peak of the Dunning-Kruger curve. That one conversation inspired the past four years of work. Your patience and utterly astounding depth of expertise (not in any way limited to the energy field) has pushed me to attain even one fraction of the gravity of your knowledge.

To Marjorie. You have a unique way of explaining incredibly complex concepts in a way that makes them seem so simple and straightforward. I learned so much from working with you, not limited to capacity calculation methods, but also how to approach a problem, gather the necessary pieces and come to a solution.

To Sandrine. You have developed such enormous expertise in so many subjects (though younger than I am). It is truly impressive to me how your mind works. Thank you for sharing part of that with me.

To Nicolas. You came in near the end of my PhD, but your inputs were no less relevant or beneficial to this work. I'm so glad we got to work together for a while and I hope we can continue to work together on related topics.

To Virginie. While you were never directly my supervisor, you have been there since the beginning offering advice and your fingerprint appears clearly on this work as well. As any of the many

interns and PhD students that you mentor would attest, your expertise is vast and your compassion boundless.

Additional thanks go to all the people at RTE in my various *pôles*–EOD-CT first and then PEPS (and now PILS)–who filled my lunches, coffee breaks and afterwork happy hours with wonderful conversation. To all the assistants at LGI and RTE who helped me stumble blindly through the many French bureaucratic processes. To any colleague who helped me reword an email when I wasn't sure of the correct phrasing. To all the other doctoral students, both at LGI and at RTE, who participated in seminars with me, who reread articles and chapters of my manuscript and with whom I shared beers and countless interesting discussions.

In many ways it was much more difficult than I thought to move to a new country, speaking a language I had studied, but never lived in. It took the better part of 3 years for me to fully feel comfortable and to be happy with my new personality in French. The fact that I ever did is due to all the friends I made here, in particular Rémy, Malix, V, H et Floco who were there for the full duration of my thesis, including all of Covid. Thanks for making me realize that I don't need to be able to pronounce *bidouille* perfectly in order to enjoy living in France.

To my family who filled our house with love, great food and so many books. I owe who I am and all my accomplishments to them.

Finally, I want to thank Nathan, for letting me go crazy when necessary, for cooking when I didn't even have the energy to boil pasta for myself and of course for your opinions on proper coding—notably the time when you made one of my codes 9,745% faster. ♡

Résumé en français

> *« Le marché intérieur de l'électricité, dont la mise en œuvre progressive est en cours depuis 1999, a pour finalité d'offrir une réelle liberté de choix à tous les consommateurs de la Communauté, qu'il s'agisse de particuliers ou d'entreprises, de créer de nouvelles perspectives d'activités économiques et d'intensifier les échanges transfrontaliers, de manière à réaliser des progrès en termes d'efficacité, de compétitivité des prix et de niveau de service et à favoriser la sécurité d'approvisionnement ainsi que le développement durable. »*[1]

Le maintien de l'équilibre instantané entre l'offre et la demande d'électricité au moindre coût pour les consommateurs est au cœur de nombreuses réglementations européennes récentes, comme l'illustre la citation ci-dessus. Cependant, l'électricité est assez unique par rapport à d'autres produits. Comme le résume (Wolak, 2021) (dans une section intitulée *Why Electricity is Different*), « il est difficile de concevoir une industrie où l'introduction de mécanismes de marché au niveau de la vente en gros et au détail est plus difficile... L'offre doit être égale à la demande à chaque instant et à chaque endroit des réseaux de transmission et de distribution. Il est très coûteux de stocker l'électricité... Enfin, la livraison du produit consommé doit se faire par le biais d'un réseau de transmission bouclé, potentiellement congestionné, et la manière dont la capacité de transmission est allouée aux différents acteurs du marché exerce une énorme influence sur leurs comportements. »[2] La restructuration radicale des monopoles verticalement intégrés en marchés concurrentiels, qui a débuté dans les années 1980 et s'est poursuivie au début des années 2000, a été traitée de plusieurs manières distinctes dans différentes régions. Il est toutefois largement reconnu qu'en raison des économies d'échelle, les réseaux de transport et de distribution entrent dans la catégorie des monopoles naturels. Les méthodes de calcul et d'allocation de la capacité de ces réseaux - au coût le plus bas pour le système - ont occupé une part importante des discussions lors de la période de restructuration et continuent aujourd'hui.

Le contexte de la transition énergétique ajoute également un aspect transformateur particulier à ce sujet, en partie en raison de l'erreur de prévision croissante entre les transactions à long terme, le marché J-1 et la répartition en temps réel. Un modèle modifié de production, souvent plus éloigné des centres de charge et un peu plus largement distribué que les centrales conventionnelles, menace de pousser le réseau existant à ses limites. Si l'investissement dans le réseau est bien sûr un élément fondamental de la solution, il deviendra également plus important d'utiliser le réseau existant aussi efficacement que possible - par exemple, en intégrant une flexibilité accrue dans le réseau de transport d'électricité pour tenir compte des flux plus variables ou en ajoutant des actifs de « Dynamic Line Rating » (DLR) pour utiliser la totalité de la capacité instantanée des lignes de transport.

[1] RÈGLEMENT (CE) No 714/2009 DU PARLEMENT EUROPÉEN ET DU CONSEIL du 13 juillet 2009 sur les conditions d'accès au réseau pour les échanges transfrontaliers d'électricité et abrogeant le règlement (CE) no 1228/2003 (noa, 2009)

[2] Ma traduction

Dans le contexte européen, depuis la libéralisation du marché européen de l'électricité, l'objectif de la gestion des échanges transfrontaliers est rapidement passé au premier plan des discussions. Les échanges n'ont cessé d'augmenter à mesure que les marchés européens se sont intégrés et harmonisés. Les méthodes utilisées pour calculer et allouer la capacité de transmission ont évolué avec ces changements et des intérêts divers et parfois contradictoires influencent ces évolutions. Dans ces circonstances, l'objectif de la Commission européenne est d'intégrer davantage les différentes politiques nationales pour créer un marché intérieur unique de l'énergie, en augmentant le domaine des échanges possibles afin d'accroître théoriquement le bien-être social global du marché européen.[3]

Afin d'éviter une déconnexion économiquement dommageable entre les marchés et la réalité opérationnel du réseau (en particulier au sujet des « flux parallèles »), deux approches se sont succédées. Au début des années 2000, la logique en Net Transfer Capacity (NTC) a été mise en place : elle permet aux acteurs d'effectuer aisément des échanges transfrontaliers dans le respect de la sécurité du réseau, mais au prix d'une schématisation très forte de la physique sous-jacente conduisant à une non-utilisation de toutes les marges disponibles. La méthode flow-based, au cœur de cette analyse, a été mise en exploitation dans la région CWE (Central Western Europe) en 2015 afin de maximiser le domaine de sécurité, avec le même niveau de risque que la méthode NTC utilisée auparavant. A la différence des NTC, la méthode flow-based permet de tenir compte des lois de Kirchhoff qui induisent une dépendance forte entre les différentes zones géographiques, comme les flux de bouclage (loop flows). En explicitant ces interactions, la méthode flow-based permet de répartir la marge physique pendant la phase d'allocation et non en amont, durant le calcul de la capacité.

Les principales contributions de cette thèse sont de trois types. Tout d'abord, elle montre que l'intérêt économique des flexibilités du réseau croît avec la pénétration des énergies renouvelables intermittentes. Ensuite, elle propose une description minutieuse et actualisée de la méthodologie flow-based opérationelle. Les travaux se distinguent de la littérature existante en donnant une vision plus complète et plus précise des aspects théoriques et opérationnels de cette méthodologie. Enfin, une évolution du flow-based est proposée qui permet de mieux intégrer les flexibilités du réseau dans l'algorithme opérationnel de couplage des marchés.

Le chapitre 2 commence par une revue de littérature sur les impacts de l'incorporation des leviers de flexibilité du réseau. Ensuite, il présente les modèles de réseau pertinents pour ce travail et plusieurs variantes qui intègrent les méthodes opérationnelles de gestion de la flexibilité du réseau, en particulier les changements de topologie. Enfin, il présente une étude de cas sur un petit réseau académique avec des énergies renouvelables variables croissantes. Si les avantages du contrôle optimal de la topologie sont généralement bien connus dans la littérature (voir la section 2.1 pour la revue de la littérature sur ce sujet), cette étude explore comment ce gain est affecté par une production variable croissante. Les résultats, présentés dans la section 2.5 montrent que les gains des actions de contrôle topologique augmentent significativement avec la pénétration des énergies renouvelables variables. L'étude et les conclusions de ce chapitre ont été réalisées avec plusieurs variantes d'OPF (« Optimal Power Flow ») sur un jeu de données académique (RTS-GMLC).

Le chapitre 3 donne plus de détails sur la méthode flow-based existante. Dans la première partie du chapitre 3, nous présentons une description globale de la méthode, d'abord théorique puis opérationnelle. Les particularités et les choix des différents GRT (Gestionnaire de Réseau de Transport) européens sont explorés à travers une analyse des données historiques de la région CWE. Plusieurs sources ont été croisées afin d'obtenir une image précise de ces données. Les modifications apportées au processus depuis l'extension à la région CORE (combinaison de la région CWE et CEE, Central Eastern Europe)

[3] Les avantages de l'intégration des marchés européens de l'électricité ont également été analysés dans la littérature, voir par exemple (Newbery et al., 2016).

sont également expliquées. La deuxième partie du chapitre 3 explore plus en détail plusieurs des paramètres d'entrée de la méthode flow-based, en particulier le type de modélisation utilisé pour la création du cas de base, les « Generation Shift Keys » (GSK), et une discussion sur l'inclusion de mesures correctives à différentes phases du processus - à la fois dans le calcul du cas de base et dans la phase de mesures correctives explicites.

Dans le chapitre 4, nous proposons une nouvelle méthode d'inclusion des changements topologiques non convexes qui est compatible avec le couplage de marché européen existant. Cette méthode est appelée l'approche multi-domaines. Elle constitue une extension de la méthode flow-based actuelle. Une brève description de l'algorithme de couplage de marché J-1 (SDAC), EUPHEMIA, est présentée dans la section 4.2.1, spécifiquement centrée sur les types d'offres utilisées dans le clearing. La méthode proposée a ensuite été validée directement dans EUPHEMIA ainsi qu'avec un modèle de simulation de clearing de marché faisant partie du projet ATLAS (voir le chapitre 4 pour la description). La méthode permet non seulement d'intégrer des contrôles topologiques binaires dans le *clearing* (détermination des offres acceptées et refusées), mais aussi d'inclure des actions correctives coûteuses. Cela permet à l'algorithme de clearing du marché d'arbitrer lui-même entre le bien-être social du marché J-1 et un coût de redispatch prévu. Plusieurs méthodes potentielles pour la création de ces multi-domaines sont proposées dans la section 4.3.4.

Enfin, le chapitre 5 présente un résumé des conclusions de ce travail. Pour des raisons de clarté, les modèles utilisés dans chaque chapitre variant légèrement, un tableau de notations est présenté au début de chaque chapitre.

Notons également qu'une liste d'acronymes est fournie au début du manuscrit et qu'une liste de tous les GRT du ENTSO-E est fournie à l'annexe D.

Contents

List of Figures

List of Tables

List of Abbreviations

AC	Alternating Current
ACER	Agency for the Cooperation of Energy Regulators
aCRA	Automatic Curative Remedial Action
aFRR	Automatic Frequency Restoration Reserves
ATC	Available Transfer Capacity
BRP	Balance Responsible Party
BZ	Bidding Zone
CACM	Capacity Allocation and Congestion Management
CB	Critical Branch
CEE	Central Eastern Europe
CGM	Common Grid Model
CNE	Critical Network Element
CNEC	Critical Network Element under Contingency
CNECRA	Critical Network Element under Contingency and Remedial Action(s)
CO	Critical Outage
CORE	Central Eastern and Western Europe, CWE + CEE
CSP	Concentrated Solar Power
CWE	Central Western Europe
D-2	Two days before real time
DA or D-1	Day Ahead
DC	Direct Current
DC-OPF	DC Optimal Power Flow
DLR	Dynamic Line Rating
DSO	Distribution System Operator
EC	External Constraint
eqt	Equipment
EUPHEMIA	Pan-European Hybrid Electricity Market Integration Algorithm
FACTS	Flexible AC Transmission System
FAV	Final Adjustment Value
FB	Flow-based
FCR	Frequency Containment Reserves
FRM	Flow Reliability Margin
FTR	Financial Transmission Right

GLPK	GNU Linear Programming Kit
GSK	Generation Shift Key
HVDC	High Voltage Direct Current Line
ID	Intraday
IGM	Individual Grid Model
ISO	Independent System Operator
LF	Load Flow
LMP	Locational Marginal Pricing
LOC	Lost Opportunity Cost
LODF	Line Outage Distribution Factor
LP	Linear Program
LSK	Load Shift Key
LTA	Long Term Allocation
LTN	Long Term Nomination
MAR	Minimum Acceptance Ratio
mCRA	Manual Curative Remedial Action
mFRR	Manual Frequency Restoration Reserves
MIC	Minimum Income Condition
MILP	Mixed Integer Linear Program
MIQP	Mixed Integer Quadratic Program
MWh	Megawatt-hour
NP	Net Position
NRA	National Regulatory Authority
NTC	Net Transfer Capacity
NWE	North-Western Europe
OPF	Optimal Power Flow
OTC	Optimal Topology Control
PAB	Paradoxically Accepted Block Offer
PCR	Price Coupling of Regions
PF	Power Flow
PRA	Preventive Remedial Action
PRB	Paradoxically Rejected Block Offer
PRMIC	Paradoxically Rejected Minimum Income Condition Offer
PST	Phase Shifting Transformers
PTDF	Power Transfer Distribution Factor
ptr	Physical Transmission Right
PV	Photovoltaic
RA	Remedial Action
RAM	Remaining Available Margin
RR	Replacement Reserves
RT	Real Time
RTE	Réseau de Transport d'Électricité
RTPV	Rooftop Photovoltaic

SP	Single Product
TSO	Transmission System Operator
UIOSI	Use-it-or-Sell-it
VZ	Virtual Zone

Chapter 1

Introduction

> *"The internal market in electricity, which has been progressively implemented since 1999, aims to deliver real choice for all consumers in the Community, be they citizens or businesses, new business opportunities and more cross-border trade, so as to achieve efficiency gains, competitive prices and higher standards of service, and to contribute to security of supply and sustainability."*[1]

Maintaining the instantaneous electricity supply and demand balance at the lowest cost to consumers is at the heart of many recent European regulations, as described in the citation above. However, electricity is quite unique compared to other commodities, complicating the issue. As summarized by (Wolak, 2021) (in a section entitled *Why Electricity is Different*), "it is difficult to conceive of an industry where introducing market mechanisms at the wholesale and retail level is more challenging...Supply must equal demand at every instant in time and at each location in the transmission and distribution networks...It is very costly to store electricity...Finally, delivery of the product consumed must take place through a potentially congested, looped transmission network, and how transmission capacity is allocated to different market participants exerts an enormous influence on their behaviour." The sweeping restructurization of vertically integrated monopolies into competitive markets beginning in the 1980s and continuing into the early 2000s was handled in several distinct manners in different regions. It is however widely recognized that due to economies of scale, both transmission and distribution networks fall under the category of natural monopolies. The methods to calculate and allocate the capacity of these networks – at the lowest system cost – make up a significant share of the discussions in the period of restructuring.

The context of the energy transition adds a particular transformative aspect to this conversation as well, in part due to the increasing forecast error between the long term transactions, the day ahead market and the real time dispatch. A modified pattern of generation, often farther from load centers and somewhat more widely distributed than conventional plants threatens to push the existing network to its limits. While network investment is of course a large piece of the solution, it will also become more important to utilize the existing network as efficiently as possible – for instance, integrating

[1] From REGULATION (EC) No 714/2009 OF THE EUROPEAN PARLIAMENT AND OF THE COUNCIL of 13 July 2009 on conditions for access to the network for cross-border exchanges in electricity and repealing Regulation (EC) No 1228/2003 (noa, 2009)

increased flexibility in the electricity transmission network to account for the more variable flows or adding dynamic line rating (DLR) assets to use the full capacity of individual transmission elements.

Zooming into the European context, since the liberalization of the European electricity market, the goal of cross-border exchange management has fast come to the forefront of the discussion. Exchanges have been steadily rising as European markets have become increasingly integrated and harmonized. The methods used to calculate and allocate transmission capacity have evolved with these changes and a variety of perspectives influence these evolutions. At the European Commission level, there is an aim to further integrate the various national policies to create a single Internal Energy Market, increasing the domain of possible exchanges in order to theoretically increase the overall European market welfare.[2]

The discussion of the links between energy markets and transmission network constraints is not new. Indeed, it is well known that since electricity flows according to Kirchhoff's laws and can only be marginally controlled, assessing the limits of how much power can be exchanged in reality is a complex process. The early discussions on this topic are largely inextricable from the quasi-global liberalization of energy markets that was launched in 1982 in Chile (Pollitt, 2004) (Serra, 2022).[3] This is due to the fact that prior to the separation of the traditional vertical monopolies, the costs associated with network congestion were internalized. As stated by (Harvey et al., 1996), "in the world of vertically integrated monopoly, the inevitable problems of the contract-path fiction could be internalized by the monopoly. In a world of choice, with multiple users competing on the same integrated system, the old fiction must be replaced with a new reality."

The restructuring of the electricity markets and the subsequent discussion of transmission rights allocation was framed by the context of the relevant national or regional policies. For instance in regions, such as large areas of the US[4], where Independent System Operators (ISOs) or Regional Transmission Organizations (RTOs)[5] were formed, the main question regarding the allocation of transmission rights was how to ensure that the transmission system owners were correctly incentivized to allow for competition in the generation sector. The US eventually settled on nodal markets (Location Marginal Pricing, LMP) with resulting long term financial transmission rights to manage the locational risks (and volatility) of the nodal prices.

In Europe, once transmission and generation ownership were fully unbundled with the Third European Package, this was less of an issue. The goal in Europe centered more around how to "improve international congestion management while respecting the fact that internal congestion management

[2]The benefits of integrating the European electricity markets has also been analyzed in the literature, see for example (Newbery et al., 2016).

[3]Note that there are those who insist on the distinction that while Chile was indeed the first country to perform significant reform in the energy sector, it did not create a proper wholesale market and the unbundling remained limited (Joskow, 2008).

[4]These somewhat global reforms were brought on by a multitude of causes. In certain areas in the US for instance, a need for increases generation capacity (and a lack of actors to provide it) was a significant driving factor (Hogan, 1992). Additionally, although some early papers contend that regulated utilities are incentivized to overbuild, in the 1980s-1990s, the US was faced with a "slowdown in generation construction" according to other sources (Einhorn, 1990).

[5]A major difference between a Transmission System Operator (TSO) or an ISO lies in the grid ownership. In ISO territories, the same company can own generation, transmission, distribution and load-serving assets. However, the operation of the transmission network lies with the ISO. In other words, the traditional definition of property rights was somewhat modified to break down the vertically integrated monopolies. In TSO territories, there is a single company who owns, maintains and operates the network, but who is not allowed to possess generation assets. See (Rious, 2007) and (Rious et al., 2008) for a discussion and literature review on the different system operator models.

remains under the sole responsibility of each TSO and may be done in different ways" (Audouin, 2002).[6] Because of this, a zonal market was chosen, with a different price per bidding zone (generally associated with national borders, although some countries encompass several zones). The financial burden rests then on the TSO to have a grid that supports the economically optimal dispatch (including grid costs) for their respective zone. The transmission rights problem is vital as it determines the wealth exchanges that can occur between electricity market participants. It has overarching links to grid ownership, transmission investment coverage, pool trading versus over-the-counter transactions, and even decisions around central or self-dispatch.

The debate concerning nodal and zonal markets is perhaps one of the most contentious surrounding the energy markets. A full discussion on the advantages or disadvantages of either model is not included in this work.[7] It is accepted, however, that there is the need for increased flexibility, both on the generation and transmission aspects of the chain. Many studies show an important benefit from the incorporation of transmission grid flexibility (see Chapter 2 for a summary of these studies). This work focuses on this aspect as well as the trade-offs between an increasing domain of possible exchanges in the day ahead market compared to the resulting decrease of grid security (which imply higher levels of redispatch costs). In the next section, we will go into more details concerning the existing European market and the capacity calculation and allocation phases in place today.

1.1 European Energy Markets

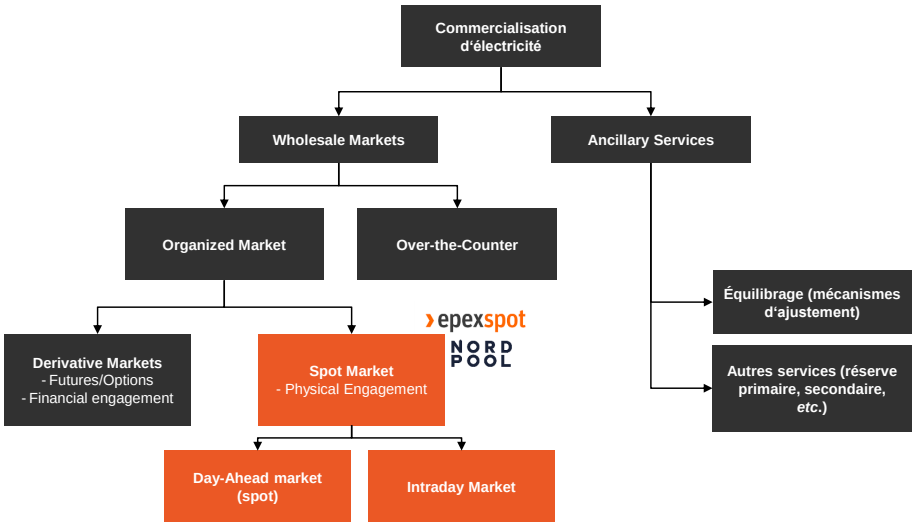

Figure 1.1: EU Energy Trading

This PhD work is centered on the European energy market structure, although the major conclusions are important for any zonal market and certain conclusions are valid across nodal markets also (see Chapter 2 for instance). This section describes the current state of affairs in the European system. A

[6] Note the distinction between international and internal congestion management. This will evolve to the definition of bidding zones, which do not always correspond only to national borders or a single TSO. Germany, for instance has a single bidding zone that is operated by four TSOs and Italy and several Nordic countries have several bidding zones operated by a single TSO.

[7] There are many studies that illustrate advantages of the different methods (see (Eicke and Schittekatte, 2022) for a summary of some of these). However, a nodal market does not seem to have any advantages related directly to the energy transition. In fact, as a zonal model reduces location-based risk for a generation plant (Ambrosius et al., 2020), it may be more prudent to allow renewable investment where there is a higher potential.

variety of different exchange mechanisms have developed in recent years. Figure 1.1 shows a basic breakdown of these.

Figures 1.2 and 1.3 show the volumes of the respective markets since 2016. We can see a very slight increase in the share of trades occurring in the day ahead market, and more notably for the intraday market.

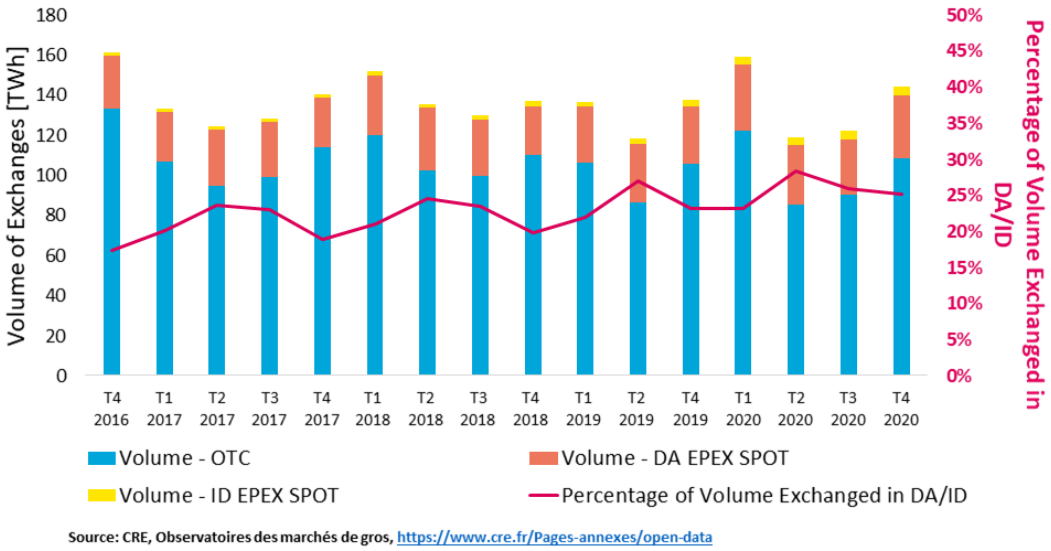

Figure 1.2: Volume of OTC Exchanges compared to Spot Markets

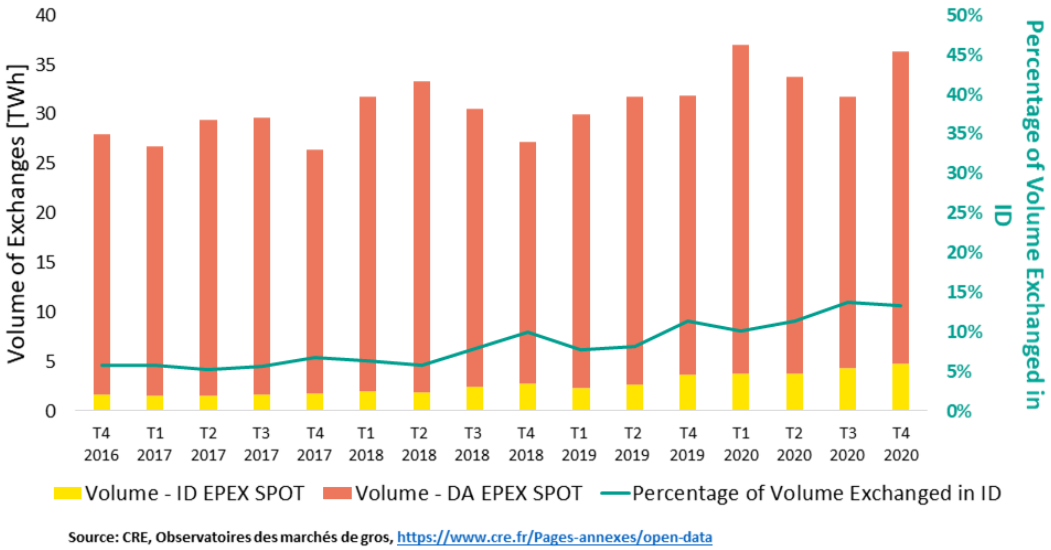

Figure 1.3: Volume of Intraday Market compared to Day Ahead Market

To integrate Kirchhoff's laws and the limits of the grid, two approaches have developed in the European zonal context: in the beginning of the 2000s, Net Transfer Capacity (NTC)—imported from North America—that hides the underlying physics from the market players, and then flow-based that exposes more the internal system constraints, yet offers an increased capacity exchange domain, with the same the risk tolerance.

The network code CACM (Capacity Allocation and Congestion Management) introduces the flow-based method as the reference method for the short-term cross-border capacity management across linked

zones. The flow-based was first implemented for the day ahead allocation for CWE (Central Western Europe). The decision—announced in November 2016 by ACER (Agency for the Cooperation of Energy Regulators) and put into practice with the Go Live on June 8, 2022—to expand this approach to the entire CORE zone (combined zone of CWE and CEE) marks the first step of this generalization.

Unlike NTC, the flow-based method makes explicit the strong physical dependence between the different (and highly meshed) geographic zones. This is an advantage of the method as it explicitly takes into account the "loop flows". However, as the flow-based method is expanded to cover a larger geographic region, it is important to keep in mind that this methodology implies – for the development of a reliable and representative security domain – a much higher level of inter-regional cooperation than NTCs. Combining regional flow-based models without a well-designed process that includes a set of harmonized and transparent rules and validations can very rapidly lead to the collapse of the method, despite the fact that theoretically, the method is unequivocally superior to the market coupling based on NTC. Indeed, average daily market welfare gains of 257 K€ (95 M€ annually) were found during the CWE parallel run in 2013 (amprion, 2020).

The flow-based method was first introduced in the literature in the early 2000s. Initial presentations of the method cite flowgate transactions (Chao et al., 2000) as the inspiration for the method (Audouin et al., 2002). At the time, it was presented in tandem with the concept of implicit transmission rights. This detail was crucial for the European network specifically. This distinction is described in Figure 1.4.

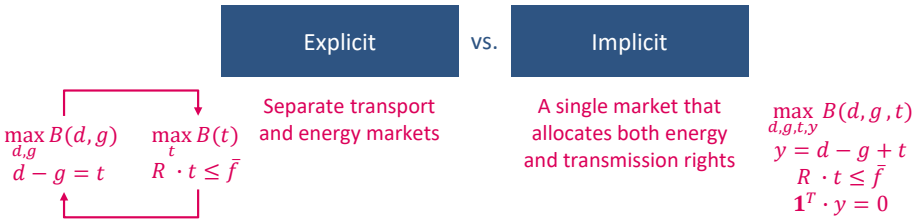

Figure 1.4: Explicit vs. Implicit Transmission Rights

Etso (European Transmission System Operators, the predecessor to ENTSO-E), described in 2001 the difficulties in applying a contract path mechanism in the European electricity system in the following way:

> *Contract path mechanisms are appropriate in longitudinal (e.g. U.S. West Coast) or two-party peninsular systems (e.g. France-Spain). Such mechanisms are inherently bound to fail in meshed networks as soon as cross-border power trade introduces significant swings in power flows, because they cannot account for the physical reality of electric power transmission. This also means that transmission capacity reservation cannot be undertaken by a single country, but has to follow a mechanism that encompasses all the interconnected countries. In a meshed network, transmission capacity cannot be partitioned : it is a common resource that has to be operated jointly and in a co-ordinated [sic] way.*[8]

This passage highlights several distinct ideas: 1) the importance of coupling the highly-meshed European network transactions, 2) the necessity to include links between all countries, not only

[8](etso, 2001)

neighboring zones, and 3) the crucial need for high levels of coordination, not only in the transaction phase, but also in the operation.

Moving forward to today, (Finck, 2021) presents a summary of the literature on the flow-based up to 2021. The author splits the literature into three categories: 1) "Conceptual work on stylized examples or reduced temporal resolution", 2) "Reduced temporal or spatial scope of real-world systems / Analysing specific aspects (mainly in CWE", and 3) "Frameworks for comprehensive system analysis considering FBMC." Across the board, any studies comparing NTC to FB found increased trading capacities in the flow-based method compared to the NTC. The results found in the literature mirror those recorded during the CWE parallel run that began in 2013, where an average daily gain of 257 K€ was found compared to ATC (see Annex 16.10 of (amprion, 2020) for detailed results).[9]

However, (Bjorndal et al., 2018) found that the increased day ahead market welfare of a domain that may be too large is compensated by higher redispatch costs, although on a model quite dissimilar to the one used in practice. This demonstrates how a careless use of any network constraint method could have an overall negative impact. It does demonstrate, on the other hand, the importance of the parameter definition by TSOs and how increasing the exchanges without thought to the physical network constraints may raise day ahead market welfare, but lower the overall welfare.

In a recent study, (Weinhold, 2021) assess some of the newer policies and the goals behind these policies: "As a result, Regulation (European Commission, 2019a) makes clear that capacity allocation has priority over congestion management and that TSOs should not restrict commercial exchange to solve internal congestion, as previously observed by ACER (2016), and explicitly requires that at least 70% of physical capacity is allocated to the market." This is referred to as the 70% minRAM rule in this and other works. This is important because physically, seen from the congested line, there is of course no difference between an internal flow or a loop flow. (Matthes et al., 2019) summarizes this conclusion as well: "Certainly a higher minRAM goes along with decreasing costs, but transmission grid's utilization increases simultaneously, resulting in an increasing demand for remedial actions." If non-costly remedial actions cannot cover this increasing demand, then the redispatch cost will easily be higher than any purported market welfare gains. (Schönheit et al., 2021a) found a similar result when analyzing different values for minimum RAM rules.

The main assets of this thesis are three-fold. First, the increasing value of transmission-level grid flexibility is shown in a system with high levels of variable renewable energy sources. Second, with the ultimate aim of presenting an updated form of the European capacity calculation, the existing flow-based method is presented in detail. This goes beyond the work in the existing literature to provide a comprehensive look at the theoretical and operational aspects in extended detail. A definition of the quality of a network security domain is proposed as part of this work and the robustness of several parameters are assessed. Thirdly, an updated version of the existing capacity calculation is proposed, allowing for improved integration of grid flexibility options and considering the operational complexities and existing market clearing algorithm.

1.2 Thesis Organization

Chapter 2 begins with a literature review on the impacts of incorporating grid flexibility methods. Next, it presents the relevant network models for this work and several variations that incorporate grid flexibility methods, in particular topology changes. Finally, it presents a case study on a small

[9]There were a few days with a slight social welfare loss, but each was linked to a misuse of the method. These are presented in the parallel run performance report (CWE TSOs, 2015).

academic network with increasing variable renewables. While the benefits of optimal topology control are generally well known in the literature (see Section 2.1 for the literature review on this topic), this study explores how this gain is affected by increasing variable production. The results, presented in Section 2.5 show that the gains from topological control actions increase significantly with the penetration of variable renewable energies. The study and conclusions in this chapter were performed with several DC-OPF variations on an academic dataset (RTS-GMLC).

Chapter 3 goes into more details regarding the existing flow-based method. In the first part of Chapter 3, we present an overarching description of the method, first theoretical and then operational. The particularites and choices of the various European TSOs are explored through light analysis of the historical CWE data. Several sources were cross-referenced in order to capture an accurate image of these inputs. Changes to the process since the expansion to the CORE region are also explained. The second part of Chapter 3 explores in more detail several of the input parameters of the flow-based method, in particular the type of modelization used for the creation of the base case, the Generation Shift Keys (GSKs), and some discussion on the inclusion of remedial actions at different phases of the process – both in the base case calculation and at the explicit remedial action phase.

In **Chapter 4**, we propose a new method for inclusion of non-convex topological changes that is compatible with the existing European zonal flow-based market coupling. This method is referred to as the *multi-domain approach*. It is an extension of the current flow-based method.

A brief description of the Single Day Ahead Market Coupling (SDAC) algorithm, EUPHEMIA, is presented in Section 4.2.1, specifically centered around the types of offers used in the clearing. The proposed method was then validated directly in EUPHEMIA as well as with a market clearing simulation model that is part of the ATLAS project. The method not only allows for the integration of binary topological controls to be integrated into the clearing, but also for costly remedial actions to be included. This allows the market clearing algorithm itself to arbitrate between the day ahead market welfare and a forecast redispatch cost. Several potential methods for the creation of these *multi-domains* are proposed in Section 4.3.4.

Finally, **Chapter 5** presents a summary of the conclusions of this work.

For clarity, since the models used in each chapter vary slightly, there is a different table of notations at the beginning of each chapter. Note also that an acronym list is provided in the beginning of the manuscript and a list of all TSOs in ENTSO-E is provided in Appendix D in case they are not defined at each usage in the text.

Chapter 2

Transmission Network Flexibility

Nomenclature

Indices	
n	Node
s(k)	Source Node of Branch, k
e(k)	End Node of Branch, k
k	Branch
g	Generator
Variables	
P_g	Real Power Generation at Generator, g
Q_g	Reactive Power Generation at Generator, g
L_n^P	Real Power Demand at Node, n (P dropped for DC-OPF)
L_n^Q	Reactive Power Demand at Node, n
F_k^P	Real Power Flow on Branch, k (P dropped for DC-OPF)
F_k^Q	Reactive Power Flow on Branch, k
V_n	Nodal Voltage Magnitudes
θ_n	Voltage Angles
δ_k	Binary variable representing breaker open/close status
z_k	Binary variable representing branch open/close status
δ_g^{UC}	Binary variable representing the unit commitment variable

P_d^{LS}	Load shedding variable
Parameters	
R_k	Line Resistance
X_k	Line Reactance
Z_k	Line Impedance
Y_k	Line Admittance
G_k	Line Conductance
B_k	Line Susceptance
$\overline{F_k^{dir}}, \overline{F_k^{inc}}$	Maximum Flow limits on branch, k, (direct/inverse directions)
$P_g^{OpRange}$	Domain representing real operation of Generator, g
P_g^{min}, P_g^{max}	Minimum stable, Maximum real power of Generator, g
$Q_g^{OpRange}$	Domain representing reactive operation of Generator, g
M_B	Big-M parameter for controllable breakers
M_K	Big-M parameter for controllable branches
c_g	Generator, g, Marginal Cost
c_w	"Wear-and-tear" cost for topological actions
c_{LS}	Load shedding cost
N_B, N_{CB}	Number of controllable breakers, branches
Sets	
$\mathcal{K}$	Set of Branches
$\mathcal{K}_B$	Set of Controllable Breakers (Modelled as branches with no flow limit)
$\mathcal{K}_{CB}$	Set of Controllable Branches
$\mathcal{K}_{\notin Flex}$	Set of Non-flexible Branches
$\mathcal{N}$	Set of Nodes
$\mathcal{G}$	Set of Generators
$\mathcal{G}_n$	Set of Generators at Node, n
$\mathcal{Z}$	Set of Zones

2.1 Introduction

Note that some of this chapter is taken directly from a previously published work:

E. Little, S. Bortolotti, J.-Y. Bourmaud, E. Karangelos, and Y. Perez, "Optimal Transmission Topology for Facilitating the Growth of Renewable Power Generation," in 2021 IEEE Madrid PowerTech, Madrid, Spain, Jun. 2021, pp. 1–6. doi:10.1109/PowerTech46648.2021.9495032.

With increasing penetration of renewable energies, more and more focus is being placed on flexibility in the electricity system. Improved flexibility is required not only on the generation and consumption sides of the system, but also in the transport, which is crucial to achieve the secure physical execution of the electricity market. Along with costly remedial actions such as the redispatch of generation units, these possibilities include topological changes (which itself includes transmission switching and bus splitting and merging, among others), phase shifting transformers (PSTs) tap changes and high voltage direct current (HVDC) line set points.

While power flow control devices and redispatch and even some topology control[1] are regularly used

[1]The extent to which system operators use topology control varies widely case by case and often

by system operators (Transmission System Operators (TSOs), Independent System Operators (ISOs), etc.), their integration in the electricity market framework remains incomplete. Their usage remains largely reserved for ensuring the security of the grid close to real time and is generally determined individually by system operators. However, as the inherent system variability increases, these tools will become more and more beneficial, not only from a security perspective, but also economically. Their integration into current market paradigms presents certain challenges that will likely require fundamental market design changes. This chapter aims to quantify the increasing advantage that arises through market integration of these levers by way of analysis of a basic case study.

From a mathematical perspective, control of HVDC lines, phase shifting transformers (PSTs) as well as other power flow devices that operate through line reactance control (FACTs) can require binary variables for their full modelization, as in (Djelassi et al., 2018). However, they are often approximated through the use of continuous variables, facilitating their integration into a variety of optimization problems (Van den Bergh et al., 2014). Optimal topology control can not be approximated in this way.

The optimal transmission switching (OTS) problem has been well-covered in the literature, beginning in the early 1980s. As described by Mazi et al. (Mazi et al., 1986) at the time:

> *"An experiment was conducted in which a power system model was set up to reflect a contingency condition resulting in a branch overload. A corrective action for this overload was calculated using a linear programming solution and resulted in a shift in generation. The same contingency condition was then presented to a system operator on a dispatcher training simulator. . . The operator's initial response to the overload was to simply switch the network. This relieved the overload and allowed the generation to remain at economic loading."*

Mazi et al. then point out that while transmission switching is an action often taken by network operators, it is not often automated or pre-calculated.

Certain aspects of this remain true today. Topology control poses a difficult problem, both in its resolution and the question of transparency to market players. The research on this topic can be split roughly into two large blocks. The first period from the early 1980s to the early 2000s (largely before the liberalisation of electricity markets) focused almost exclusively on the technical aspects of the problem. Reference (Van Amerongen and Van Meeteren, 1980) introduced the problem as a method to correct overloads after N-1 events. It was found early on that the problem was quite complex[2] and thus the large part of the research focused on fast heuristics, decomposition and other methods to reduce the search space.

Reference (Rolim and Machado, 1999) performed a literature review in 1999 and found optimization problem search spaces limited by: operator experience (Bakirtzis and Meliopoulos, 1987) (Schnyder and Glavitsch, 1990), sensitivity factors (Bacher and Glavitsch, 1986) (Mazi et al., 1986), off-line analysis (Koglin and de Medeiros, 1985) (Bertram et al., 1990), branch and bound heuristics (Gorenstin, B. et al., 1987), loop flow analysis (Freitas e Silva and Machado, 1993), Z-matrices (Makram et al., 1989), electrical distance, and development of specific strategies based on flow direction. Up to this point, reference (Rolim and Machado, 1999) found that the most common objectives of optimal transmission switching were solving branch overloads and voltage problems (Bakirtzis and Meliopoulos, 1987) (Rolim et al., 1995). Some studies also looked at minimizing losses (Dodu et al., 1981) (Schnyder and

lacks transparency. Reference (Hedman et al., 2011a) elaborates on the operational parameters for some system operators.

[2] See (Lehmann et al., 2014) for in depth complexity analysis of the problem.

Glavitsch, 1990) and some preventive security enhancement (Glavitsch, H. et al., 1984) (Schnyder and Glavitsch, 1990). They found that the large majority of the literature concentrated on corrective remedial actions, rather than preventive.

While this type of research continues to this day, a new block of research began developing in the early 2000s analyzing the economic aspects of the problem. This was driven by several factors. Firstly, the somewhat global liberalization of electricity markets brought about a reframing of the context of the problem itself. In addition, in the past, the added value from automation of grid flexibility was limited as the flows resulting from conventional power production sources were relatively stable and well-known. The addition of variable renewable energies brought a renewed interest in this area as power flows become more unpredictable and irregular (not to mention more highly-distributed farther from load centers, where power lines were previously dimensioned for more regular flows).

Reference (O'Neill et al., 2005a) proposed dispatchable transmission asset auctions. A series of papers co-optimizing unit commitment or economic dispatch and optimal transmission switching, published between 2009 and 2012, found gains of between 3-25% of total cost due to transmission switching (Fisher et al., 2008) (Hedman and Oren, 2009) (Hedman et al., 2011a). Reference(Hedman and Oren, 2009) used the $B\theta$ form of the DC-OPF and limited the total number of switches allowed by the algorithm to make the problem tractable. This method was expanded to include N-1 contingencies in (Hedman et al., 2009). Reference (Goldis et al., 2017) developed a PTDF approach to improve the computational time of the co-optimized problem. Often in these studies, the problem was decomposed, iterating between a unit commitment with fixed topology and an optimal transmission switching problem with fixed generation (Hedman et al., 2011a). Reference (Han and Papavasiliou, 2016) found 0.3–2.03% reduction in total cost in zonal electricity markets using a similar decomposition.

Beyond the obvious gains of optimizing the grid topology for different dispatch profiles, (Hedman et al., 2008), (Hedman et al., 2011b) and (O'Neill et al., 2005a) analyzed the specific economic sensitivities related to optimal transmission switching. These authors found that the total gain from optimal transmission switching could be approached with a limited number of switching operations. However, solutions with almost identical total savings led to large differences in both LMPs (Locational Marginal Prices, also referred to as nodal prices) and the wealth transfers between market participants. Since the problem is quite large and unlikely to attain an exact optimum in operation, this poses a problem for transparency to market players. In addition, the changes in topology can lead to revenue inadequacy regarding the long-term FTR (Financial Transmission Rights) market. The implication is that a reconsideration of LMP-based market trading would be useful to exploit the benefits of optimizing the transmission topology. Similar sensitivities of zonal prices were found by (Mekonnen and Belmans, 2012) and (Mekonnen et al., 2013) of the flow-based market coupling to PST and HVDC parameters.

To summarize, the technical and economic benefits of optimal transmission switching are established in the literature. The goal of this chapter is to expand the existing studies by focusing on a current aspect, the need to accommodate increasing amounts of variable renewable power generation through the transmission system. Unlike the optimal transmission switching analyses performed by (Hedman and Oren, 2009) and (Hedman et al., 2008), this study focuses on bus splitting and merging rather than switching branches in and out of service, which are often more complicated from an operational perspective (Goldis et al., 2017). Specifically, this chapter examines how the use and economic value of transmission switching increase with the growth of renewable power generation.

Section 2.2 describes the basic equations for modeling transmission networks. Section 2.3 explicits the methodology used for this study, followed by a description of the case study in Section 2.4 and results in Section 2.5.

2.2 Network Modeling

2.2.1 AC Optimal Power Flow Equations

The original AC optimal power flow (OPF) is often traced back to (Carpentier, 1962), and indeed this is one of the earliest and most elegant descriptions of the problem. However, the problem - and its resolution under any number of hypotheses goes even further back (Ricard, 1946). Around this same time, Boiteux published his seminal paper on marginal price theory (Boiteux, 1956) leading Carpentier 1962 to include "une interprétation économique des variables duales" as well. An introduction to the approximations made for a DC-OPF calculation are also introduced in this early work:

> *"APPROXIMATION 2 [Utilisable pour un calcul rapide (simulation)]. — Les tensions sont fixes et égales en tout point. On ne tient pas compte du réactif. Les angles (θ_i — θ_α) sont suffisamment petits pour qu'on néglige $(\theta_i$—$\theta_\alpha)^3$."*[3]

We can write a generic optimal power flow model in the following way, for instance following the style of (Lin and Magnago, 2017):

$$\min_{x,\,u} \quad f(x) \tag{2.1a}$$

$$\text{s.t.} \quad g(x,p) = 0 \quad (\lambda) \tag{2.1b}$$

$$h(x,p) \leq 0 \quad (\mu) \tag{2.1c}$$

In this form, x and p represent the variable vector and a parameter vector, respectively. The vector x may include active and reactive power, voltage magnitudes, phase shift angles, and so on, whereas p would contain the generator and transmission technical constraint limits. $f(x,u)$ is the objective function, which has a wide variety of possible goals, including economic dispatch or loss minimization among others. $g(x,u,p)$ represents the power flow with λ, its Lagrange multiplier – either a uniform, zonal or nodal price depending on the geographical scale balanced. Finally, $h(x,u,p)$ represents any additional constraints, including but not limited to generation operational limits and network constraints. Therefore μ represents the respective dual values, for instance congestion rents for network constraints.

We will now mention a few definitions for AC circuits. For a branch k, defined between a source bus, s(k), and an end bus, e(k), we have the following terms:

$$\begin{aligned}
\text{Resistance} &:= R_k \text{ [Ohms]} \\
\text{Reactance} &:= X_k \text{ [Ohms]} \\
\text{Impedance} &:= Z_k = R_k + \mathrm{j}X_k \text{ [Ohms]} \\
\text{Admittance} &:= Y_k = \frac{1}{Z_k} = G_k + jB_k \text{ [Siemens]} \\
\text{Conductance} &:= G_k = \frac{R_k}{R_k^2 + X_k^2} \text{ [Siemens]} \\
\text{Susceptance} &:= B_k = \frac{-X_k}{R_k^2 + X_k^2} \text{ [Siemens]}
\end{aligned}$$

[3] Translation: APPROXIMATION 2 [Usable for a rapid calculation (simulation). — The voltages are fixed and equal at all points. We do not take into account reactive power. The angles (θ_i — θ_α) are sufficiently small that we can neglect $(\theta_i$—$\theta_\alpha)^3$.

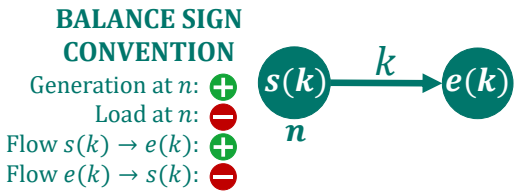

Figure 2.1: Sign Conventions

For clarification, Figure 2.1 shows the sign conventions for the following discussion.

The polar representation of the AC power flow equations using a standard pi transmission model (see (Rosellon and Kristiansen, 2013) for a nice derivation of the flow equations) are as follows:

$\forall k \in K$:

$$F_k^P = +G_k V_{s(k)}^2 - G_k V_{s(k)} V_{e(k)} cos(\theta_{s(k)} - \theta_{e(k)}) - B_k V_{s(k)} V_{e(k)} sin(\theta_{s(k)} - \theta_{e(k)}) \quad (2.2)$$

$$F_k^Q = -B_k V_{s(k)}^2 - G_k V_{s(k)} V_{e(k)} sin(\theta_{s(k)} - \theta_{e(k)}) + B_k V_{s(k)} V_{e(k)} cos(\theta_{s(k)} - \theta_{e(k)}) \quad (2.3)$$

where F_k^P and F_k^Q are the real and reactive power flow on the oriented branch k, respectively. $V_{s(k)}$, $V_{e(k)}$, $\theta_{s(k)}$ and $\theta_{e(k)}$ are the voltage magnitudes and angles at the source and end nodes of each branch, k.

These equations define the flow on the line, both real and reactive as a function of voltage magnitudes and phase angles at the nodes of the system.[4] These are necessary for the formulation of the AC optimal power flow (OPF):

$$\min_{P,Q,V,\theta} \quad f(x) \quad (2.4a)$$

$$\text{s.t.} \quad \sum_{g \in \mathcal{G}_n} P_g - L_n^P - \sum_{k \in \mathcal{K} | s(k)=n} F_k^P + \sum_{k \in \mathcal{K} | e(k)=n} F_k^P = 0 \qquad \forall n \in \mathcal{N} \quad (2.4b)$$

$$\sum_{g \in \mathcal{G}_n} Q_g - L_n^Q - \sum_{k \in \mathcal{K} | s(k)=n} F_k^Q + \sum_{k \in \mathcal{K} | e(k)=n} F_k^Q = 0 \qquad \forall n \in \mathcal{N} \quad (2.4c)$$

$$V_{min} \leq V_n \leq V_{max} \qquad \forall n \in \mathcal{N} \quad (2.4d)$$

$$(F_k^P)^2 + (F_k^Q)^2 \leq (S_k^{max})^2 \qquad \forall k \in \mathcal{K} \quad (2.4e)$$

$$\theta_{min} \leq \theta_{s(k)} - \theta_{e(k)} \leq \theta_{max} \qquad \forall k \in \mathcal{K} \quad (2.4f)$$

$$P_g \in P_g^{OpRange} \qquad \forall g \in \mathcal{G} \quad (2.4g)$$

$$Q_g \in Q_g^{OpRange} \qquad \forall g \in \mathcal{G} \quad (2.4h)$$

where F_k^P and F_k^Q are defined as in Equations set 2.2 and 2.3, respectively. Equation set 2.4 shows a standard AC-OPF problem with a set of basic constraints. The objective function, Equation 2.4a, can vary depending on the issue in question. Some common functions are cost minimization (economic dispatch), minimization of line losses, voltage maximization or surplus maximization (for these last two, the minimum in Equation 2.4a would be replaced by a maximum, or a negative sign added). For the purposes of this work, we use either cost minimization or surplus maximization, which are of course equivalent if demand is offered at the maximum market price.

Constraints 2.4g and 2.4h represent the active and reactive generation limits.[5] These can take into account simply a minimum and maximum value. Depending on whether the optimization occurs over multiple time steps or not, ramping or minimum duration constraints could be included as well. Constraints 2.4b and 2.4c represent the nodal balance equations (Kirchhoff's current law) for both real and reactive power. Equation 2.4e is a proxy for the thermal line flow limit. Finally, Equations 2.4d and 2.4f[6] give the limits on the voltage magnitude and angle. This list of constraints is in no way

[4] For more details on AC-OPF modelizations, see for instance (Sliwak, 2021) or (Josz, 2022).

[5] Note that these are interrelated.

[6] Note that this constraint is not necessarily a physical equipment limit, but it is generally added to improve resolution of the problem.

exhaustive; for instance, we will discuss later in this chapter the addition of contingencies and flexible topology to the OPF formulation.

2.2.2 DC Optimal Power Flow Equations

Given the definitions of real and reactive power flow in Equations 2.2 and 2.3, we can see that the AC-OPF problem is nonlinear and the objective function often nonconvex. In some conditions, the feasible domain may even be non connex. This vastly complicates the resolution of the problem. For this reason, this work uses the commonly accepted linearization known as the DC approximation (see Appendix F for some analysis of an AC versus DC load flow on the CWE scale). The power flow equations are formulated through the application of several assumptions[7]:

1. Voltage magnitudes differ negligibly and are close to a nominal value

The value of 1 comes specifically from the use of per unit values.

$$V_i \approx V_j \approx 1$$

This first assumption reduces Equations 2.2 and 2.3 to:

$$\forall k \in K:$$

$$F_k^P = +G_k - G_k cos(\theta_{s(k)} - \theta_{e(k)}) - B_k sin(\theta_{s(k)} - \theta_{e(k)}) \tag{2.5}$$

$$F_k^Q = -B_k - G_k sin(\theta_{s(k)} - \theta_{e(k)}) + B_k cos(\theta_{s(k)} - \theta_{e(k)}) \tag{2.6}$$

2. Small angle approximation

$$sin(\theta) \approx \theta$$
$$cos(\theta) \approx 1$$

We next assume that the phase angle between nodes remains quite small, giving:

$$\forall k \in K:$$

$$F_k^P = -B_k(\theta_{s(k)} - \theta_{e(k)}) \tag{2.7}$$

$$F_k^Q = -G_k(\theta_{s(k)} - \theta_{e(k)}) \tag{2.8}$$

3. Line resistance is negligible compared to line reactance

$$B_k = \frac{X_k}{R_k^2 + X_k^2} \approx \frac{1}{X_k} \tag{2.9}$$

4. Ignore reactive power

This is technically not an assumption in its own right as it stems from the previous assumptions, but due to its importance, we highlight it here. This leads us to a single equation that represents the real power flow on a line k (defined as the line from s(k) to e(k)):

$$F_k = B_k(\theta_{e(k)} - \theta_{s(k)}) = \frac{1}{X_k}(\theta_{e(k)} - \theta_{s(k)}) \tag{2.10}$$

[7]The validity of these assumptions depends heavily on the network in question as well as several other factors. A comparison of AC and DC modeling is interesting, but out of the scope of this work, although some data from 2007 is analyzed in Appendix F. Many works discuss the often questionable validity of DC modeling applied to certain problems, many of which are summed up nicely in (Stott et al., 2009)

Note that we have dropped the notation P from F_k^P (becomes F_k) for ease in the next sections and chapters since we will continue to use the DC approximation. We apply this change to all relevant variables.

Applying the four assumptions described above, we can now formulate what is often referred to as the Bθ version of the DC-OPF:

$$\min_{P,\theta} \quad f(x) \tag{2.11a}$$

$$\text{s.t.} \quad \sum_{g\in\mathcal{G}_n} P_g - L_n - \sum_{k\in\mathcal{K}|s(k)=n} F_k + \sum_{k\in\mathcal{K}|e(k)=n} F_k = 0 \qquad \forall n \in \mathcal{N} \tag{2.11b}$$

$$F_k - \frac{1}{X_k}(\theta_{e(k)} - \theta_{s(k)}) = 0 \qquad \forall k \in \mathcal{K} \tag{2.11c}$$

$$-\overline{F_k^{inv}} \le F_k \le \overline{F_k^{dir}} \qquad \forall k \in \mathcal{K} \tag{2.11d}$$

$$\theta_{min} \le \theta_{s(k)} - \theta_{e(k)} \le \theta_{max} \qquad \forall k \in \mathcal{K} \tag{2.11e}$$

$$P_g \in P_g^{OpRange} \forall g \in \mathcal{G} \tag{2.11f}$$

2.3 Methodology

The aim of this chapter is to analyze optimal topology control on systems with increasing penetration of variable renewable energies. More specifically, we aim to assess two facets of this topic: firstly, how increasing system variability calls for the usage of a wider variety of grid flexibility actions; and secondly how the economic benefits of grid flexibility evolve as the generation side of the electricity system becomes more variable.

In order to analyze these two aspects, a full year study was run with a DC-OPF performed on each hour of the year. Several scenarios with increasing wind production were generated and the results from three variations of the DC-OPF were compared: 1) a DC-OPF without flexible topology; 2) a DC-OPF with optimal topology control (OTC); and 3) a generation economic dispatch, ignoring the transmission network. The no-network (or copper plate) variation gives a lower limit of the total production cost and when compared to the first variation, assigns a value to the added system cost due specifically to network constraints. The second variation, with OTC, allows for analysis of how the expansion of use and variability of optimal grid flexibility actions could benefit the customer in future energy systems.

The lossless DC-OPF formulation used for this study includes the nodal balance constraints (Equation 2.11b), generation limits (Equation 2.11f, and branch flow limits (Equation 2.11d) as in (Fisher et al., 2008) among others. Constraints imposing full grid connectivity were also included as shown in (Djelassi et al., 2018). Breakers are treated as branches with an infinite flow limit and no susceptance. For the DC-OPF with OTC, the constraints were added for each breaker with the possibility to be split, following the patterns of constraints 2.4f and 2.11d:

$\forall k \in \mathcal{K}_B$:

$$-(1-\delta_k)M_B \le \theta_{s(k)} - \theta_{e(k)} \le (1-\delta_k)M_B \tag{2.12}$$

$$-\delta_k M_B \le F_k \le \delta_k M_B \tag{2.13}$$

where $\mathcal{K}_B$ is the set of controllable breakers, M_B is a parameter sufficiently large to render the inequality ineffective according to the breaker status variable, δ_k is the binary variable representing the breaker open/closed status, F_k is the flow on branch k, and $\theta_{s(k)}$ and $\theta_{e(k)}$ are the voltage angles on the origin

and end nodes, respectively. While the majority of control actions considered in the case study were splitting and merging buses, a small set of controllable branches are included as well. To that end, the following constraints were included for each branch that can be open or closed:

$\forall k \in \mathcal{K}_{CB}$:

$$-(1 - z_k)M_K \leq -F_k + B_k(\theta_{s(k)} - \theta_{e(k)}) \leq (1 - z_k)M_K \tag{2.14}$$

$$-\overline{F_k^{inv}} z_k \leq F_k \leq \overline{F_k^{dir}} z_k \tag{2.15}$$

where $\mathcal{K}_{CB}$ is the set of controllable branches, z_k is the binary variable representing the branch open/closed status, M_K is a parameter similar to M_B described above and B_k is the susceptance. In order to assess the idealized system flexibility, no limits are placed on the number of control actions that can be used.

The objective function minimizes the variable production cost. For the DC-OPF with OTC, a small wear-and-tear cost was also added to the objective function for each line that is opened or bus that is split.[8] The possibility for load shedding at a very high cost was included in the objective function for all three DC-OPF variations. The objective function is as follows[9]:

$$\min \sum_{g \in \mathcal{G}} c_g P_g + c_w(N_B - \sum_{k \in \mathcal{K}_B} \delta_k) + c_w(N_{CB} - \sum_{k \in \mathcal{K}_{CB}} z_k) + c_{LS} P_d^{LS} \tag{2.16}$$

where $\mathcal{G}$ is the set of generators with the cost and production represented by c_g and P_g. N_B and N_{CB} are the number of controllable breakers and branches, c_w is the wear-and-tear cost associated with the control actions and c_{LS} and P_d^{LS} are the load shedding cost and quantities.

For each scenario and DC-OPF variation, the total system cost and the dispatch were calculated. Finally, the nodal prices were calculated by rerunning a DC-OPF with all binary variables fixed as described in (O'Neill et al., 2005b). For the purposes of this study, renewable power generation is considered as a free resource (no cost), hence prioritized by the chosen objective function (5). Curtailment of renewables is considered at no additional cost.

2.3.1 DC-OPF Variations

As described in the previous section, three lossless DC-OPF variations were used for this study.

[8] Note that this penalty cost was not included in the total production cost calculation summarized in the tables and graphs hereafter.

[9] Note that the two middle terms of Equation 2.16 are included only in the DC-OPF with OTC.

2.3.1.1 DC-OPF without flexible topology (No OTC)

Similar to the optimization problem 2.11, the first version of the DC-OPF used in this chapter is as follows:

$$\min_{P,\theta} \quad \sum_{g\in\mathcal{G}} c_g P_g + c_{LS} P_d^{LS} \tag{2.17a}$$

$$\text{s.t.} \quad \sum_{g\in\mathcal{G}_n} P_g - L_n - \sum_{k\in\mathcal{K}|s(k)=n} F_k + \sum_{k\in\mathcal{K}|e(k)=n} F_k = 0 \qquad \forall n\in\mathcal{N} \tag{2.17b}$$

$$F_k - \frac{1}{X_k}(\theta_{e(k)} - \theta_{s(k)}) = 0 \qquad \forall k\in\mathcal{K} \tag{2.17c}$$

$$-\overline{F_k^{inv}} \le F_k \le \overline{F_k^{dir}} \qquad \forall k\in\mathcal{K} \tag{2.17d}$$

$$\theta_{min} \le \theta_{s(k)} - \theta_{e(k)} \le \theta_{max} \qquad \forall k\in\mathcal{K} \tag{2.17e}$$

$$\delta_g^{UC} P_g^{min} \le P_g \le \delta_g^{UC} P_g^{max} \forall g\in\mathcal{G} \tag{2.17f}$$

Equations 2.17a-2.17f follow the same pattern that we have seen in the previous section.

2.3.1.2 DC-OPF with optimal topology control (OTC)

Next, we have the full DC-OPF used in this chapter, but this time, we include the constraints for optimal topology control.

$$\min_{P,\theta} \quad \sum_{g\in\mathcal{G}} c_g P_g + c_w(N_B - \sum_{k\in\mathcal{K}_B}\delta_k) + c_w(N_{CB} - \sum_{k\in\mathcal{K}_{CB}} z_k) + c_{LS} P_d^{LS} \tag{2.18a}$$

$$\text{s.t.} \quad \sum_{g\in\mathcal{G}_n} P_g - L_n - \sum_{k\in\mathcal{K}|s(k)=n} F_k + \sum_{k\in\mathcal{K}|e(k)=n} F_k = 0 \qquad \forall n\in\mathcal{N} \tag{2.18b}$$

$$F_k - \frac{1}{X_k}(\theta_{e(k)} - \theta_{s(k)}) = 0 \qquad \forall k\in\mathcal{K}_{\notin Flex} \tag{2.18c}$$

$$-\overline{F_k^{inv}} \le F_k \le \overline{F_k^{dir}} \qquad \forall k\in\mathcal{K}_{\notin Flex} \tag{2.18d}$$

$$\theta_{min} \le \theta_{s(k)} - \theta_{e(k)} \le \theta_{max} \qquad \forall k\in\mathcal{K}_{\notin Flex} \tag{2.18e}$$

$$-(1-\delta_k)M_B \le \theta_{e(k)} - \theta_{s(k)} \le (1-\delta_k)M_B \forall k\in\mathcal{K}_B \tag{2.18f}$$

$$-\delta_k M_B \le F_k \le \delta_k M_B \qquad \forall k\in\mathcal{K}_B \tag{2.18g}$$

$$-(1-z_k)M_K \le -F_k + \frac{1}{X_k}(\theta_{e(k)} - \theta_{s(k)}) \le (1-z_k)M_K \forall k\in\mathcal{K}_{CB} \tag{2.18h}$$

$$-\overline{F_k^{inv}} z_k \le F_k \le \overline{F_k^{dir}} z_k \qquad \forall k\in\mathcal{K}_{CB} \tag{2.18i}$$

$$\delta_g^{UC} P_g^{min} \le P_g \le \delta_g^{UC} P_g^{max} \quad \forall g\in\mathcal{G} \tag{2.18j}$$

2.3.1.3 Copper Plate Economic Dispatch

The copper plate model ignores the network flow limit constraints:

$$\min_{P,\theta} \quad \sum_{g\in\mathcal{G}} c_g P_g + c_{LS} P_d^{LS} \tag{2.19a}$$

$$\text{s.t.} \quad \sum_{g\in\mathcal{G}_n} P_g - L_n - \sum_{k\in\mathcal{K}|s(k)=n} F_k + \sum_{k\in\mathcal{K}|e(k)=n} F_k = 0 \qquad \forall n\in\mathcal{N} \tag{2.19b}$$

$$F_k - \frac{1}{X_k}(\theta_{e(k)} - \theta_{s(k)}) = 0 \qquad \forall k\in\mathcal{K} \tag{2.19c}$$

$$\theta_{min} \le \theta_{s(k)} - \theta_{e(k)} \le \theta_{max} \qquad \forall k\in\mathcal{K} \tag{2.19d}$$

$$\delta_g^{UC} P_g^{min} \le P_g \le \delta_g^{UC} P_g^{max} \forall g\in\mathcal{G} \tag{2.19e}$$

2.4 Case Study

2.4.1 Network and Data Description

The network used for this study is based on the modified RTS-96 in (Barrows et al., 2020), which is a modernized version of the original RTS-96 network (Grigg et al., 1999).[10] Some simplifications were made to this data: namely, the piecewise linear cost model used in the original data set was reduced to a simple marginal price, minimum power output was zero for all plants, and storage was not included as intertemporal constraints were not modeled.

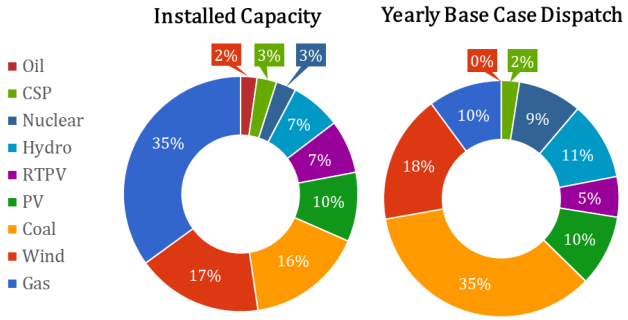

Figure 2.2: System Generation by Fuel

Reference (Barrows et al., 2020) artificially places the RTS-96 network in the Southwest United States in order to have yearly renewable data. The network is characterized by high load in the summer, fairly steady PV production throughout the year and increased average wind production in the winter months. The installed capacity and energy dispatched in this base case scenario are shown in Figure 2.2.

2.4.2 Determining Topology Control Actions

The modified RTS-96 system did not originally include grid flexibility controls. A subset of the network buses were selected as controllable as well as a few branches. In order to choose which buses would be considered for control actions, an analysis was performed using two seasonally representative months: January and July. All buses were allowed to split or merge and those that changed position more than a certain threshold (set at 15% of the time) were selected for the case study.

While the study focuses largely on bus splitting or merging, four lines per zone were additionally considered for transmission switching as they are lines that have a parallel counterpart. In total, 30 topological actions are included in the system. 18 out of the 73 nodes were deemed controllable. These are shown with their location in the network in Figure E.5.

2.4.3 Generation Scenarios

Several scenarios with increasing wind capacities were generated from the base case data described above. We consider that the resource at each of the plant locations had not yet been fully utilized and could thus be increased up to three times that of the base case. Twelve scenarios were generated wherein all wind power plants increase their power output proportionally from 0-300% of the base case capacity, or 0-7.52 GW of installed capacity.

[10]The data can be found at https://github.com/GridMod/RTS-GMLC.

2.5 Results

2.5.1 Effect of Increasing Generation Variability on Usage of Grid Flexibility Controls

We first analyze the effect of increasing renewable energy penetration on the usage of transmission switching. As the wind power generation increases from scenario to scenario, there is an increase in the number of topological changes that are used, shown in Figure 2.3. Below the 50%-Scenario, a maximum of 7 changes occur between any two hours. This goes up to around 20 maximum changes between time steps for cases with more variable generation. Indeed, the scenarios from the lowest wind scenario to the base case level have no changes between time steps more than 75% of the time. This reduces to around 50% of the time around the 200%-Scenario and stays relatively steady for the cases with higher wind generation. It is important to note that while the variability of the topology increases quite quickly between the 50%-Scenario and the 150%-Scenario, the increase in topological changes hits an inflection point and begins to level off after a certain threshold.

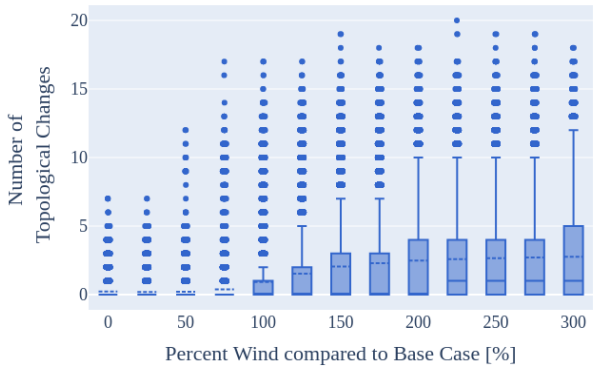

Figure 2.3: Number of Topology Changes for Each Scenario

This same threshold is also noticeable in the examination of the number of unique topologies used in each system shown in Figure 2.4. This plot shows the number of unique combinations of breaker positions in the system. The number of different topologies increases quickly between the 75%-Scenario and the 150%-Scenario, but the number of topologies used increases by less and less after this point. This, along with the results shown in Figure 2.3 is key as the number of actions that can be used in practice is limited. Figure 2.3 demonstrates the fact that the ideal number of actions enacted by a system operator between time steps remains fairly steady above a certain wind penetration level. While the number of topologies increases, even in the 300%-Scenario, the base topology (all lines closed) is used almost half of the hours of the year.

2.5.2 Economic Benefits of Topology Control Actions

Figure 2.5 compares the total cost in the three different situations: copper plate, base network with no grid flexibility and base network with optimal topology control across the various renewable capacity scenarios. The top plot demonstrates the decrease in production cost for each of the three variations as the amount of renewables increases. The difference between the copper plate and the results without topology control are shown in the top line (red) in the bottom plot. The difference in annual

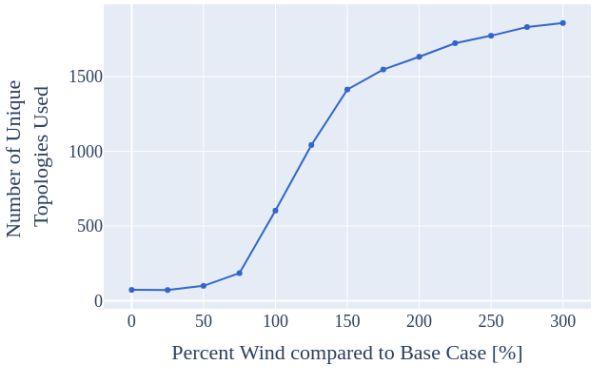

Figure 2.4: Number of Unique Topologies for Each Scenario

production cost between the two variations moves from $40 thousand to $66 million as more lower cost energy sources are included in the system. This is over 18% difference. This value comes solely from the network constraints of the system and gives an upper limit to the possible benefits gained through flexibility. The lower line (blue) in the bottom plot gives the difference between the optimal topology control and the base network without grid flexibility. While the largest rate of change occurs between the 50% and 150% scenarios, the gains from the use of grid flexibility continue to increase throughout all scenarios, up to $20 Million, over 7% of the total production cost. As the wind production increases by a factor of 3 (between the 100%- and 300%-Scenarios), the amount gained due to OTC increases by a factor of 3.4.

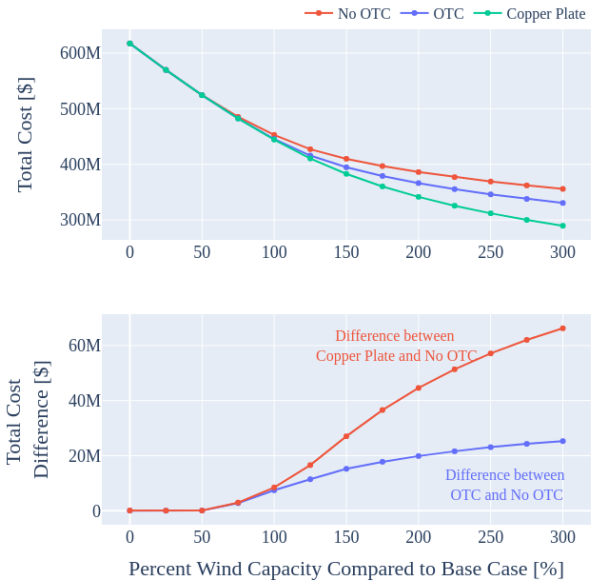

Figure 2.5: Total Cost Gained due to Topological Control Actions

Already the reduction in system cost due to OTC shown in Figure 2.5 alludes to the fact that a larger amount of renewables are dispatched through the use of grid topology actions. Figure 2.6 shows the wind curtailment on the hours where there is thermal generation – in other words, it does not include

the hours where demand was met with only renewable energy. As a consequence, the copper plate case is shown to have zero wind curtailment for all scenarios, while any curbing of wind generation in the other two cases is due solely to network constraints. The grid flexibility actions allow for a reduction in curtailment of up to 1.6 TWh. The difference in the curves continues to increase as well as more wind is introduced into the system.

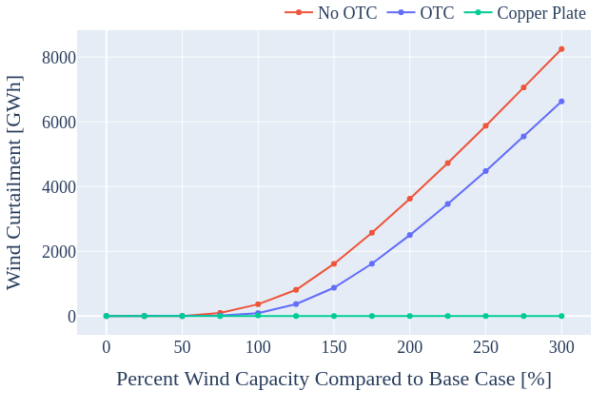

Figure 2.6: Sum of Wind Curtailment Across All Hours with Thermal Generation

Figure 2.7 shows the average variance over the year of data of the nodal prices across the buses of the system. This value can be used as an indicator of the congestion in the system. The case with optimal topology control shows a lower geographical variance as the amount of congestion in the system is reduced.

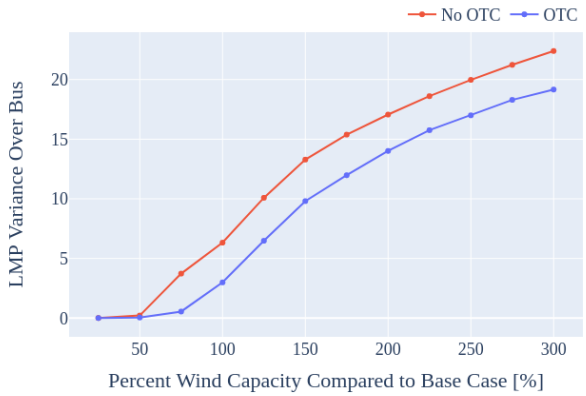

Figure 2.7: Nodal Price Variance

2.6 Conclusion

This research analyzes how the use of optimal topology controls facilitates the inclusion of renewable energies. As shown through the analysis of a case study, optimal topology control impact on dispatch and cost becomes more important as the energy system grows more variable. While the ideal number of topological actions used increases with the penetration of wind generation, the economic benefit

from their use increases along the same axis. In fact, an increase in wind production of a factor of 3 leads to a gain in total system cost by a factor of 3.4 from optimal use of topological controls.

Traditionally, there has been some pushback to market integration of topology optimization especially in nodal markets where switching a line or splitting a bus could render the FTR (Financial Transmission Rights) markets revenue inadequate(Hedman et al., 2011b). These results show that there will be more and more situations where system operators should be incentivized to use these mechanisms, whether for system security or economic reasons. Their development and integration with existing market designs is thus crucial as variable renewable energies become a larger percent of the dispatch.

Chapter 3

The Flow-Based Capacity Calculation

Nomenclature

Indices	
i,j,n	Node
s(k)	Source Node of Branch, k
e(k)	End Node of Branch, k
k	Branch
g	Generator
z	Zone
c	Contingency
l	Critical Network Element and Contingency
Variables	
P_g	Real Power Generation at Generator, g
L_n	Real Power Demand at Node, n
y_n^N	Generation Load Balance (Nodal Net Position) at Node, n
y_z^Z	Generation Load Balance (Zonal Net Position) for Zone, z
F_k	Real Power Flow on Branch, k
F_k^0	Reference Flow in the Base Case on Branch, k
V_n	Nodal Voltage Magnitudes
θ_n	Voltage Angles
δ_k	Binary variable representing breaker open/close status

z_k	Binary variable representing branch open/close status
δ_k^{UC}	Binary variable representing the unit commitment variable
P_d^{LS}	Load shedding variable
NP_z	Zonal Net Position for Zone, z
Parameters	
R_k	Line Resistance of Branch, k
X_k or $X_{i,j}$	Line Reactance of Branch, k, or Branch between Nodes i,j
Z_k	Line Impedance of Branch, k
Y_k	Line Admittance of Branch, k
G_k	Line Conductance of Branch, k
B_k	Line Susceptance of Branch, k
$\overline{F_k^{dir}}, \overline{F_k^{inv}}$	Maximum Flow limits on branch, k (direct/inverse directions)
$P_g^{OpRange}$	Domain representing real operation of Generator, g
P_g^{min}, P_g^{max}	Minimum, Maximum real power of Generator, g
M_B	Big-M parameter for controllable breakers
M_K	Big-M parameter for controllable branches
c_g	Generator, g, Marginal Cost
c_w	"Wear-and-tear" cost for topological actions
c_{LS}	Load shedding cost
N_B, N_{CB}	Number of controllable breakers, branches
$D_{z,k}^Z$	Zonal PTDF Factor for Zone, z, on Branch, k
$D_{n,k}^N$	Nodal PTDF Factor for Node, n, on Branch, k
RAM_l	Remaining Available Margin on CNEC, l
NP_z^{ref}	Zonal Reference Program (Base case net position) for Zone, z
Sets	
$\mathcal{K}$	Set of Branches
$\mathcal{K}_B$	Set of Controllable Breakers (Modelled as branches with no flow limit)
$\mathcal{K}_{CB}$	Set of Controllable Branches
$\mathcal{K}_{¢Flex}$	Set of Non-flexible Branches
$\mathcal{N}$	Set of Nodes
$\mathcal{N}_i$	Set of Nodes connected to Node, i
$\mathcal{G}$	Set of Generators
$\mathcal{G}_n$	Set of Generators at Node, n
$\mathcal{Z}$	Set of Zones
$\mathcal{C}$	Set of Contingencies
$\mathcal{CNEC}$	Set of Critical Network Elements and Contingencies
Matrices and Vectors	
$\boldsymbol{A}$	Network Incidence Matrix, $[\mathcal{K}x\mathcal{N}]$
$\boldsymbol{\beta}$	Branch Susceptance Matrix, $[\mathcal{K}x\mathcal{K}]$
$\boldsymbol{\Psi}$	$\boldsymbol{A\beta A}$, $[\mathcal{N}x\mathcal{N}]$
$\boldsymbol{\Gamma}$	$\boldsymbol{\beta A}$, $[\mathcal{K}x\mathcal{N}]$
$\boldsymbol{y^N}$	Vector of Nodal Net Positions
$\boldsymbol{F}$	Vector of Branch Flows
$\boldsymbol{\theta}$	Vector of Phase Angles
$\boldsymbol{D^N}$	Nodal Power Transfer Distribution Matrix
$\boldsymbol{G^{sh}}$	Generation Shift Key (GSK) Vector
$\boldsymbol{f^0}$	Vector of Reference Flows

3.1 Introduction

In the previous chapter, we discussed the increasing value of grid flexibility in systems with higher levels of variable renewable energy. The next steps are to look directly at how to integrate these conclusions into a market environment, specifically the European zonal market. For this, we begin by analyzing the existing method of network capacity calculation and allocation in Europe, specifically the zonal flow-based model. The use of this model – originally introduced to the CWE region in 2015 – is expanding, now covering the full CORE region and currently under an external parallel run phase in the Nordic Capacity Calculation Region as well. The CORE region of Europe covers 13 countries[1] and the 16 TSOs that own and operate the transmission networks in these countries.

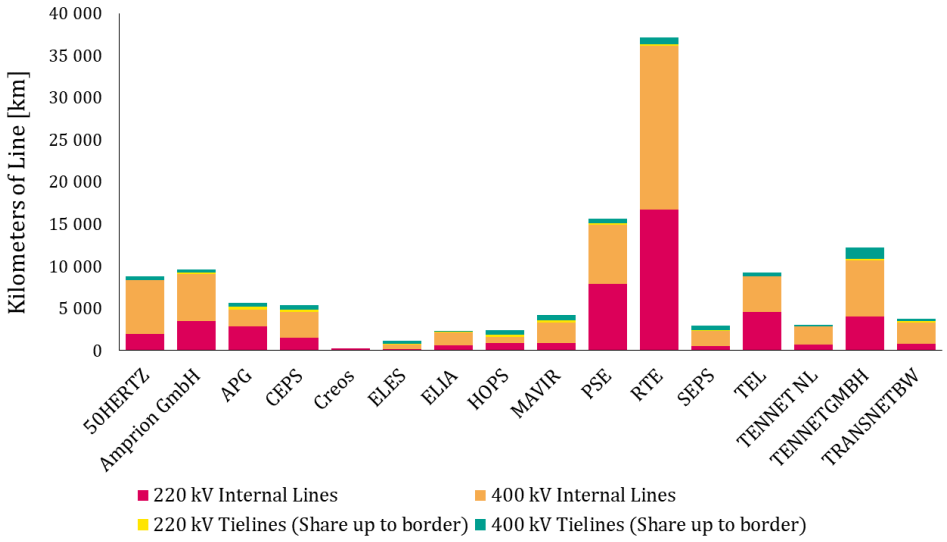

Figure 3.1: Kilometers of Line by TSO in CORE

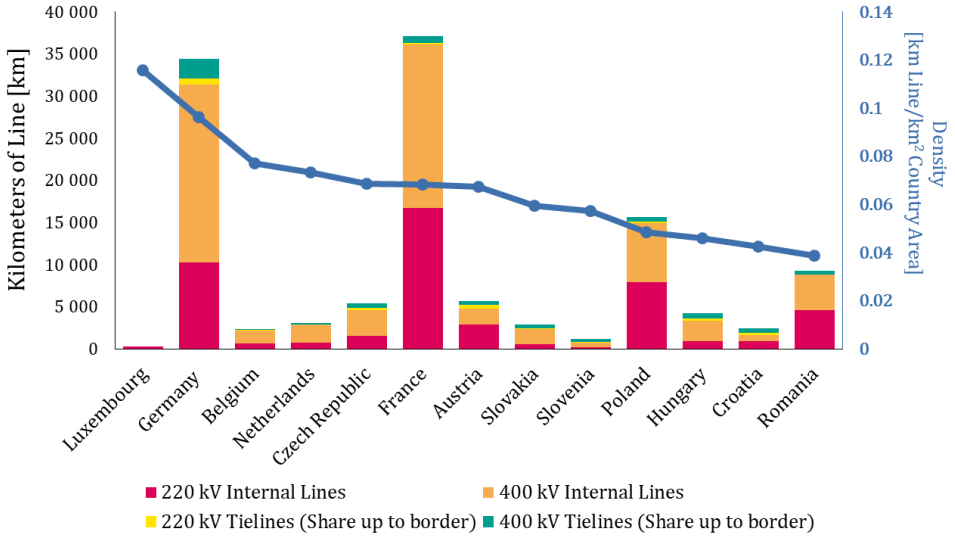

Figure 3.2: Kilometers and Density of Lines by Country in CORE

Figures 3.1 and 3.2 show the kilometers of 220kV and 400kV lines by TSO and by country, respectively,

[1]Austria, Belgium, Croatia, the Czech Republic, France, Germany, Hungary, Luxemburg, the Netherlands, Poland, Romania, Slovakia and Slovenia

for the CORE region.[2] Figure 3.2 additionally shows the density of lines compared to the area of the country.[3]

The flow-based method was initially put in place in 2015 in CWE, Central Western Europe. The goal for this move was to increase the quality of the network constraints given to the market coupling. Recent European-level political directives are pushing to increase European exchange capacities to augment the day ahead market welfare, while maintaining satisfactory levels of electricity supply security. This desire to expand interconnections coincides with increasing system variability brought on by rising use of intermittent renewable energy sources. The initial capacity calculation model, known as the Available Transfer Capacity (ATC) method (still in place in several countries in Europe), is limited in several ways. It treats each direction of each border as an independent constraint and ignores the interdependencies of the flows brought on by Kirchhoff's laws. To account for this lack, in the highly meshed European grid, the physical margin on the elements impacted by the cross-border exchanges must be allocated ex ante between the likely market directions. This assumption is likely to over-constrain the market if the assumed market direction turns out to be erroneous. However, both methods are meant to respect the security level required, including N-1 (and for some rare branches, N-2 as well) constraints. However, for the same level of network security, the flow-based method will theoretically always include the ATC domain, as shown in Figure 3.3.

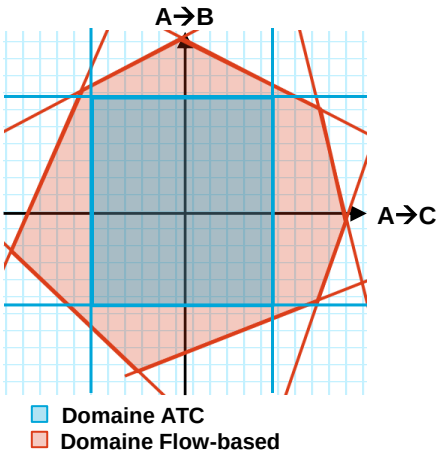

Figure 3.3: ATC and Flow-based Security Domains

Because of this, there was a marked gain in day ahead market welfare during the external parallel run in 2013, shown in Figure 3.4.[4]

The flow-based method, unlike the ATC method, takes into account explicitly the interdependent effects of the exchanges between other zones. The literature on the flow-based method has expanded

[2]Sources: Kilometers of lines taken from CORE Static Grid Model (Version 20220905): https://www.jao.eu/static-grid-model. Country areas found on Wikipedia.

[3]Note that both of the above figures only include the 220kV and 400kV lines. The inclusion of lower voltage levels in the considered transmission network depends on the TSO. For instance, RTE descends well below the majority of the European TSOs, including as far down as 63 kV, while in most other countries this level is already considered as the distribution system.

[4]Note that the *Flow Based Intuitive* method mentioned in this graphic involved the addition of a constraint limiting non-intuitive flows – flows in the opposite direction of the price indicators. This is a concept that is true also for nodal markets and discussed at length in (Wu et al., 1996). Eventually this additional constraint was abandoned due to the associated reduction of market welfare.

[5]Image from Annex 16.10 of (amprion, 2020). ATCMC: ATC market coupling; FBMC: Flow Based market coupling; FBIMC: Flow Based Intuitive market coupling; Infinite: Market coupling under infinite ATC;

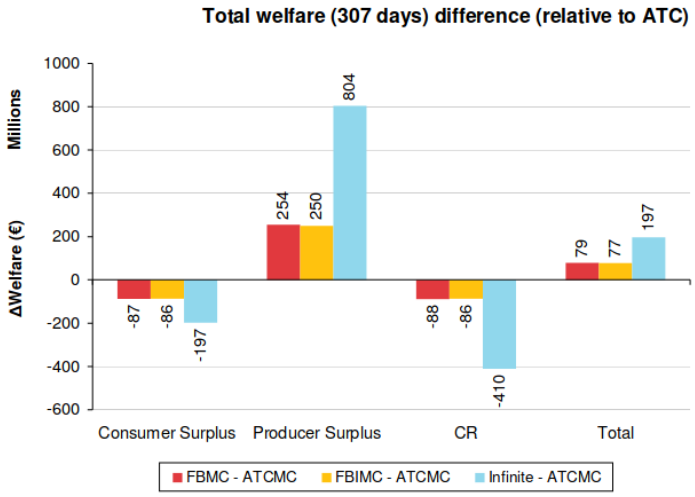

Figure 3.4: Social Welfare Gains from CWE Parallel Run[5]

significantly since it was initially put in place and the concepts behind the flow-based calculation are becoming well-known in electricity modeling literature. (Van den Bergh et al., 2016) and (Marien et al., 2013) give descriptions of the method that touch on the key principles. Much of the early literature highlights issues with the existing method, especially focusing on the lack of transparency of the calculation of certain parameters (notably, the Generation Shift Keys, GSKs, the Flow Reliability Margin, FRM, and the choice of Critical Network Elements, CNE, that are included as constraints) (Marien et al., 2013) (Felten et al., 2021) (Schönheit et al., 2021b) (Voswinkel et al., 2019), although there has been a push for more transparency and the new CORE method clarifies some points that were previously less clear. There are also several studies that work to expand the current method, either through the explicit inclusion of HVDC lines (Müller et al., 2017)[6] or transmission switching (Lete and Papavasiliou, 2020). The gains of the flow-based method compared to the NTC method are widely acknowledged in the literature and a overview of the different studies and their geographical scales can be found in (Finck, 2021).

It is crucial to note the tradeoffs regarding the determination of the "quality" of a given flow-based domain. The quality of a network security domain for a day ahead market relies on a balance between the market welfare generated by a larger domain in this forward market and the security level of the network constraints closer to real time. One can obtain a larger domain by artificially increasing the margin on network elements that is available for allocation in each phase or by filtering the network elements included as constraints. However, doing so without concern for the physical flows resulting from these additionally permitted exchanges will likely lead to increased redispatch costs and a decrease in the overall social welfare considering all stages of the energy system operation. Theoretically, if the bidding zones were constructed in such a way that the structural congestion was found largely at the borders, a small set of cross-border and close-to-the-border lines should represent accurately the network constraints. In the current situation[7], while it is possible to include all internal branches, the domain is likely to be quite small, and possibly empty depending on the base case used to calculate the domain.

Additionally, as more variable renewable energy sources are incorporated into the existing energy system,

[6] In fact, the choice of the set points of the HVDC line ALEGrO between Germany and Belgium has now been integrated directly into the market coupling. This is addressed in more detail in Section 4.2.2.1

[7] Notably with the large structural congestions running between the northern wind production and the southern load centers in Germany

the larger the potential forecast error between the day ahead and real time situations. The network constraints therefore must allow the market to opt for the direction of the best welfare, especially given that there is already updated information between the forecast used for the capacity calculation (using data forecast two days before real time, D-2) and the capacity allocation in the day ahead market. It is therefore crucial to gain the correct balance between increasing exchange capacity and including grid security constraints. In order to properly determine the quality of a given flow-based domain, it is important to model a redispatch phase in order to identify the cost tradeoffs that arise from the given security domain.

This chapter adds several aspects to the existing literature. First, a full description of the operational aspects of the model that are often ignored in the literature is provided. A light explicative analysis of some historical data from CWE and the new developments of the method for the CORE region is presented in this chapter. Several of the somewhat less transparent TSO-specific choices are elucidated through a combination of these analyses and the cross-referencing of multiple documentation sources.

Additionally, an assessment of the robustness of certain flow-based parameter choices is performed on a small case study. This analysis focuses on three key parameters of the flow-based method: 1) the base case calculation, 2) the generation shift keys (GSKs) and 3) the inclusion of remedial actions across different phases. While these have each been assessed to a certain degree in the literature, we bring several additional aspects to light that are rarely treated.

The base case calculation is somewhat less addressed in the existing literature compared to the other two parameters. The majority of studies use some form of DC-OPF to mimic the operational process (Finck, 2021). However, in particular with the addition of contingencies and remedial actions, several questions arise surrounding the effects of different types of modelization. To that end, for the base case calculation, we address the level of grid security constraints – and associated remedial actions – included in the process. Three different models for grid security constraints are applied and their impacts on the resulting flow-based domain are assessed. Secondly, the effects of different GSK calculation methods – perhaps the most widely treated of these parameters in the literature – are studied across two phases: the day ahead market clearing and a redispatch phase that represents the security level of the market clearing output. Notably, they are found to be less susceptible to large welfare differences when we consider the combination of the two stages than has been previously seen in the literature. Thirdly, an example of the impacts from the remedial actions and their inclusion in both the base case calculation and explicitly in the flow-based method are shown as well.

Section 3.2 describes the theoretical zonal flow-based model (zonal shift factor), beginning from the $B\theta$ DC-OPF formulation developed in the previous chapter (Section 2.2). Next, Section 3.3 goes into more detail relating to the operational practices, and the complications that arise in reality. In Section 3.4 we add to the existing literature on the breakdown of the importance of different parameters inherent to the flow-based model. This section notably contributes to the understanding of the operational parameters of the flow-based method in relation to a small case study – the same RTS-GMLC network analyzed in the previous chapter. Finally, Section 3.5 summarizes the results, concludes and presents a few of the many paths of further study surrounding the flow-based method.

3.2 Theoretical Description

3.2.1 Nodal Shift Factor (PTDF) DC-OPF

In Chapter 2, we demonstrate the $B\theta$ formulation of the DC-OPF problem. In order to arrive at the zonal flow-based model currently in use in Europe today, we will first introduce the nodal shift factor

DC-OPF formulation and then show the additional assumptions necessary for the zonal flow-based model.

The shift factor formulation was created initially as a way to improve resolution of the DC-OPF and to directly express line flow with respect to nodal balances. With the $B\theta$ formulation, the number of constraints grows quickly, especially as we add in contingencies (see Section 3.2.3). One way to reduce the size of the problem is through smart use of the shift factor formulation. (Goldis, 2015) demonstrate large speed gains using the PTDF method. Some results from Chapter 3 of that work are shown in Figure 3.5. In this figure, the values are in seconds and $B\theta - DS$ refers to the Dual Simplex method with the $B\theta$ formulation, $B\theta - BR$ to the Barrier method (still with the $B\theta$ formulation), and Ψ refers to the shift factor formulation. There is a huge difference in computational time between the $B\theta$ and shift factor formulations, especially when considering contingencies.

Table 3.1: LP Formulation Results

	Without Contingencies			With Contingencies		
	$B\theta$ - DS	$B\theta$ - BR	Ψ	$B\theta$ - DS	$B\theta$ - BR	Ψ
Avg.	0.65	0.54	0.12	37.28	80.24	.67
Min.	0.42	0.50	0.06	14.49	26.80	0.64
Max.	0.91	0.62	0.14	74.37	541.09	0.70
Sum.	12.95	10.86	2.32	745.68	1,604	13.48
sDev.	0.13	0.03	0.02	14.31	129.69	0.02

Figure 3.5: Time Savings from PTDF method in (Goldis, 2015)

We will now present the derivation of the shift factor formulation, beginning with the $B\theta$ formulation used in the previous chapter. As a reminder, Equations 3.1a-3.1f show the $B\theta$ formulation:

$$\min_{P,\theta} \quad f(x) \tag{3.1a}$$

$$\text{s.t.} \quad \sum_{g\in\mathcal{G}_n} P_g - L_n - \sum_{k\in\mathcal{K}|s(k)=n} F_k + \sum_{k\in\mathcal{K}|e(k)=n} F_k = 0 \qquad \forall n \in \mathcal{N} \tag{3.1b}$$

$$F_k - \frac{1}{X_k}(\theta_{e(k)} - \theta_{s(k)}) = 0 \qquad \forall k \in \mathcal{K} \tag{3.1c}$$

$$-\overline{F_k^{inv}} \le F_k \le \overline{F_k^{dir}} \qquad \forall k \in \mathcal{K} \tag{3.1d}$$

$$\theta_{min} \le \theta_{s(k)} - \theta_{e(k)} \le \theta_{max} \qquad \forall k \in \mathcal{K} \tag{3.1e}$$

$$P_g \in P_g^{OpRange} \forall g \in \mathcal{G} \tag{3.1f}$$

For ease in notation, we will begin by defining the net position of a node as the balance of production and consumption at that node:

$$y_n^N = \sum_{g\in\mathcal{G}_n} P_g - L_n \tag{3.2}$$

We will focus on constraints 2.11c and 2.11b and rewrite them in the following manner:

$$\text{Balance at node n:} \quad y_n^N = -\sum_{k\in\mathcal{K}|s(k)=n} F_k + \sum_{k\in\mathcal{K}|e(k)=n} F_k = 0 \tag{3.3}$$

$$\text{where Flow on line k:} \quad F_k = -\frac{1}{X_k}(\theta_{e(k)} - \theta_{s(k)}) \tag{3.4}$$

At this point, it becomes more straightforward to move into matrix notation. To that end, we define the incidence matrix – which represents the connectivity of a network – and the nodal susceptance

matrix :

$$\text{Incidence matrix} := \boldsymbol{A}^{[\mathcal{K}x\mathcal{N}]} = \begin{bmatrix} a_{1,1} & \cdots & a_{1,n} \\ \vdots & \ddots & \vdots \\ a_{k,1} & \cdots & a_{k,n} \end{bmatrix} \quad \text{where } a_{k,n} = \begin{cases} 1 & \text{if } n \text{ is source of } k \\ -1 & \text{if } n \text{ is end of } k \\ 0 & \text{otherwise} \end{cases}$$

$$\text{Branch Susceptance Matrix} := \boldsymbol{\beta}^{[\mathcal{K}x\mathcal{K}]} = \begin{bmatrix} b_{1,1} & \cdots & b_{1,k} \\ \vdots & \ddots & \vdots \\ b_{k,1} & \cdots & b_{k,k} \end{bmatrix} \quad \text{where } b_{i,k} = \begin{cases} \frac{1}{X_k} & \text{if } i = k \\ 0 & \text{otherwise} \end{cases}$$

We can therefore rewrite Equations 3.3 and 3.4 in matrix form as:

$$\boldsymbol{y^N} = \boldsymbol{\Psi\theta} \tag{3.5}$$

$$\boldsymbol{F} = \boldsymbol{\Gamma\theta} \tag{3.6}$$

where

$$\boldsymbol{\Psi}^{[\mathcal{N}x\mathcal{N}]} = \boldsymbol{A^T\beta A} = \begin{bmatrix} \psi_{1,1} & \cdots & \psi_{1,j} \\ \vdots & \ddots & \vdots \\ \psi_{i,1} & \cdots & \psi_{i,j} \end{bmatrix} \quad \text{where } \psi_{i,j} = \begin{cases} -\sum_{n \in \mathcal{N}_i} \frac{1}{X_{i,n}} & \text{if } i = j \\ \frac{1}{X_{i,j}} & \text{if } j \text{ is connected to } i \\ 0 & \text{otherwise} \end{cases}$$

$$\boldsymbol{\Gamma}^{[\mathcal{K}x\mathcal{N}]} = \boldsymbol{\beta A} = \begin{bmatrix} \gamma_{1,1} & \cdots & \gamma_{1,n} \\ \vdots & \ddots & \vdots \\ \gamma_{k,1} & \cdots & \gamma_{k,n} \end{bmatrix} \quad \text{where } \gamma_{k,n} = \begin{cases} -\frac{1}{X_k} & \text{if } n \text{ is source of } k \\ \frac{1}{X_k} & \text{if } n \text{ is end of } k \\ 0 & \text{otherwise} \end{cases}$$

Note that in order for $\boldsymbol{\Psi}$ to be invertible[8], we remove the rows and columns referring to the reference node for all relevant matrices. Equation 3.5 can therefore be written as:

$$\boldsymbol{\theta} = \boldsymbol{\Psi^{-1}y^N} \tag{3.7}$$

which, if we insert this into 3.6 gives:

$$\boldsymbol{F} = \boldsymbol{\Gamma\Psi^{-1}y^N} = \boldsymbol{\beta A}(\boldsymbol{A^T\beta A})^{-1}\boldsymbol{y^N} \tag{3.8}$$

We define the nodal power transfer distribution factor (PTDF) matrix as:

$$\text{Nodal PTDF} = \boldsymbol{D^N} := \boldsymbol{\beta A}(\boldsymbol{A^T\beta A})^{-1} \tag{3.9}$$

Note that these values rely solely on the grid characteristics, specifically the reactance of the transmission lines. Finally, this gives the shift factor formulation of the DC-OPF:

$$\min_{P} \quad f(x) \tag{3.10a}$$

$$\text{s.t.} \quad \sum_{g \in \mathcal{G}} P_g - \sum_{n \in \mathcal{N}} L_n = 0 \tag{3.10b}$$

$$-\overline{F_k^{inv}} \leq \sum_{n \in \mathcal{N}} D_{n,k}^N y_n^N \leq \overline{F_k^{dir}} \qquad \forall k \in \mathcal{K} \tag{3.10c}$$

$$P_g \in P_g^{OpRange} \forall g \in \mathcal{G} \tag{3.10d}$$

The shift factor formulation has the main benefit that the shift factor matrix can be calculated in advance of market or dispatch planning. As a result, it is used in the majority of operational practices. The formulation can easily be modified to include contingencies through the use of LODF (see (Goldis et al., 2017) for an explanation of this).

[8]There are also other conditions, such as the connexity of the network.

3.2.2 Zonal Shift Factor Formulation (Zonal Flow-Based)

To get to the zonal flow-based (or shift factor) formulation, it is necessary to make assumptions about the internal generation pattern. We begin by decomposing Equation 3.10b into 3 separate equations:

$$\sum_{g\in\mathcal{G}_n} P_g - L_n = y_n^N \quad \forall n \in \mathcal{N} \tag{3.11}$$

$$\sum_{n\in\mathcal{N}_z} y_n^N = y_z^Z \quad \forall z \in \mathcal{Z} \tag{3.12}$$

$$\sum_{z\in\mathcal{Z}} y_z^Z = 0 \tag{3.13}$$

and writing:

$$F_k = \sum_{n\in\mathcal{N}} D_{n,k}^N y_n^N \tag{3.14}$$

Because we will be making some additional assumptions about the internal generation pattern, we perform a Taylor expansion around an initial operating point, s_o (here on out referred to as the base case).

$$(y_z^Z)^{new} = y_z^Z\Big|_{s_0} + \sum_{n\in\mathcal{N}_z} \frac{\partial y_z^Z}{\partial y_n^N}\Big|_{s_0} \Delta y_n^N \quad \therefore \quad \Delta y_z^Z = \sum_{n\in\mathcal{N}_z} \frac{\partial y_z^Z}{\partial y_n^N} \Delta y_n^N \tag{3.15}$$

$$F_k^{new} = F_k^0 + \sum_{n\in\mathcal{N}} \frac{\partial F_k}{\partial y_n^N} \Delta y_n^N \tag{3.16}$$

Using a finite difference to approximate the partial derivative, we have:

$$\frac{\partial y_z^Z}{\partial y_n^N} \approx \frac{\Delta y_z^Z}{\Delta y_n^N} \tag{3.17}$$

This allows us to rewrite 3.15 as:

$$\Delta y_n^N = \sum_{n\in\mathcal{N}_z} \frac{\Delta y_n^N}{\Delta y_z^Z} \Delta y_z^Z \tag{3.18}$$

We define the following term as the generation shift key (GSK):

$$\text{Generation Shift Keys} := G_{n,z}^{sh} = \frac{\Delta y_n^N}{\Delta y_z^Z} \tag{3.19}$$

The GSKs are discussed in more detail in the following section, but they are one of the most important potential sources of inaccuracy.

From the Equation 3.18, we can then rewrite Equation 3.16 to give us the flow in terms of zonal net position:

$$F_k^{new} = F_k^0 + \sum_{n\in\mathcal{N}} \frac{\partial F_k}{\partial y_n^N} \frac{\partial y_n^N}{\partial y_z^Z} \Delta y_z^Z = \boldsymbol{f^0} + \boldsymbol{D^Z \Delta y_z^Z} \tag{3.20}$$

$$\text{where Zonal PTDF} := \boldsymbol{D^Z} = \sum_{n\in\mathcal{N}} \frac{\partial F_k}{\partial y_n^N} \frac{\partial y_n^N}{\partial y_z^Z} = \boldsymbol{D^N G^{sh}} \tag{3.21}$$

Finally, we can write the whole zonal shift factor OPF as:

$$\min_{P} \quad f(x) \tag{3.22a}$$

$$\text{s.t.} \quad \sum_{g \in \mathcal{G}_z} P_g - \sum_{n \in \mathcal{N}_z} L_n = y_z^Z \qquad \forall z \in \mathcal{Z} \tag{3.22b}$$

$$\sum_{z \in \mathcal{Z}} y_z^Z = 0 \tag{3.22c}$$

$$-\overline{F_k^{inv}} \leq F_k^0 + \sum_{z \in \mathcal{Z}} D_{z,k}^Z \Delta y_z^Z \leq \overline{F_k^{dir}} \qquad \forall k \in \mathcal{K} \tag{3.22d}$$

$$P_g \in P_g^{OpRange} \forall g \in \mathcal{G} \tag{3.22e}$$

As discussed in Section 2.2, the market price is the Lagrange multiplier of the balance equation. Since we now have one balance equation per zone, there is a single price per zone.

Note that the PTDFs are different if the initial topology is different as well as in each different network state considered. However, if we assume that the GSKs and the topology are relatively constant across similar forecast scenarios, these values are not subject to large effects from forecast errors. The reference flows, on the other hand, can be highly impacted by these errors.

3.2.3 Contingencies and Remedial Actions

We saw in Chapter 2 the gains from utilizing flexible transmission assets in a simple DC-OPF. However, in reality a more complex approach is generally applied, taking into account contingencies (N-k) and corresponding remedial actions. In the literature, this is a vast field, with many different methods of contingency modeling, a few of which we will demonstrate here. Figure 3.6 shows an example of the different operational phases and how they each might apply to a generic flow-based domain. The different thermal limits shown in Figure 3.6 (1-min, 10-min, 20-min) are an example of how a TSO (or ISO) might operate.[9] In reality, they may be for different temporal phases. Additionally, it is important to recall that here we are using a static model, which is somewhat limited. No dynamic impacts of applying these actions are taken into account. Additional dynamic analysis is always performed by system operators before application of these actions.

In the case shown there, we can identify three types of remedial actions:

1. **Preventive Actions (PRA)** are taken in anticipation of an outage. These consist of a single set of actions that must be consistent with the network state in N (prior to an outage) as well as the moment immediately after an outage. These would therefore already be in place in Box 1 and Box 2 of Figure 3.6.
2. **Automatic Curative Actions (aCRA)** include a set of automatic actions that are applied in a very short time period directly after an outage, as shown in Box 3 of Figure 3.6.
3. **Manual Curative Actions (mCRA)** are the actions that a system operator will undertake manually. The number of these actions is limited due to the time frame. These are represented by Box 4 of Figure 3.6.

For the purposes of this work, three different methods of contingency modeling were applied:

1. Preventive Mode
2. 2-Stage Corrective Mode
3. 3-Stage Corrective Mode

[9] These example temporal limits are taken from the RTE constraints in the CWE published data, shown in Section 3.3.2.2

In the next examples, we represent solely the line constraint part of the problem.

1 Preventive Mode

This mode optimizes two phases of operation: normal and post-contingency mode. It uses only preventive remedial actions, no curative.

$$\min \quad C(x_o) \tag{3.23a}$$

$$\text{s.t.} \quad f_0(x_o, p_o) \leq f^{max} \tag{3.23b}$$

$$f_c(x_o, p_c) \leq f^{max} \quad \forall c \in \mathcal{C} \tag{3.23c}$$

where p_o are the input parameters relating to the base case and p_c are those input parameters under a contingency (or set of contingencies), c. These parameters include fixed network topology, technical parameters of the generation, and load. The variables are contained in x_o which includes generation dispatch and status of any topological actions considered (or potentially PST tap positions or HVDC set points). Of the three models presented here, preventive mode is the most constrained since only one set of generation and topology can be applied to all contingency situations.

2 2-Stage Corrective Mode

This mode optimizes separate sets of remedial actions across normal and each post-contingency phase of operation, meaning that we now include one set of curative remedial actions.

$$\min \quad C(x_o, x_c) \tag{3.24a}$$

$$\text{s.t.} \quad f_0(x_o, p_o) \leq f^{max} \tag{3.24b}$$

$$f_c(x_o, x_c, p_c) \leq f^{max} \quad \forall c \in \mathcal{C} \tag{3.24c}$$

$$||x_o - x_c|| \leq \Delta v \tag{3.24d}$$

The variables referring to the curative remedial actions are represented by x_c. In this case, we will have a different optimal topology and dispatch for the N state and each contingency. Δv represents the maximum accepted difference of state between x_o and x_c. This could, for instance, represent a limit on the number of topological constraints performed by the operator. This type of modelization leaves out the automatic curative actions.

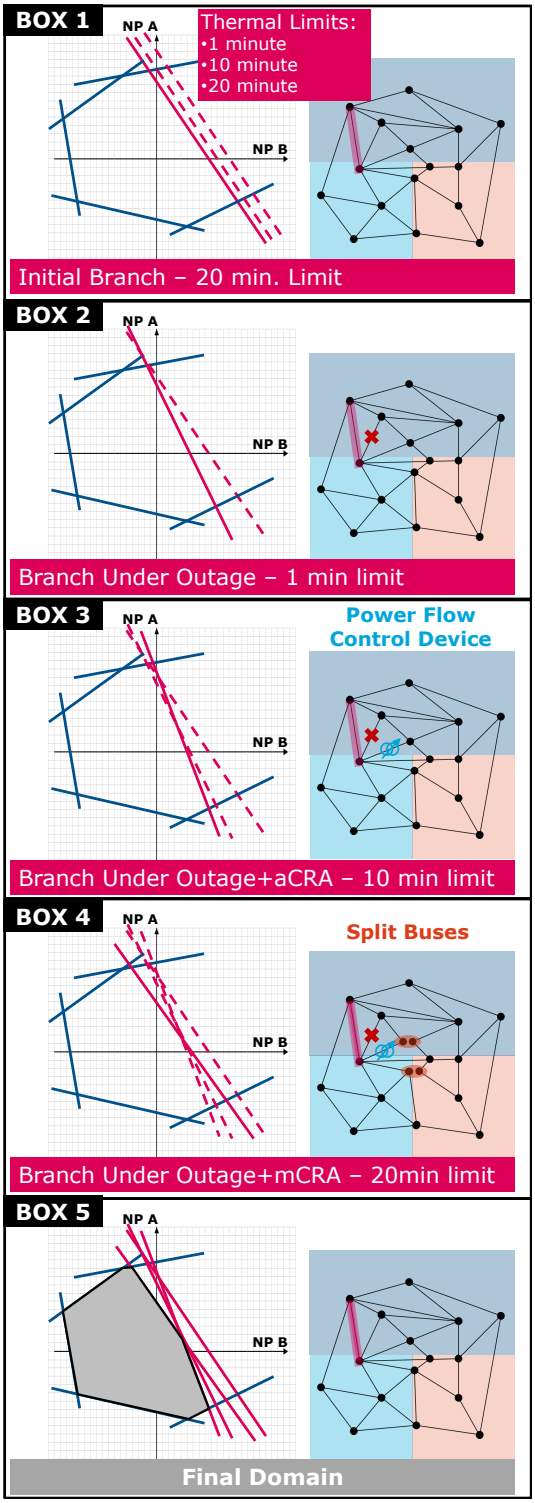

Figure 3.6: Operational Phases

3 3-Stage Corrective Mode

Finally, we have the 3-stage corrective mode which adds an intermediate operational phase, representing a higher thermal line limit which can be held for a limited period of time until some manual curative remedial actions can be put in place by the system operator. Again, we do not include automatic curative remedial actions in this modelization for simplification purposes. However, it would be possible

to add a third set of variables with a second relaxed limit to include this stage.

$$\min \quad C(\boldsymbol{x_o}, \boldsymbol{x_c}) \tag{3.25a}$$

$$\text{s.t.} \quad f_0(\boldsymbol{x_o}, p_o) \leq f^{max} \tag{3.25b}$$

$$f_c(\boldsymbol{x_o}, p_c) \leq f^{max,relaxed} \quad \forall c \in \mathcal{C} \tag{3.25c}$$

$$f_c(\boldsymbol{x_o}, \boldsymbol{x_c}, p_c) \leq f^{max} \quad \forall c \in \mathcal{C} \tag{3.25d}$$

$$||\boldsymbol{x_o} - \boldsymbol{x_c}|| \leq \Delta v \tag{3.25e}$$

In this type of modelization, there will be a single optimized dispatch and topology for N and a relaxed form of N-1 as well as an additional redispatch or topology for longer-term post-contingency operations. As above, Δv represents the maximum accepted difference of state between $\boldsymbol{x_o}$ and $\boldsymbol{x_c}$. $f^{max,relaxed}$ represents a higher constraint limit, theoretically modeling a higher thermal line limit that can be held for a limited amount of time.

The 3 modeling modes shown here are simplifications of reality as they do not represent all the thermal limits shown in the boxes. In preventive and 2-stage corrective, we only use the most constraining thermal limit, the 20-minute thermal limit. 3-stage corrective adds an additional limit, represented by $\widetilde{f_o}^{max,relaxed}$.

Box 1 represents the base case (or N) situation (with preventive actions already in place), and the Equations 3.23b, 3.24b and 3.25b. Box 2 is the situation immediately after an outage, before the system operator has a chance to implement any remedial actions. The state shown in Box 2 is modeled in 3-stage corrective mode by Equation 3.25c and in preventive mode by Equation 3.23c, although in this case we only use a single thermal limit, which is the most constraining thermal limit (20-min). Box 3 represents the state after the usage of automatic curative remedial actions. Box 4 is after additional remedial actions, a limited number of manual actions performed by the system operator to stabilize the system.

Each of these different limits is represented by a different flow-based constraint. Box 5 shows the resulting flow-based domain. In reality, different TSOs apply the rules in slightly different methods. Since the flow-based model is a proxy for full network modelization, TSOs have different balances of internalizing their own constraints or explicitly including them in the flow-based domain. The next section describes the reality of the application of the method in operation.

3.3 Operational Practices

As described in previous sections, the network code CACM (Capacity Allocation and Congestion Management) introduces the flow-based method as the reference method for the short-term cross-border capacity management across highly-meshed zones. The zonal flow-based method was initially put into place for the day ahead allocation in the CWE region in 2015. The decision—announced in November 2016 by ACER (Acency for the Cooperation of Energy Regulators)—to expand this approach to the entire CORE zone (combine zone of CWE and CEE) marked the first step of this generalization. After an extended parallel run phase, the Go Live for the CORE region occurred on June 8, 2022. The flow-based method is undergoing the external parallel run phase in the Nordic capacity calculation region as well, with an expected Go Live near the end of 2022.

In practice, there are many issues that add complexity to the flow-based capacity calculation (or indeed any capacity calculation taking into account the effects of contingencies, a variety of uses of remedial actions, different regional methodologies, and at such a large scale). Some of these will be

addressed in this section. The inputs to the calculation – and the variety of approaches to these[10] – are addressed in Section 3.3.2. The process itself is detailed in Section 3.3.3. The process and inputs have both changed significantly between the original CWE region and the CORE region. Both models will be referenced in the following sections.

3.3.1 Flow-based Calculation - In Operational Terms

Figure 3.7 shows a basic version of the operational process in the context of the current European day ahead market.

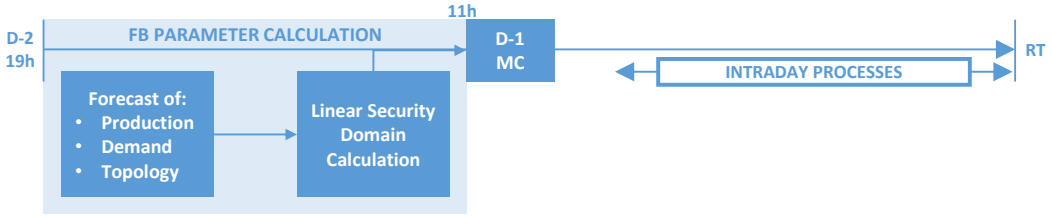

Figure 3.7: Basic Flow-based Process

Beginning two days before delivery, hereafter referred to as D-2, each TSO submits a forecast, estimating the real time load, grid topology and generation—both renewable and conventional – with agreed upon export/import positions. The different forecasts are then merged into a single vision of the entire flow-based region, known as the Common Grid Model. This is a node-level forecast which is then used to calculate the flow-based parameters that define the constraints applied during the market clearing.

In this section, we will redefine some of the formulas from the previous section in the operationally-used terms for clarity. For instance, in the market clearing, Equation 3.22d becomes:

$$\forall l \in CNECRA : \sum_{z \in Z} D^{Z}_{z,l} * NP_z \leq RAM_l \tag{3.26}$$

In these equations, CNECRA is the set of Critical Network Elements, considered under a set of Contingencies (N-1) with a set of preventive and curative Remedial Actions associated.[11] This list can only include network elements impacted significantly by cross-border flows. As a reminder, at the scale of the European power network, including all branch and outage constraints would often leave an empty domain of possible exchanges due to nonrepresented remedial actions (especially on voltage levels below 400 kV). Z is the set of bidding zones included in the flow-based market clearing, NP is the net position—the net import or export—of each respective zone, and D^{l}_{z} is the zonal Power Transfer Distribution Factor (PTDF), or the sensitivity of the flow on the specific network element to an increase in the zonal net position. Finally RAM is the Remaining Available Margin, the margin of capacity that remains to be allocated during the day ahead market clearing on each critical network element. Note that the variable in the equation has changed from ΔNP_z to NP_z. This is due to the fact that the reference program of the base case (the zonal net position in the base case) is included in the RAM.

We can write:

$$\Delta NP_z = NP_z - NP^{ref}_z \tag{3.27}$$

[10] Although, it is notable that there has been a huge effort of harmonization and increased transparency in the new CORE methodology, compared to the original CWE method.

[11] This is different for the CORE implementation.

The NP_z^{ref} is then encompassed in the RAM on the right hand side of Equation 3.26. There are a few other values included in the RAM (and more specifically into the term $F_l^{ref'}$), shown in Fig. 3.8. These will be explained fully in this section.

$$RAM_l = F_l^{max} - F_l^{ref'} - FAV_l - FRM_l \tag{3.28}$$

$$\text{where } F_l^{ref'} = F_l^{ref} + \sum_{z \in Z} D_{z,l}^{Z} (NP_z^{LTN} - NP_z^{ref}) \tag{3.29}$$

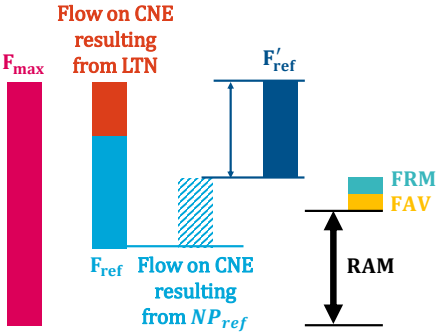

Figure 3.8: Calculation of the Remaining Available Margin (RAM)

F_l^{ref} is the flow on the network element found in the forecast described at the beginning of this section (and calculated by a full load flow). The forecast net positions (often referred to as the reference program or RefProg) result from the sum of pre-day ahead, day ahead and intraday forecast exchanges. Once the actual pre-day ahead exchanges are known (nomination of long-term rights), it is necessary to allow the market clearing algorithm to allocate only the capacity that remains. We therefore compute adapted Reference flows, $F_l^{ref'}$, by subtracting the effect of the reference program and adding the effect of the nominated exchanges (linear adaptation performed by using the PTDF factors). This corresponds to the translation of ΔNP_z to NP_z. Additional TSO-defined parameters such as the Flow Reliability Margin (FRM) and the Final Adjustment Value (FAV) deal with a variety of uncertainties. These will be discussed further in Sections 3.3.2.4 and 3.3.2.5 respectively.

Initially the nodal PTDFs are calculated using a DC load flow[12] or the matricial multiplication showed above:

$$D_{l,n}^{N} = \frac{\partial F_l}{\partial NP_n} \approx \frac{\Delta F_l}{\Delta NP_n} \tag{3.30}$$

As described in Section 3.2.1, these represent the change in the flow on a line due to a unit change in nodal net position. Next, the Generation Shift Keys, G^{sh}, are calculated. These parameters map how a change in zonal net position translates to each node of the grid. The actual method for calculating these varies widely between TSOs and is assessed further in Section 3.3.2.3. In general they take a subset of the production plants in the zone, often referred to as the "market-driven" plants; in other words, those plants that will change production based on the market clearing. For the majority of TSOs, this means that nuclear and renewables are excluded.

$$G_{sh_z} = \frac{\partial NP_n}{\partial NP_z} \approx \frac{\Delta NP_n}{\Delta NP_z} \tag{3.31}$$

The GSKs, covered in more depth in Section 3.3.2.3, are one of the main sources of approximation in the model. Realistically, the generation will change non-linearly in each zone, so this representation

[12]Note that for the Nordic region, this is to be an AC load flow (Energinet et al., 2015).

is quite a simplification. Merit order GSKs, for instance, cannot be used in the flow-based method. The assumptions in the GSKs are covered by the Flow Reliability Margin (FRM), discussed in Section 3.3.2.4.

As shown in Section 3.2.2, the zonal PTDF can be calculated from Equations 3.30 and 3.31.

$$\text{Zonal PTDF} = \boldsymbol{D^Z} = \boldsymbol{D^N G^{sh}} \tag{3.32}$$

The full flow-based constraint is therefore:

$$\forall l \in CNECRA: \sum_{z \in Z} D^Z_{z,l} * NP_z \leq RAM_l \tag{3.33}$$

or, if expanded with the definitions from above:

$$\forall l \in CNECRA: \tag{3.34}$$

$$\sum_{z \in Z} D^Z_{z,l} * NP_z \leq F^{max}_l - (F^{ref}_l + \sum_{z \in Z} D^Z_{z,l}(NP^{LTN}_z - NP^{ref}_z)) - FAV_l - FRM_l \tag{3.35}$$

3.3.2 Inputs

The official terms for the method involve a somewhat overwhelming number of acronyms, which have changed several times during even just the duratiConclusionon of this thesis work. In this section, the official CORE terms are referenced, although we aim to include the terms used in past documents (e.g. CWE) as well as the new terms and their corresponding meanings. The full list of terms is not comprehensive, but the official CORE documentation includes a glossary for all terms (TSOs, 2018a).

To illustrate several of the inputs and operational particularities, we look at the published data for a sampling of 10 dates over the course of approximately a year for the CWE region.

3.3.2.1 Two Day Ahead Individual/Common Grid Models (D-2 IGM/CGM)

Previously 2-Days Ahead Congestion Forecast (D2CF)

Initially, the TSOs coordinate to agree upon a set of net positions in order that the overall zone will be balanced. It is not clear how this reference program is determined in CORE. According to the CWE Flow Factor Study (Hagedorn, 2017c) (Hagedorn, 2017a) (Hagedorn, 2017b), the reference program was determined using historical days, following the following calendar:

- "*for Tuesday to Friday: D-1 (most recent program)*
- *for Monday: D-3 (previous Friday)*
- *For Saturday and Sunday: D-7 (previous week)*
- *For bank holidays and specific outages, a reference day is determined and fixed in a separate calendar approved by all CWE TSOs.*"[13]

It is likely the process in CORE follows a similar pattern. Once the reference program is determined, each TSO will generate its own forecast of the expected situation in real time and respecting the prescribed zonal balance. Each TSO separately generates an individual grid model (IGM) that represents their best guess for the nodal production and load in real time.

According to the GSK Monitoring Study (CWE TSOs, 2022), in the CWE region, there were two types of calculations for the D-2 IGM: 1) the "best forecast approach" and 2) the "RefProg" approach. The

[13](Hagedorn, 2017b)

former is not described in much detail, but is used by the German TSOs, the Austrian TSO (APG), and the Netherlands TSO (TenneT NL). The method is described as:

> *"using the best possible forecast of the system state at D-2. This includes the latest available topology including planned outages for the dedicated business day, the best forecast of renewables and power plant schedules as well as a load forecast.*[14]

APG, TransnetBW and TenneT DE have an additional specification in that they do not generate their own forecast of production plans, but rather use a forecast generated directly by power plant operators, combined with their own load and topology forecast.

The second method is used by Elia and RTE. Both shift their initial forecast using the calculated GSKs (described below). However, there remain many details of the calculation of these base cases that are not transparent. In any case, all TSOs must comply with the commonly agreed set of zonal balances in order for the overall system to be balanced, which means that, depending on their internal D-2 IGM process, they may have to equalize the situation (based on nodal load or generation updates.

From a theoretical point of view, having a base case close to the market outcome is ideal. (Felten et al., 2021) among others, identify that, "the better the D-2 forecasts of TSOs become, the higher is the expected cost-effectiveness in the CWE electricity markets." Indeed, the confidence range of a flow-based domain is determined by the base case forecasts, as described by (Audouin, 2002) in one of the first works developing the flow-based model in the literature. This comes from the fact that the flow-based method (and any linearization-based method) is a bit of a circular problem: to have a good linear representation of an inherently non-linear phenomenon, one needs to start from a point close to the output. If the base case is too far from the market outcome, the grid constraints may be less representative.

3.3.2.2 Critical Network Element and Contingency (CNEC)

Previously Critical Branch, Critical Outage, CBCO, also previously associated with specific remedial actions, CBCORA)

Prior to the CORE methodology which includes an explicit remedial action optimization, TSOs assigned remedial actions to specific network elements. This has changed with the addition of the remedial action optimization stage (see Section 3.3.2.7) in the CORE implementation.

The term *Critical Branch* was changed to *Critical Network Element* to clarify the fact that transformers or other network elements besides lines could be considered as well. *Critical Outage* turned into *Contingency*, again to broaden the sense. The definition remains the same as the original definition and includes the

- *"Trip of a line, cable, or transformer,*
- *Trip of a busbar,*
- *Trip of a generating unit,*
- *Trip of a (significant) load,*
- *Trip of several elements."*[15]

Each critical branch is considered under a subset of the contingencies specified above, as well as certain other conditions, depending on the TSO. For instance, as described in Figure 3.6, RTE considers

[14](CWE TSOs, 2022)

[15]*Documentation of the CWE FB MC solution As basis for the formal approval-request*. May 9 2014.

most branches with 3 different thermal limits corresponding to the amount of time that each branch can endure at each limit: a 1-minute thermal limit, a 10-minute thermal limit and a 20-minute (or permanent) thermal limit. In the CWE region, this allowed for the consideration of specific remedial actions. The 1-minute thermal limit is the highest value, and no remedial actions can be performed in this time. The 10-minute limit allows already for the activation of certain automatic remedial actions and the 20-minute allows for a certain number of manual remedial actions. Table 3.2 shows an example of this from the CWE data published for October 6, 2021.

Critical Branch Name	Outage Name	RAM [MW]	Fmax [MW]	Fref [MW]
Revigny - Vigy 1 [OPP] - 1′	Faux Fresnay - Mery sur Seine 1 [DIR]	1755	2238	293
Revigny - Vigy 1 [OPP] - 10′	Faux Fresnay - Mery sur Seine 1 [DIR]	1467	1950	293
Revigny - Vigy 1 [OPP] - 20′	Faux Fresnay - Mery sur Seine 1 [DIR]	1274	1678	214

Table 3.2: Example of a French CNEC in the CWE region on October 6, 2021[16]

This network element (Revigny - Vigy 1), considered under a single outage (Faux Fresnay - Mery sur Seine 1) has a maximum flow, based on the three different thermal limits as discussed in the previous paragraph. Looking at the reference flow (Fref) column, we can see that there are some manual remedial actions considered that would be activated in a curative manner, changing the flow seen on this line.

Looking at a specific day of data (2021.11.03), we can see the number of CNECs varies by TSO. Interestingly, even the number of CNEC by TSO varies hourly, often following a peak/off-peak pattern. This can be seen in Figure 3.9 and in Figure 3.10, which shows a zoomed in view of the TSOs with fewer CNECs. Note that this particular graphic does not include the branches added during the LTA inclusion phase (see Section 3.3.3.4). These are shown in Appendix E.

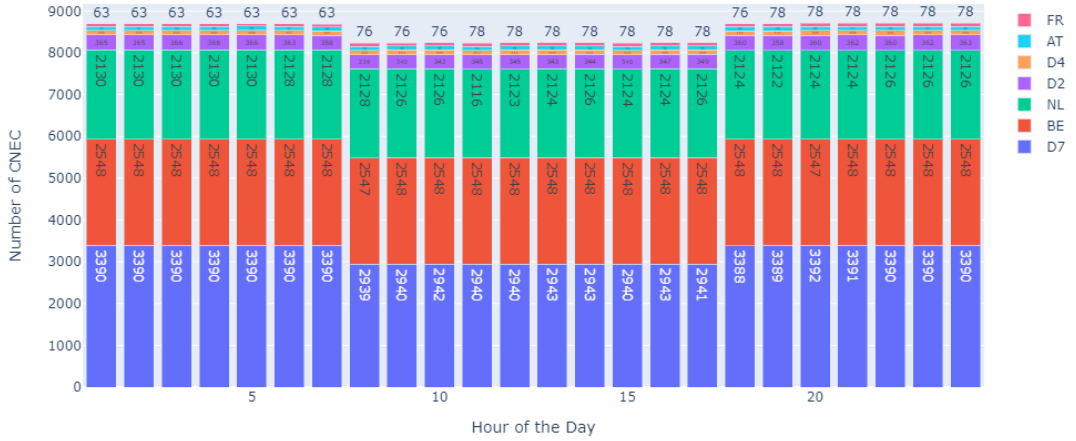

Figure 3.9: Hourly Variations of number of CNEC by TSO

3.3.2.3 Generation (or Load) Shift Keys (GSKs or LSKs)

The generation shift keys are crucial to the final quality (see Section 4.1 for a discussion on the quality of a domain) of the flow-based domain. Currently these key parameters are generated largely through TSO experience. The different methods used by the German and Austrian TSOs are detailed in (amprion et al., 2015) and a more general description of the accepted methods can be found in (ENTSO-E, 2016). They have been analyzed quite a bit in the literature. Many articles comparing

[16] Data available through the JAO utility tool at https://www.jao.eu/implict-allocation.

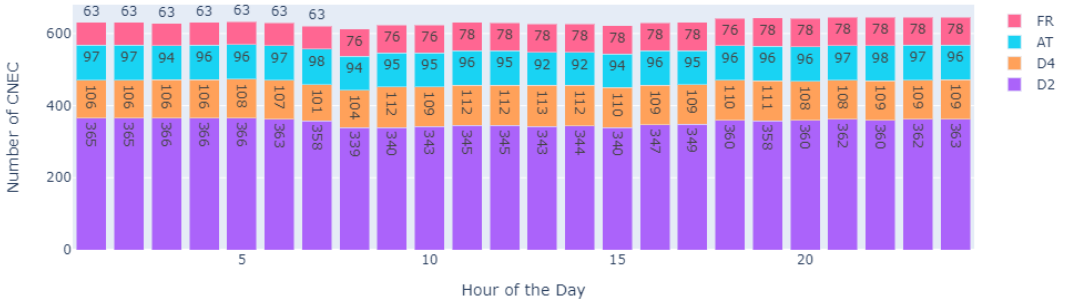

Figure 3.10: Hourly Variations of number of CNEC by TSO - Zoomed to TSOs with Less CNEC

different GSK methods land on the somewhat unsatisfying conclusion that there is no universal "best" GSK (Dierstein, 2017) (Schönheit et al., 2020) and that it depends highly on the generation dispatch, which evidently varies. Others looks at other ways to calculate these factors, for example with statistical models (Sebestyén et al., 2018).

It is important to remember that because GSKs are based on the P_{NP} (see Equation 3.19), they include assumptions about both the generation and the load at the specified node. The key to choosing a representative GSK varies on the network. The GSKs represent how the internal generation pattern will change in the market (compared to the forecast base case). Because of this, in practice they almost always represent a change in generation, ignoring the load aspect (the assumption being that the forecast load is closer to the market demand and that demand response is limited). However, load shift keys (LSKs) or GSK-LSK combinations are technically permitted (ENTSO-E, 2016) and could be useful under certain conditions. It may even be possible to envision negative GSKs in certain cases, which possible as long as the sum of all GSKs in a zone is 1.

The GSK method chosen by each TSO can vary along several axes, notably:

1. The selection of nodes to include in the shift key list
2. The calculation method
3. The temporal resolution

Although full information on the GSK methods chosen by each TSO remains somewhat unclear, by cross-referencing several studies, we can get some idea of the choices made by the CORE TSOs.

1 Selection of Nodes
In general, all TSOs aim to include "market-driven plants" in the GSK selection. How this is actually interpreted for each TSO is a bit less clear. In (CWE TSOs, 2022) and (TSOs, 2018b), we find a few specifications. For instance, Amprion specifies that they include "middle and peak load power plants" which included "hard coal, gas and hydro" up until 2019 when they removed hydro power plants from the list. RTE specifies "all flexible and controllable production units connected to RTE's network in D-2 CGM." None of the TSOs currently include nodes representing load centers with the exception of one specific use. SEPS (Slovakian TSO), ELES (Slovenian TSO) and HOPS (Croatian TSO) include some nodes with only load, but only in order to represent generation located at lower voltage levels.

2 Calculation Method
The general format of the calculations is:

$$\frac{\chi^{unit}}{\sum_{unit \in Units_z} \chi^{unit}} \tag{3.36}$$

where χ^{unit} represents the value referred to in Tables 3.3.2.3 and 3.4 and the unit can either be a generation or load unit.

Table 3.3. GSK Classification by TSO[18].

Country	TSO	GSK Method
Austria	APG	P_{max}
Belgium	Elia	$P_{max} - P_{min}$
Croatia	HOPS	N
Czech Republic	CEPS	P_g
Netherlands	TenneT TSO B.V.	$P_{max} - P_{min}$ †
France	RTE	P_g
Germany	50Hertz	Statistical ‡
	Amprion	$P_{max} - P_{min}$
	TenneT Germany	$P_{max} - P_{min}$
	TransnetBW	$P_{max} - P_{min}$
Hungary	MAVIR	P_g
Poland	PSE	P_g
Romania	Transelectrica	P_g
Slovakia	SEPS	N
Slovenia	ELES	Statistical ‡

†The maximum and minimum values are in fact the participation of the generator in a maximum export and maximum import scenario, respectively.

‡It is not fully clear what model is used. Likely it is similar to the process described here (Schonheit and Sikora, 2018).

Note that while the German TSOs each have their own individual method for GSK calculation, they are merged into a single-country vision using the TSO market share before entering the flow-based process. This is detailed in (CWE TSOs, 2022) and (amprion et al., 2015).

The Nordic region has declared 9 possible GSK strategies that TSOs can choose from, shown below in Table 3.4.

3 Temporal Resolution
Since the GSKs are not published, the temporal resolution chosen by the TSOs in CORE is difficult to assess. However, there seem to be three main strategies:

1. Constant
2. Peak and Off-Peak
3. Hourly

The documentation for the CWE flow-based process (amprion, 2020) specifies:

- *"APG, Elia and TTB use GSKs according to their GSK concept, which means constant values over the day.*
- *The German TSOs have two GSKs for two different periods of a day as described above (peak, off-peak).*

[18]Information taken from (CWE TSOs, 2022), (TSOs, 2018b), (Hagedorn, 2017b), (Hagedorn, 2017a), (CWE TSOs, 2015) and (amprion et al., 2015).
[19]The data here comes from (Energinet et al., 2015)

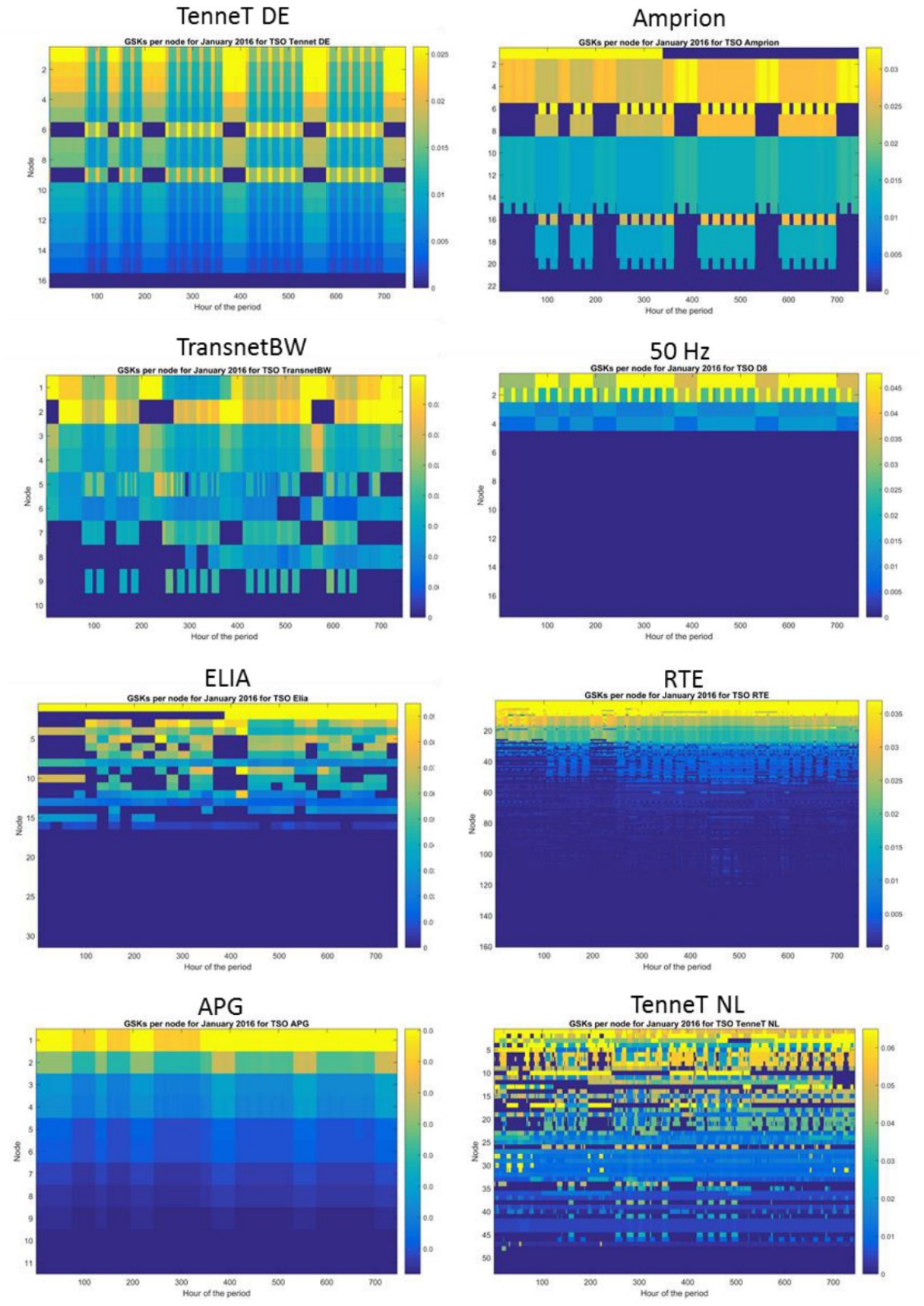

Figure 3.11: Geographic and Temporal Differences by TSO from (Hagedorn, 2017a)

Generation	Load	Description
k_g	k_l	Custom factors determined by operator experience
$max(P_g - P_{min}, 0)$	0	Relative to the generator's capacity to lower its production
$max(P_{max} - P_g, 0)$	0	Relative to the generator's capacity to increase its production
P_{max}	0	Relative to generator's maximum installed capacity
1	0	Equal factors for all generators
P_g	0	Relative to generator's production in the basecase
P_g	P_d	Generators and load participate according to their basecase productiondemand
0	P_d	Load participates according to basecase demand
0	1	Equal factors for all load

Table 3.4: GSK Calculation Methods - Nordic Region[19]

- *Since RTE is using pro-rata GSK, the values in the French GSK file change every hour.*

The CWE Flow Factor Competition Study (Hagedorn, 2017a) shows some of the geographical and temporal variations of the different TSO methods (Figure 3.11).

In April 2022, the final version of CWE GSK Monitoring Study (CWE TSOs, 2022) was published analyzing the choices of the different CWE TSOs. The study is notable as it performs analysis of the actual system data, although in the published version, branches, generators and nodes are anonymized or hidden for several TSOs. The study focuses on comparisons between net positions calculated at different points of the day. There are several different comparisons meant to identify errors at different phases of the process, from the beginning of the flow-based process to the day ahead dispatch and even to the real time dispatch.

Most of the conclusions of the study are relatively straightforward: GSKs at nuclear plants have low forecast error; the highest forecast error occurs at nodes with high levels of renewable generation – which are generally not accounted for in GSK methods – or at nodes with pumped hydro – which is particularly variable in close to real time markets and reserves. Some TSOs were found to be more successful than others in their chosen combination of forecast method and GSK.

3.3.2.4 Flow Reliability Margin (FRM)

The flow reliability margin, FRM, is a term used to cover the potential forecast errors between the beginning of the flow-based calculation two days before real time and the real time flows. In the CWE region, the goal of the FRM is specifically to cover risks from:

1. "Unintentional flow deviations due to operation of load-frequency controls
2. External trade (both trades between CWE and other regions, as well as trades in other regions without CWE being involved)
3. Internal trade in each bidding area (i.e. working point of the linear model)

4. Uncertainty in wind generation forecast
5. Uncertainty in Load forecast
6. Uncertainty in Generation pattern
7. Assumptions inherent in the Generation Shift Key (GSK)
8. Topology
9. Application of a linear grid model"[20]

It is notable that in the CORE documentation, item number 3 is not included in the definition of the FRM. The process is somewhat more defined and leaves less discretion to the TSOs. In fact, the calculation of the FRM for CORE is performed by the coordinated capacity calculator, and not separately by each TSO.

According to the CORE documentation (TSOs, 2018a) (TSOs, 2018b), the FRMs are calculated in three stages from historical data:

First, the "expected flows" are calculated by modifying the D-2 CGM with the remedial actions chosen by TSOs, recomputing the reference flows[21] and adjusting this flow to the commercial exchanges that were realized in real time using the PTDFs.

$$\forall l \in CNEC, \forall z \in \mathbb{Z}$$
$$f_l^{exp} = f_l^{ref} + D_{l,z}^{Z}(NP_z^{real} - NP_z^{ref}) \tag{3.37}$$

Second, the 90th percentiles of the probability distributions of the error between the expected flow and the actual flow values are calculated. This can be done for each CNEC (set of line and contingency) or for just the base case (set of lines without any contingency). Among the 15 CORE TSOs, ELES, Elia, CREOS, HOPS and RTE apply the second case, implying that for every network element considered, there is a single FRM value for every contingency case. As described in (TSOs, 2018b), the ability to choose between those two options is permitted "in order to let Core TSOs have an option to reflect their attitude towards risk acceptance". In other words, the choice between the two options allows TSOs to determine how they deal with contingencies in their own zone. The third step of the calculation is an optional reduction of the calculated FRM values under normal weather conditions. This introduces a somewhat odd inconsistency with the fact the FRMs are supposed to be considered constant over time.

One difficulty with the calculation of the FRM is a basic lack of data. For zones that are not in the CWE region, there is no statistical data to use in order to calculate the necessary FRM values. For those zones, a temporary value of 10% of the maximum line limit will be used for the first two and a half years after the go-live.

The FRMs are deemed not to vary temporally and are calculated on a yearly basis (mid-year updates can occur if new lines are added). This method seems somewhat problematic at first glance as a yearly value can not capture any variations in forecast error due to seasonal effect, peak vs. off-peak, week vs. weekend, etc. The issue with adding temporally variable FRMs is purely a data issue. In order to have a large enough sample size for seasonal (or more fine-grained temporal resolution), the analysis would have to include more than one historical year of data. Due to the evolution of the transmission grid over time, previous years' flows may have little relevance to the current grid situation and therefore would negatively impact the statistical relevance of the FRM.

[20](amprion, 2020)

[21]Note that since the topology may change with remedial actions, the PTDFs should be recalculated at this step, but it is unclear if this is done in practice.

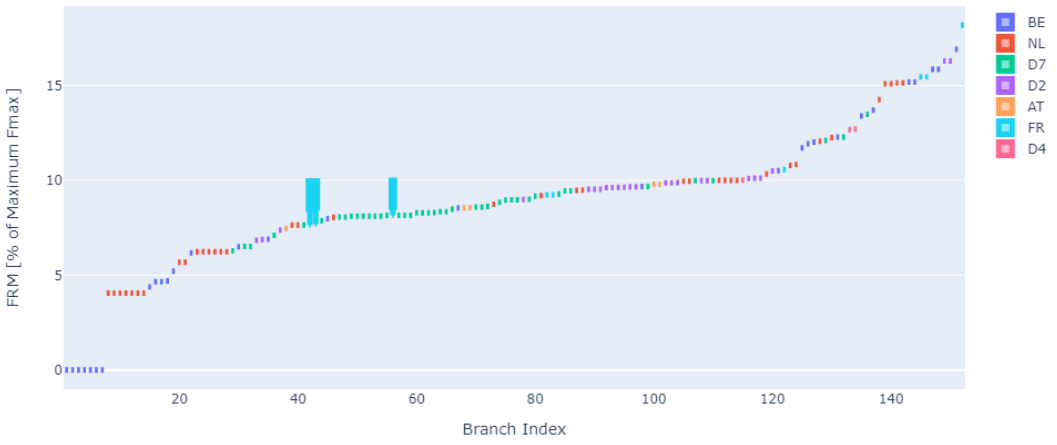

Figure 3.12: FRM Values for a sampling of 10 dates in CWE

Figure 3.12 shows the values of FRMs for branches in CWE as a percentage of their maximum Fmax[22]. The values over the past year range between 0 and 20% of the maximum flow limit. There are only three branches with an FRM that varies across the sampled days, shown in Figure 3.13. In fact, they are all linked to a single network element, defined for three separate thermal limits. In practice, only one of these will be constraining.

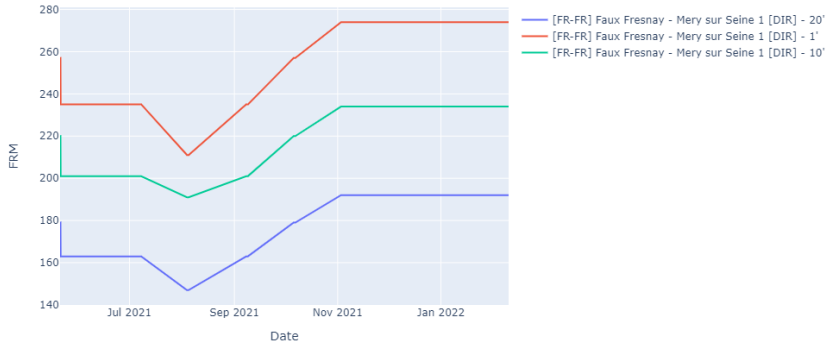

Figure 3.13: Variable FRM over time - CWE Data

3.3.2.5 Final Adjustment Value (FAV)

This term is used by TSOs to increase or decrease slightly the RAM on a CNEC. This parameter can only be applied in exceptional circumstances and must be comprehensively explained to regulatory authorities. It can be used in the case of 1) an exceptional contingency or outage, 2) to represent remedial actions that are not taken into account correctly during the remedial action optimization phase, 3) data errors that result in overestimations of cross-zonal capacity, and 4) to cover reactive power flows on certain highly-influenced network elements.

For the ten sampled days of the CWE data, the FAV was zero for every branch.

[22]The maximum Fmax is used since the Fmax changes over time for many lines.

3.3.2.6 External Constraints (ECs)

Similar to the process of introduction of the FAV, the external constraints are additional allocation constraints that can be added by TSOs to deal with certain limitations of the flow-based method. External constraints come in the form of a limit on either the net position of a specific bidding zone or a limit on the total CORE net position (which is not always set to zero, due to commercial exchanges with the areas outside CORE, e.g. Italy). Currently, three external constraints have been permitted by the regulatory authorities.

1 Stability Issues
Firstly, ELIA and TenneT B.V. are allowed to include external constraints in order to avoid stability problems. Since the flow-based is based on a DC load flow, frequency, voltage and dynamic stability issues are somewhat ignored. While for the most part, the error arising from the DC approximation remains negligible, some cases require special consideration and the external constraint is added to account for these constraints. The values for these constraints are based on offline studies that are updated on at least a yearly basis. These external constraints were applied in CWE region as well. Elia imposes a maximum import limit in order to ensure sufficient generation on their own grid to avoid voltage collapse and transient phenomena. In the CWE data from 2021, we can see the TenneT NL limits. There is an upper limit of 6500 MW that applies every day from 8 am until midnight and a lower limit of 5750 MW that applies until 7 am. There are also external constraints that represent the limits of ALEGrO (see Section 4.2.2.1), 1000 MW in each direction. Figure 3.14 shows these external constraints for the last year. [23]

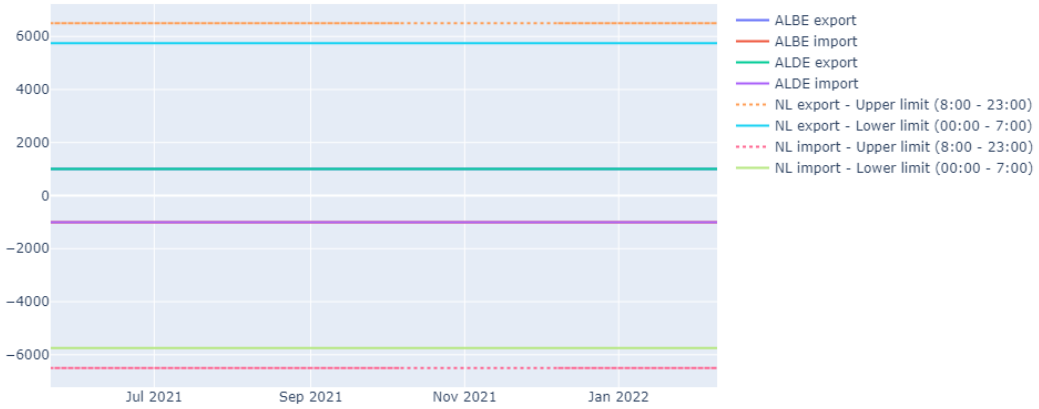

Figure 3.14: External Constraints for CWE

2 Extreme Forecast Errors in GSKs
The second case of external constraints deals with situations that are too far away from the forecast reference flows to be validated in the later stages. This type of constraint is applied to account for the errors resulting from linearized GSKs. Only TenneT B.V. (Netherlands TSO) can currently

[23] A master thesis completed in 2015 in a partnership between TU Delft and Tennet B.V. analyzes specifically a translation from voltage stability constraint values (primarily relating to the first case of external constraint justification) to net position limitations, and ultimately proposes scenario-based external constraints (or even more advanced considerations) to fully allow for secure operation while allowing for increased exchanges (van Leeuwen, 2015).

apply this type of external constraint with an interesting rationale. Their GSKs are tuned in a way as to avoid "extensive and not realistic under- and overloading of the units for foreseen extreme import or export scenarios" (CWE TSOs, 2022). Essentially, they impose limits that relate to the minimum and maximum power available in a set of "swing" generators. If the net position were to vary outside of this range, there would be a significant reduction in the accuracy of the flow on their CNECs. They rationalize the exclusive use of this type of constraint through the ratio of their interconnection capacity and total installed capacity; with a high interconnection capacity compared to their total installed capacity, they have limited flexible generation capacity to cover a rather large feasible region. A calculation of the increase uncertainty introduce by the linear GSKs is performed in parallel with the voltage collapse and stability analyses, and both sources of information are used to justify the values given for the external constraints.

3 Central Dispatch
Finally, PSE (the Polish TSO) is permitted to define bi-directional external constraints in order to ensure sufficient line flow capacity for balancing. They have this exception due to their central dispatch model.

3.3.2.7 Remedial Actions

The handling of remedial actions is one of the biggest differences between the CWE Flow-based process and the CORE process. In the CWE process, the remedial actions were associated to critical network elements. There was no explicit remedial action optimization phase and little coordination between TSOs. The CORE process added an explicit remedial action optimization phase.[24]

Figure 3.15 shows the remedial actions given by each TSO in the CORE parallel run.[25] Note that this does not mean that these will be chosen during the remedial action optimization phase described in Section 3.3.3.3.

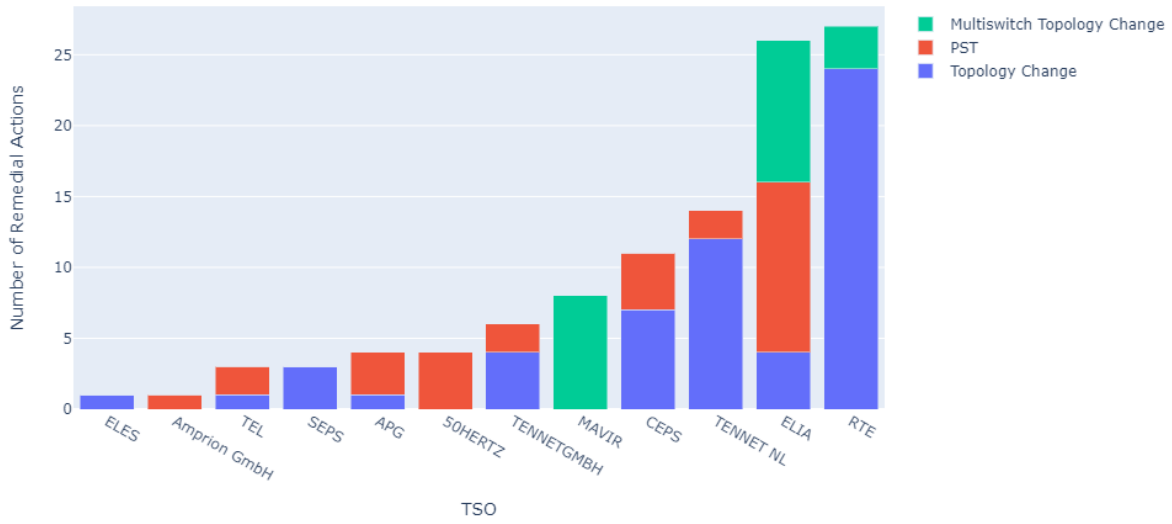

Figure 3.15: Remedial Actions by TSO in CORE Static Grid Models

[24]The documentation for this phase is described here: https://farao-community.github.io/docs/. This step will be discussed in a bit more detail in the next chapter, in Section 4.2.2.3
[25]The data is accessible at https://www.jao.eu/static-grid-model

3.3.3 Process (in the CORE region)

One of the main goals of this work is to explicit the operational complexities that surround the capacity calculation methods. The following section describes in detail the process applied to the CORE region. Much of the process remains the same as that applied to CWE. However, there are several differences that will mentioned, notably the inclusion of a common remedial action optimization.

In the official publications of the CORE day ahead capacity calculation method, the process is separated into seven distinct stages, described in the following seven subsections:

1. Initial Flow-based Computation
2. Determination of Relevant CNECs
3. Remedial Action Optimization
4. Intermediate Flow-based Computation
5. Capacity Validation
6. Pre-Final Flow-based Calculation
7. Final Flow-based Computation

3.3.3.1 Initial Flow-based Calculation

For the initial calculation, each TSO provides their list of branches of CNEC (see Section 3.3.2.2 for definition) that may be significantly impacted by either cross-border exchanges or by the remedial actions that will be chosen in the third step.

The calculation of the F_{max} is based on the standard pi-model for transmission networks:

$$F_{max} = \sqrt{3} I_{max} U cos\varphi \tag{3.38}$$

The I_{max} can vary per market time unit to incorporate Dynamic Line Rating (DLR). The I_{max} can also represent a temporary line limit, i.e. a thermal limit that is permittable for a specific time period. Each TSO has their own temporal distinctions for thermal line limits. In the CWE flow-based implementation, these different line limits can be seen explicitly. Table 3.2 shows a small extract of the CWE data published by JAO, where we can see that for this French line, there are 3 different thermal line limits: a one-minute limit, a ten-minute limit and a 20-minute (or permament) line limit.

Looking at the data from CWE, it appears that several TSOs already use DLR. Figure E.1 shows the strategies applied by each TSO for the Fmax of their lines. From this figure it seems the two of the German TSOs and the Netherlands already use DLR on several branches. In the 10 sampled days, the variation on these lines ranges between 20 and 200 MW, which is a significant change. While Transet seems to maintain steady daily Fmax values, some of their branches do change over time. RTE, Elia and APG have daily variations according to other criteria. APG, for instance seems to have Fmax values that are higher at night than during the day.

We can also note one other data anomaly in Figure E.1. Several of the lines of the Belgian TSO have extremely high values of Fmax. Excluding a potential data error, this can occur for a variety of reasons. For instance, if a TSO thinks that they have a remedial action that is sufficient to render a branch non constraining, but will not be properly modeled, they may multiply the branch by a sufficient margin to "push" it out of the flow-based domain.

3.3.3.2 Determination of Relevant CNECs

The CNECs initially determined by the TSOs are separated into two groups: 1) those whose flow is heavily impacted by cross-border exchanges and 2) those who are impacted by remedial actions to be chosen in the next phase. Those in the first group are determined by calculating the maximum zone-to-zone PTDF.

The first group is chosen based on a sensitivity criteria of 5%. Note that this sensitivity refers to the **zone-to-zone** PTDFs, and not the **zone-to-slack** PTDFs. It is calculated with the following formula:

$$\forall l \in CNEC:$$

$$Sensitivity_l = \max_z(D^Z_{z,l}) - \min_z(D^Z_{z,l}) \tag{3.39}$$

Note that this is mathematically equivalent to taking the maximum zone-to-zone PTDF.

The second group is chosen based on TSO experience. These network elements are not allowed to limit the cross-zonal capacity; they are only "monitored" during the process. This means that they can not constrain the market clearing result, but they are included in the remedial action optimization phase described in the following section.

3.3.3.3 Remedial Action Optimization

The Remedial Action Optimization (RAO) phase of the flow-based process "consists of a coordinated optimization of cross-zonal capacity within the Core CCR by means of securing and enlarging the flow-based domain in the foreseen operating point of the grid." (TSOs, 2018a). The optimization problem currently described in the documentation is:

$$\max \quad \min_l\left(\frac{RAM_l}{\sum_{(A,B)\in connectedBZs}|D_l^{A\to B}|}\right) \tag{3.40a}$$

$$\text{s.t.} \quad \text{Flow-based Line Flow Constraints} \tag{3.40b}$$

$$\text{PST Tap Ranges} \tag{3.40c}$$

$$\text{Curative Action Limit} \tag{3.40d}$$

$$\text{Maximum Additional Loading of Monitored CNEC} \tag{3.40e}$$

The final constraint, 3.40e, is applied to several network elements – deemed *monitored* – that are included in the constraints, to ensure they are not overloaded by the remedial actions chosen. However, they are not included in the objective function, nor in the flow-based domain.

3.3.3.4 Intermediate Flow-based Computation

This second flow-based parameter calculation takes into account the remedial actions that were chosen in the previous stage. It also includes previously allocated capacities from any long-term auctions. Long term markets currently use the ATC method (although this is in the process of changing, see (ACER, 2021)). Due to this fact, and the fact that the forecast has changed in the interceding time, there is a chance that the domain of long term allocations is not included in the flow-based domain, as shown in 3.16. At this stage of the process, the long term nominations – which of the long term allocations will physically occur – are not yet known.[26] Virtual branches are therefore added to include the corners of the long term allocations that may not be included in the flow-based domain. The algorithm for the LTA inclusion is described in detail in (N-Side, 2019). The LTA branches make up

[26]LT capacity rights are auctioned as options, meaning that which of the long term allocations will physically occur is only known at nomination time - just before the market clearing of the FBMC, when

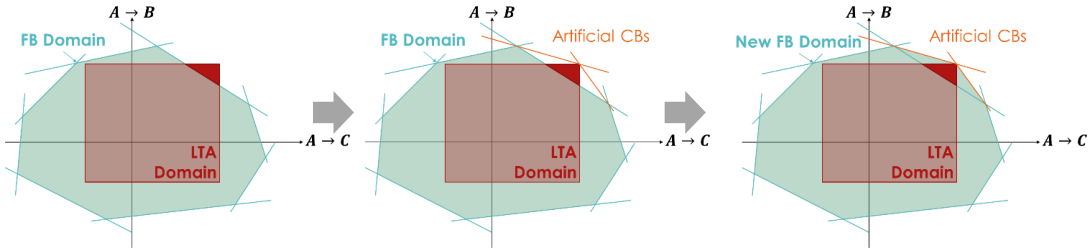

Figure 3.16: Inclusion of Long Term Allocations

a large portion of the flow-based domain. This phase was similar for the CWE region. The number of LTA branches varies significantly (and somewhat randomly) across different time steps. We can see the number of LTA CNECs across 10 sampled days in the CWE region by TSO in Figure E.4 in Appendix E.

It is also at this stage that the margin for CNECs is adjusted to the value required by the *70% Minimum RAM* rule of the Clean Energy Package.[27] This rule maintains that 70% of the RAM of cross-border lines must be used for exchanges, rather than internal flows. Some version of this has been in place for several years, beginning at 20% and slowly increasing to the desired 70%. It is not clear how this value relates to the physics of electricity flows. In any case, there remains to be some work for TSOs to fully integrate this constraint (ACER, 2022). At this stage in the process, any CNEC with a margin below the legal requirement will have a margin – termed Adjustment for Min RAM (AMR) – added to ensure compliance. The values of AMR for CWE over 10 historical days are shown in Figure 3.17. The data shown in the box plots represents only the branches with a non-zero value, while the line on the secondary y-axis shows the percentage of branches with an AMR of zero. Still over 90% of branches have a value of zero, although this has decreased in 2022 as the rules tighten.

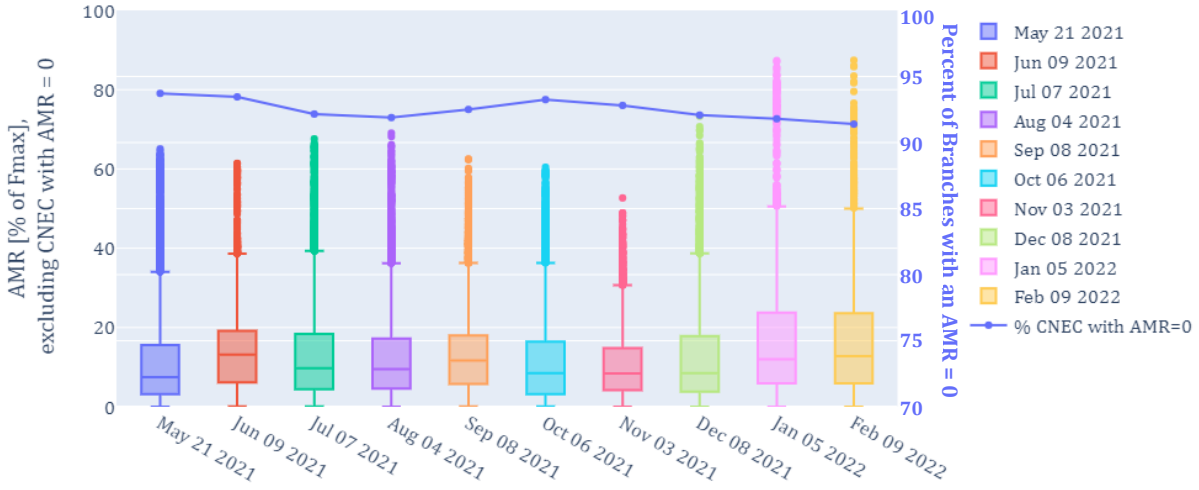

Figure 3.17: Adjustment for Min RAM

their owners decide how much of they option they will actually use. NB: after the market clearing, they will receive a pay-back for the non-used part of their rights (priced at day-ahead price spread between zones).

[27] https://energy.ec.europa.eu/topics/energy-strategy/clean-energy-all-europeans-package_en

3.3.3.5 Capacity Validation

The capacity validation stage consists of a coordinated check of the flow-based domain at this stage by all involved TSOs. In very extreme cases, TSOs can reduce the capacity of certain CNECs. At this stage, they can modify the FAV (Section 3.3.2.5) in the case of 1) input data error, 2) exceptional outage, 3) necessary reactive power flow coverage, or 4) insufficient remedial actions. This is also when TSOs can request for certain branches an exception to the 70% Minimum RAM rule described above in case of security concerns.

3.3.3.6 Pre-Final Flow-based Calculation

This stage involves a third calculation of the flow-based parameters, this time integrating any updates from the capacity validation phase. This phase also includes the flow-based presolve, where any unconstraining branches are removed. The full size of the flow-based power transfer distribution factor (PTDF) matrix can be quite enormous, given the number of CNECs that are taken into account. However, the size of the matrix given to EUPHEMIA only includes the rows that are constraining. This is done through an iterative optimization (called the presolve) where the RAM on each branch is maximized maintaining all other constraints. If the optimal RAM remains the same, than the branch is redundant and is eliminated. Otherwise, it is kept as a constraining branch. This process is represented in Figure 3.18.

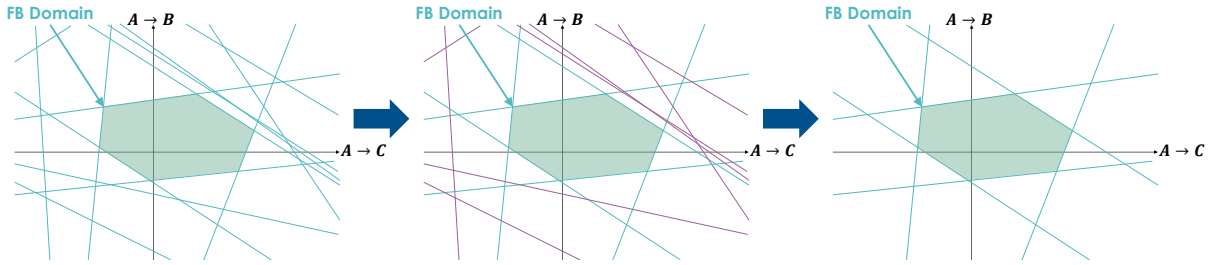

Figure 3.18: Presolve

3.3.3.7 Final Flow-based Computation

Finally, long term nominations (LTN) and external constraints are included before the publication of the final flow-based domain. Long term nominations shift the domain to the point that includes the effect of nominated quantities from long term exchanges, as shown in Figure 3.19

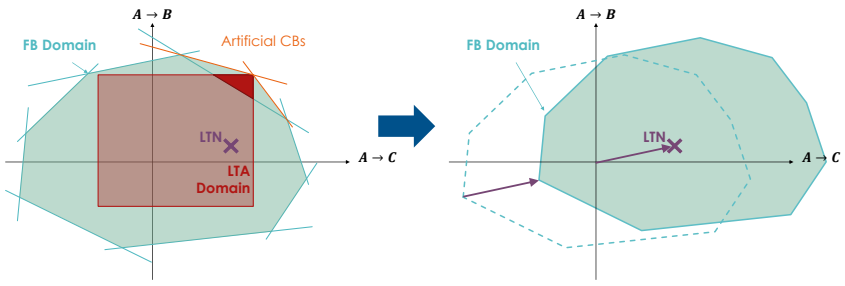

Figure 3.19: Long Term Nomination Shift

3.3.4 Some Discussion on the above process

> *"Allowing for a higher minimium RAM, or for a higher maximum zone-to-zone threshold, is likely to lead to a higher amount of costly remedial actions required in order to maintain operational security. At the same time, the less-constrained capacity domain is supposed to allow for a higher socio-economic welfare. The balance between those two numbers is hard to quantify."*
>
> - Explanatory note on the day-ahead and intraday common capacity calculation methodologies for the CORE CCR. June 4 2018

As described further in the same document, the balance between including all the internal branches, only some or none comes down to an arbitrage between the TSOs' ability to model ex ante the remedial actions available to them – including redispatch and the associated cost – to ensure compliance with the N-1 rule and the day ahead system cost. This anticipation is all the more difficult as generation changes that occur closer to real time – either in intraday, balancing or redispatch market phases – are more prevalent.

Assuming a certain level of liquidity (and therefore competitive pricing) in closer-to-real time markets, the crucial values to set in the day ahead market are the unit commitments of generation plants that require lengthy start-up durations or other modifications of their dispatch. However, in systems with increasing variable renewables, this is already called into question as a reference point. The forecast error between day ahead and real time (not to mention between D-2 when the network constraints are calculated and real time) is only going to increase for the time being, highlighting the need for flexible markets and products.

3.4 Robustness of Parameter Choices on a Small Case Study

Here we look at the RTS-GMLC case study (described in Chapter 2) and present different effects on the flow-based domain from variations on three specific aspects:

1. Base Case Calculation (Section 3.4.1)
2. Generation Shift Keys (Section 3.4.2)
3. Remedial Actions (Section 3.4.3)

3.4.1 Base Case

The first input that we look at in a bit more detail is the base case calculation. In the actual operational process, the base case is formed as described in Section 3.3.2.1. As a short reminder, a reference program of zonal net positions is first determined in a coordinated manner. Then, each TSO performs their best forecast for their internal load and non-dispatchable generation. This is then balanced using dispatchable generation to match the agreed-upon reference program. However, the details of these power flow stages is at the discretion of the TSO. Due to their large sizes (several thousands of substations), operational base cases are demanding in data preparation and computation time, whereas non-disclosure agreements ususally limit the reseracher's ability to publish illustratie detailed facts. Some valuable insights may be extracted from a fictitious base case mimicking the operational scale on a smaller scale.

In the literature, a DC-OPF is generally used to mimic the operational processes [Finck 2021]. This can lead to certain effects that do not correspond to reality. For instance, if different security level constraints are applied to forecast the internal generation pattern of the base case than those used in the flow-based domain calculation, the reference flows of the contingency-associated CNEC may be too high, leading to negative RAM values. Since the final flow-based domain is meant to be N-1 secure, not including these constraints in the base case calculation can lead to problems with empty domains.

3.4.1.1 Temporal Variation

To begin with, we can get an idea of the seasonal and hourly variance of the base case net positions in Figure 3.20. The RTS-GMLC system contains three zones; therefore the complete balance information can be represented in two dimensions.This plot shows the base case for the RTS-GMLC system across 4 different 2-week seasonally-variant periods. For these cases, a security constrained OPF (SCOPF) following the three-stage corrective model described in Section 3.2.3 was used. The color of the marker represents the hour of the simulation.[28]

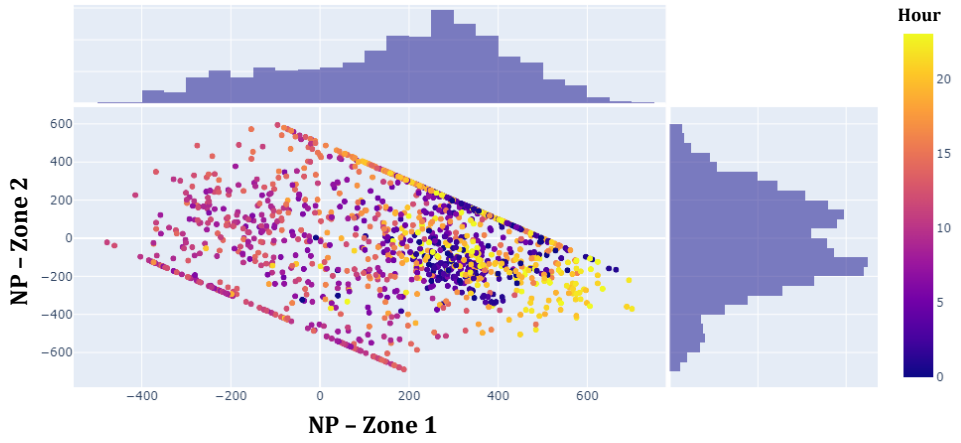

Figure 3.20: Temporal Variation of Base Case Values

We can see a few interesting things from the resulting flow-based domains. Figure 3.21 shows the flow-based domains from the extreme points of Figure 3.20. We can see that a very different set of net positions does not automatically lead to a significantly different flow-based domain. Note that the domains seem to extend well beyond the cloud of points in the upper left and lower right corners. This is normal since the flow-based domain is a visualization only of the network constraints, and does not include any generation constraints.

3.4.1.2 Constraint Inclusion

Looking a little closer, we can generate the base case using the two methods of modeling contingencies and remedial actions demonstrated in 3.2.3, as well as a simple DC-OPF. We ran these different modeling variations over a month (January) of the RTS-GMLC network with an hourly time step. Figure 3.22 shows these points for the net position of Zone 1 and 2, where the color of the marker represents the type of model applied.

We can see in the figure where the net positions were limited by the different security levels, preventive mode being the most limiting. Interestingly, the corrective mode is similar to the DC-OPF (no N-1)

[28]This analysis uses the 3-stage corrective method and GSKs of type RemRange (see Table 3.6).

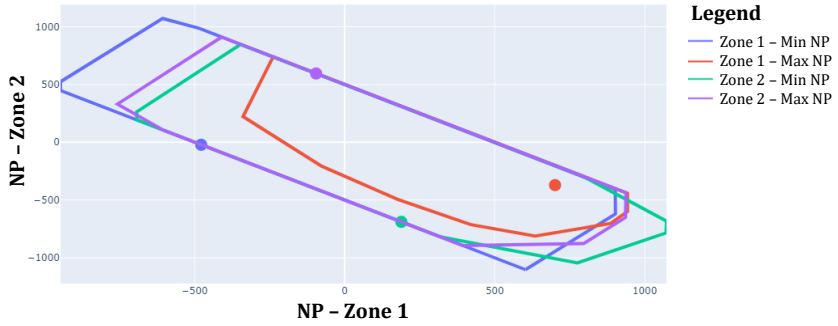

Figure 3.21: Extreme Points of Temporal Variation of Base Case Values

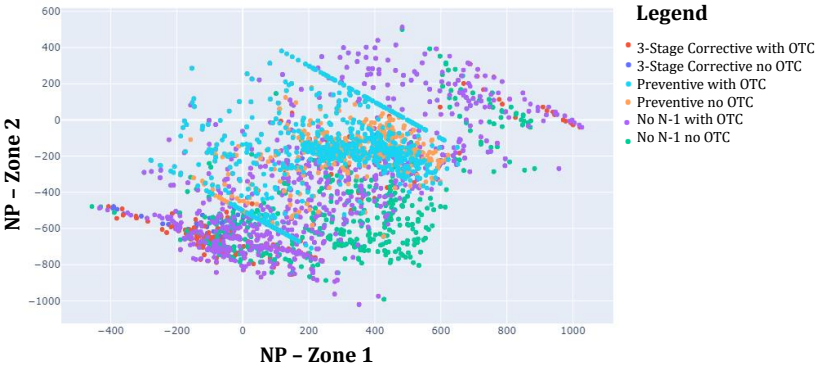

Figure 3.22: Constraint Inclusion Variations for Base Case Calculation

and the feature that actually makes the difference is the inclusion of topological remedial actions. This will be discussed in a bit more detail in the next section.

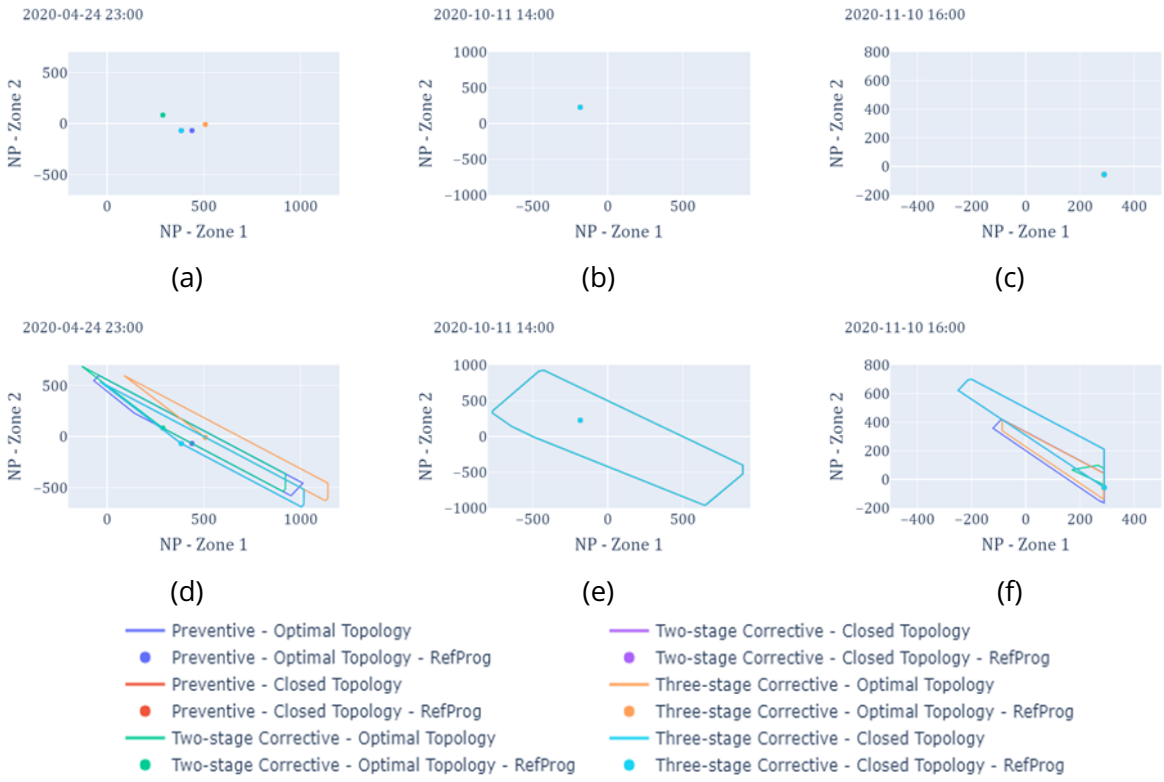

Figure 3.23: Various Effects of Base Case Variations on the Resulting Flow-Based Domains

To highlight the importance of the basecase forecast (not only the reference program of net positions), Figure 3.23 shows three specific cases. The three top images (Figures 3.23a, 3.23b, and 3.23c) show the reference programs and the bottom images (Figures 3.23d, 3.23e, and 3.23f) show the resulting flow-based domains. Figure 3.23d shows that having different reference programs will generally lead to some amount of difference in the flow-based domains. However, when we have the same reference program, we can have either the same resulting domain, as in Figure 3.23e, or significantly different domains, as in Figure 3.23f. This final column of images shows how crucial the internal forecast is to the final flow-based domain. A well forecast net position is not as important as a well forecast internal position.

3.4.2 GSKs

The GSKs are another of the most important parameters of the flow-based method to be addressed. They are perhaps the most-often treated in the literature, and often the most criticized. They capture an attempt to linearize a definitively non-linear phenomenon and thus can have a high impact on the ending results. Figure 3.25 show the effects of several GSK variations on six statistically different timesteps for the RTS-GMLC system. This gives an example of the possible variation in flow-based domain shape. In the examples shown here, we hold the other parameters of the base case calculation and remedial action inclusion constant, using a 3-stage corrective SCOPF with optimal topology control to generate the base case. A maximum of 4 curative actions (only non-costly) and a minimum PTDF filter of 0.05 were applied. As other studies have previously found, the GSKs change the domain quite a bit. What remains to be seen is how exactly they impact the security level of the domain. In order to analyze a bit more in depth the effects of different generation shift key (GSK) methods on the security level of the domain, we performed a more in depth study using the RTS-GMLC network. The

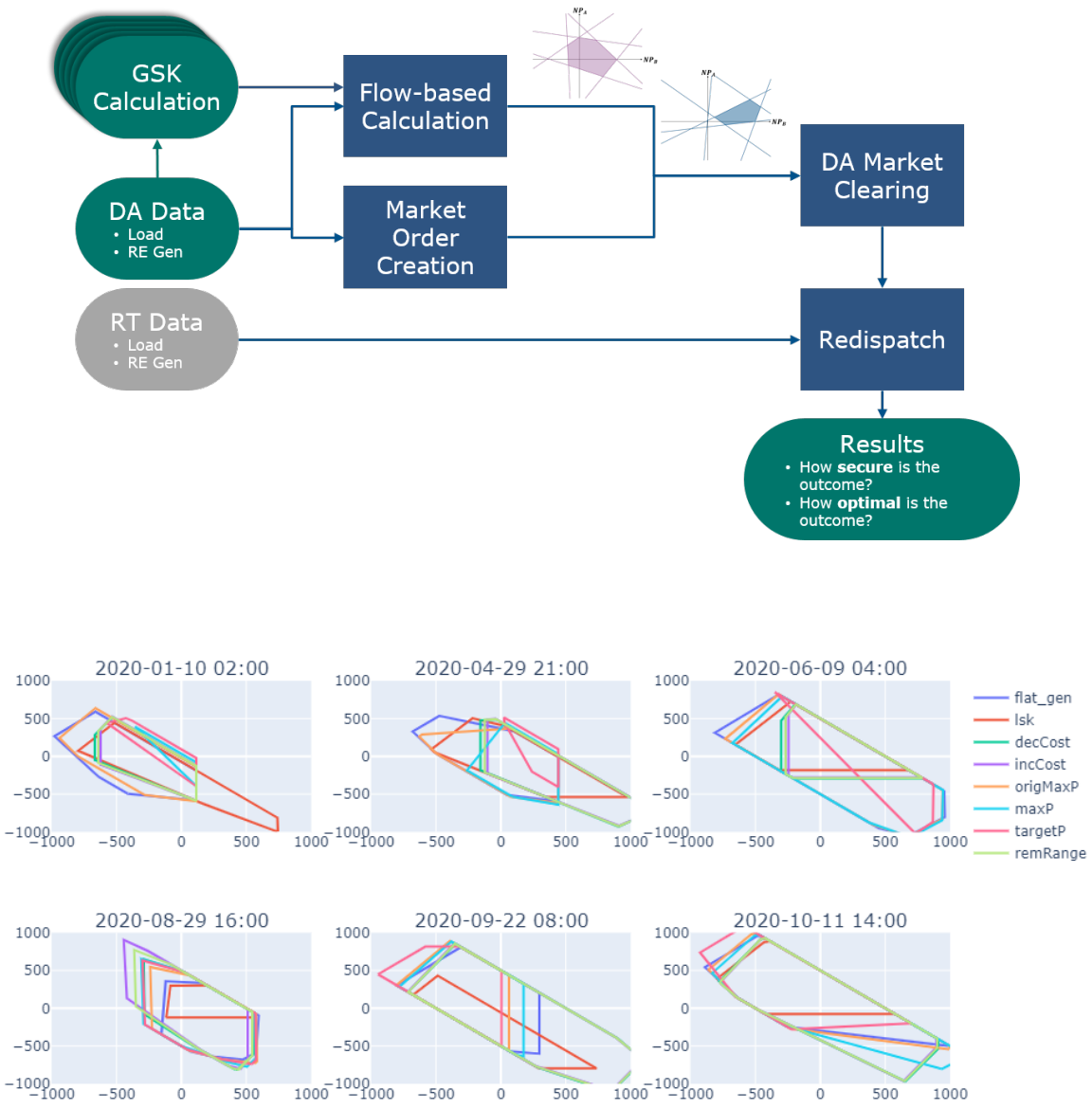

Figure 3.25: Example of GSK effect on Flow-based Domain Variation

goal of the study was to analyze not only the ability of a certain GSK to allow the best market clearing result, but also to assess the security of the market clearing outputs of each GSK method. To that end, we follow the process shown in Figure 3.24. The analysis concerns both the day-ahead electricity market welfare as well as the real-time physical system security. At a first stage the multi-domain and (current) single-domain flow-based methods are compared based on forecasted data, in terms of the resulting day-ahead market welfare. At a second stage, the effect on the system security is compared under real-time operational data. Some details of the redispatch model are explained in Appendix G.

Four two-week periods were selected from the data set, representing varied load, PV and wind profiles. These are shown in Table 3.5.[29] Five different GSK calculation methods were assessed, shown in Table 3.6.

[29]Note that the end date marks the end of the period and is not included in the study period, i.e. the first study period includes 366 hours, January 8, 2020 00:00 to January 21, 2020 23:00.

	Start Date	End Date
1	January 8, 2020	January 22, 2020
2	April 8, 2020	April 22, 2020
3	July 1, 2020	July 15, 2020
4	October 14, 2020	October 28, 2020

Table 3.5: Two-Week Periods Used in GSK Assessment Study

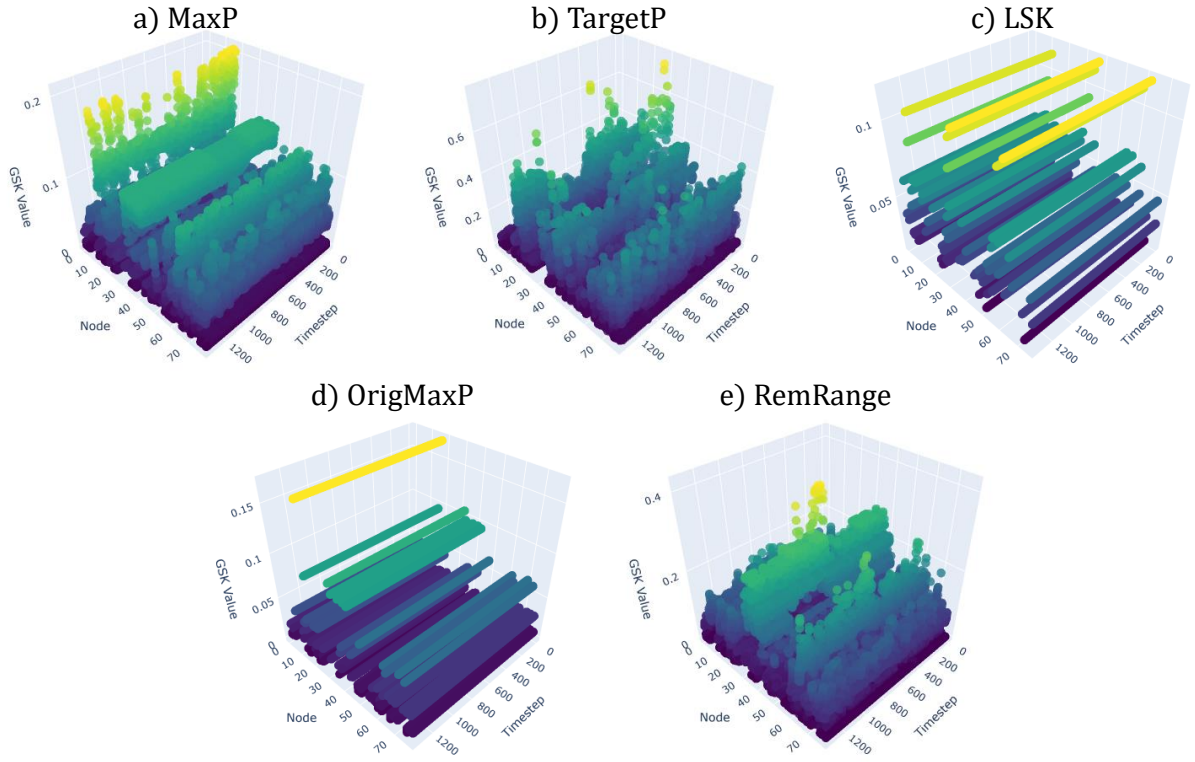

Figure 3.26: GSK Temporal and Geographic Variations

Reference Term	Name	Calculation
OrigMaxP	Original Max P[30]	$\forall g \in G: gsk_g = \frac{P^i_{gmax}}{\sum_{g \in Z} P^i_{gmax}}$
TargetP	Basecase Prod.	$\forall g \in G: gsk_g = \frac{P_{g_{BC}}}{\sum_{g \in Z} P_{g_{BC}}}$
MaxP	Hourly Max P[31]	$\forall g \in G: gsk_g = \frac{P^h_{gmax}}{\sum_{g \in Z} P^h_{gmax}}$
RemRange	Remaining Operating Range	$\forall g \in G: gsk_g = \frac{(P^h_{gmax} - P_{g_{BC}})}{\sum_{g \in Z} (P^h_{gmax} - P_{g_{BC}})}$
LSK	Load Shift Key	$\forall d \in D: gsk_d = \frac{P_d}{\sum_{d \in Z} P_d}$

Table 3.6: GSK Calculation Methods used in Assessment Study

Figure 3.26 shows the variation both in time and in geographical location of the different GSK methods

[30] Installed capacity of the plant
[31] Maximum production available at that hour (specifically different for variable renewables)

explored in this section. We can see that as expected the OrigMaxP variation does not vary in time. The LSK variation does not either since the input data had constant nodal participation factors.[32] Figure 3.27 shows the box plot of the different GSK types. We can see that for this network, the

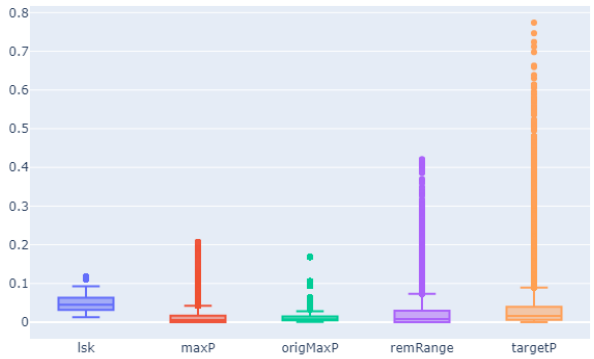

Figure 3.27: Box Plot of GSK Values by Type

targetP method can lead to incredibly high values. This means that at those time steps, there is one plant producing almost 80% of the zonal generation. However, the median of all the GSK values remains below 10% of the zonal generation.

Next, we can see the difference in the flow-based domains generated by each different GSK method in Figure 3.28. These plots show results from all time steps of the study. The color represents how often each point (representing a given configuration of net positions) in the mesh appears in the flow-based domain of that GSK across the four two-week study periods. Finally, Figures 3.29 and 3.30 show the

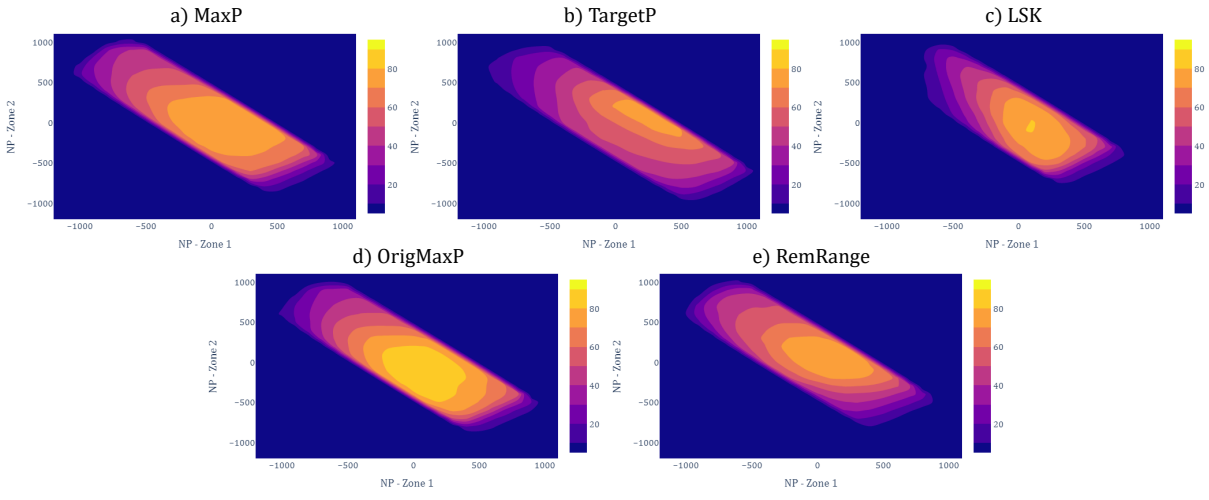

Figure 3.28: Contour Plots of Flow-based Domains

cost differences across the two phases and the total, in absolute values and then percent differences compared to the minimum cost GSK, respectively. Interestingly, we can see that whenever a GSK had a much lower cost market clearing dispatch, it had a higher redispatch cost. This aligns with some of

[32] In future work, it would be better to modify this.

our hypotheses regarding the *quality* of a flow-based domain. Occasionally it seems using a certain GSK leads to a larger domain of possible exchanges in the market clearing. However, in the cases we see here, this gain significantly reduced when we look at the resulting redispatch cost. In the end, the percent differences of total cost for the different GSK methods were almost identical, with less that 1% difference.

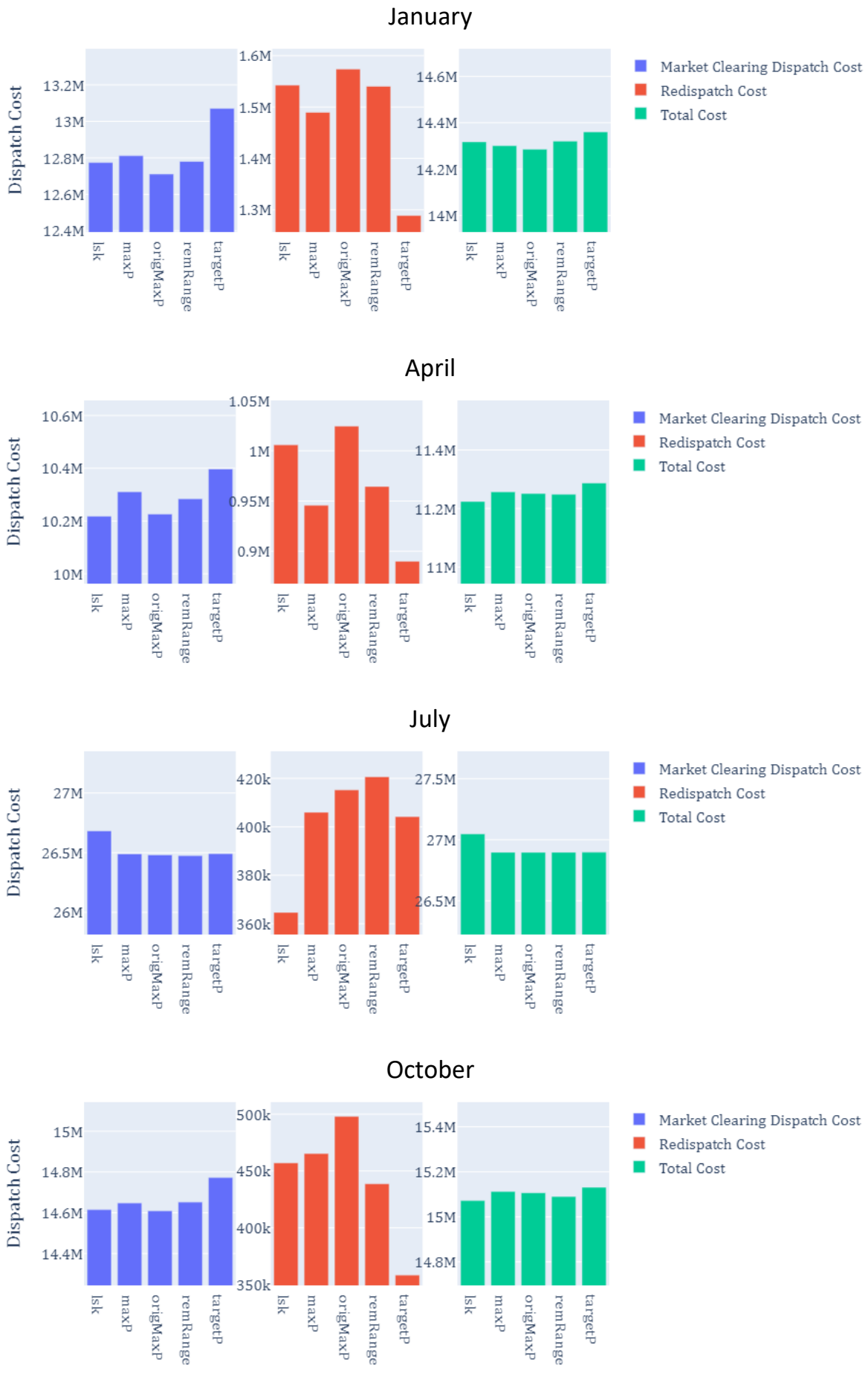

Figure 3.29: Cost Differences - GSK Analysis

Figure 3.30: Percent Cost Differences - GSK Analysis

3.4.3 Remedial Actions

Finally, we look at some effects of the inclusion of remedial actions on the flow-based domain. This incorporates multiple aspects of the process. First, as we see in Figure 3.22, the inclusion of remedial action optimization in the base case calculation already has an impact on the resulting domain. Looking a little closer at this specific case, Figure 3.31 shows the range of the reference programs for each of the zones in 6 cases. Looking at the net positions for zone 1, we notice that the limits for the 3-stage corrective and the DC-OPF with no N-1 included are not in fact that different. What makes a larger difference is the inclusion (or lack thereof) of optimal topology control in either case. This is true to a lesser extent for the other zones where less remedial actions are activated.

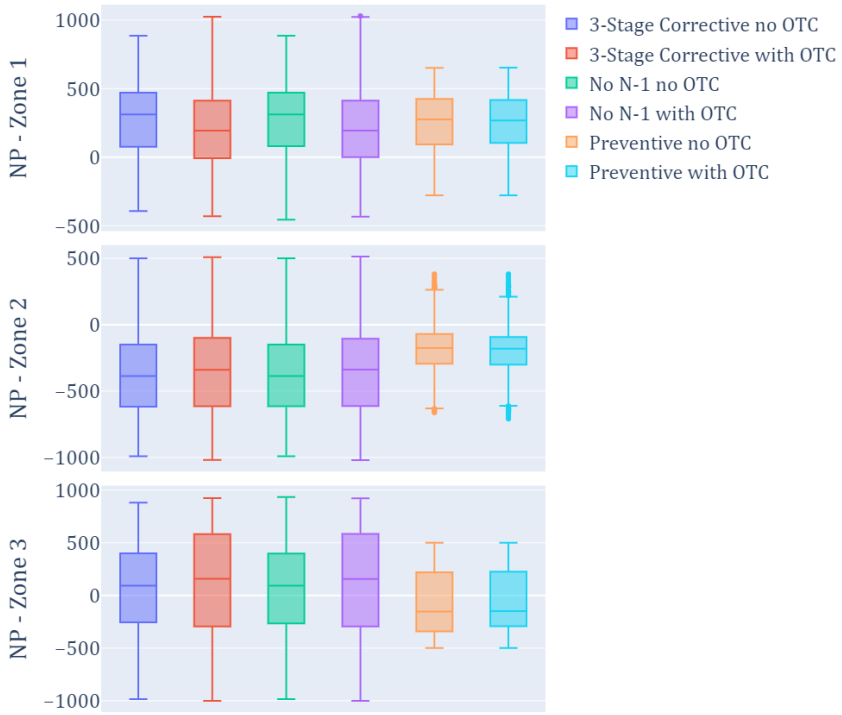

Figure 3.31: Remedial Action Effect on Minimum and Maximum Net Positions

Then there is the matter of including explicitly a remedial action optimization phase during the flow-based process.

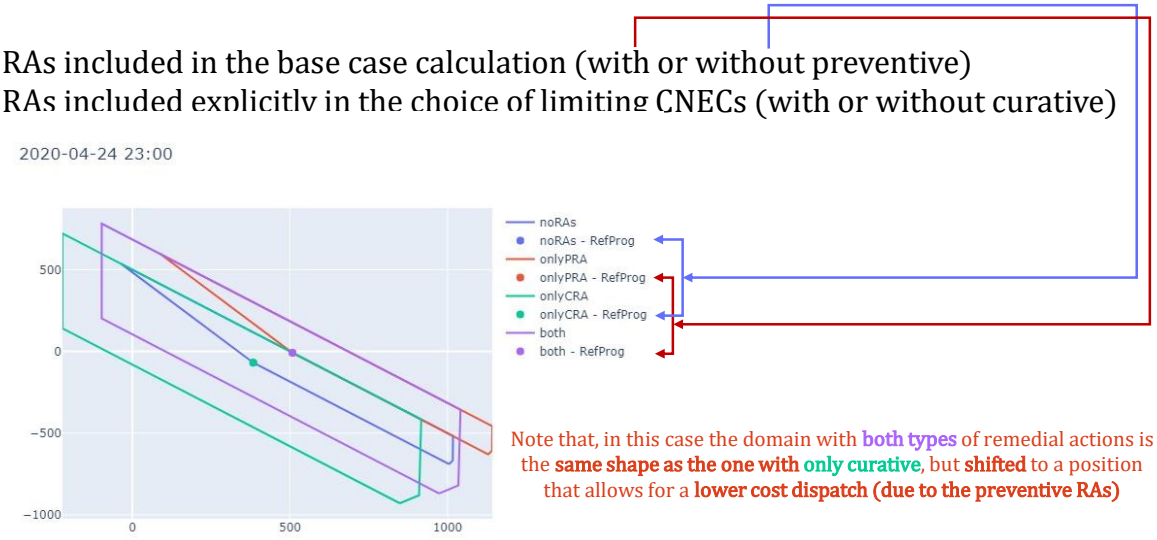

Figure 3.32: Remedial Action Inclusion Effects

3.5 Conclusion

This chapter presented a wide perspective around the existing capacity calculation method, beginning with an in-depth look at the operational constraints, specifically at the different applications of the method by the various TSOs. The gains from the integration of the flow-based method as the standard model for the highly-meshed European network are clear, both in the literature and the results from the parallel runs. One of the main focuses of this chapter is to clarify the level of harmonization and the reasons for which a lack of harmonization can still be found regarding several of the flow-based parameters. For instance, the use of the external constraints is particular to the network characteristics of the specific TSO, while the most representative GSK may depend not only on the particular installed capacity of each TSO, but also on the hourly balance pattern.

In this chapter, we show the variety of impacts that can occur to modify the flow-based domain – taking into account more or less network constraints or flexibility, for instance. We show how temporal variations as well as different types of outage modelling in the base case might impact the resulting flow-based domain. More importantly, we show that just knowing the reference program (the set of zonal balances) is nowhere near enough information to try to forecast the similarities between different flow-based domains. Interestingly, in the same small case study, we saw little overall welfare difference between GSK calculation methods, when a redispatch phase was included. It will be important to validate these results on a real case study for this result to be fully conclusive. A brief demonstration showed the impacts of including remedial action modeling at different phases.

As mentioned briefly in Section 3.1, the measure of the *quality* of a flow-based domain can be difficult to quantify. From the European level, there is a desire to have larger domains, updated more frequently, with the aim to increase the overall European market welfare. However, if increasing the domain of possible exchanges simultaneously increases the difference between how the grid is modeled within the market clearing algorithm and the actual network flows that might physically limit the exchanges, there is likely to be an increased redispatch cost.

We can attempt to visualize this arbitrage a bit using the two different DC-OPF models described in the first chapter. The following plot, Figure 3.33 shows the optimal cost at each set of net positions. On the left is the version with all constraints (as well as optimal topology, but no N-1 or complex

remedial actions as we have used elsewhere in this chapter) and on the right is the same plot, but this time, using the copper plate model, without network constraints. At each of the points in the graphic, an OPF was run, and the plots show a heat map of the optimal minimum dispatch cost, while forcing the zonal balance to the x and y values. The color scales are identical, with dark blue representing the lowest cost dispatch and red the highest. Finally, Figure 3.34 shows the difference between the two, in the feasible space of the network.

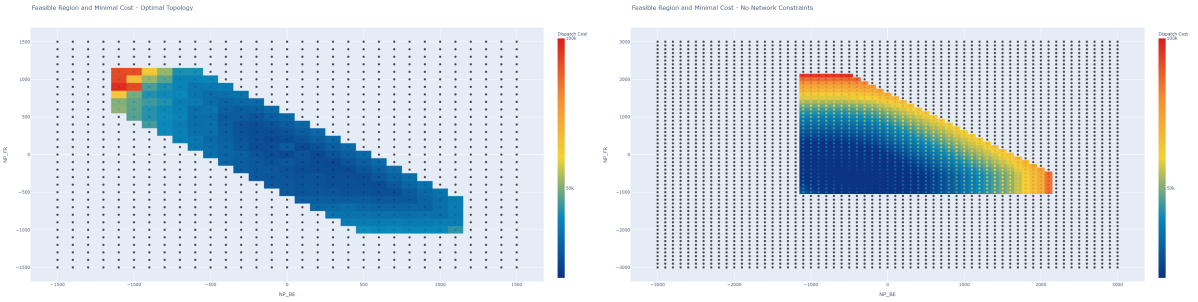

(a) DC-OPF with Optimal Topology Control (b) DC-OPF with No Network Constraints

Figure 3.33: Heatmap of Optimal Dispatch Cost at Set Net Positions

What we see is that at the same set of net positions, we often have a difference in cost that comes from network constraints. Subplot 3.33b represents the social welfare (really the cost minimization, no load price) and shows where the market coupling will go with no network constraints. This means that the reduction of variable space to net positions can incur a cost even with a perfectly represented flow-based domain, unless we consider a "perfect" flow-based domain as only covering the part of this plot where there is zero cost difference.

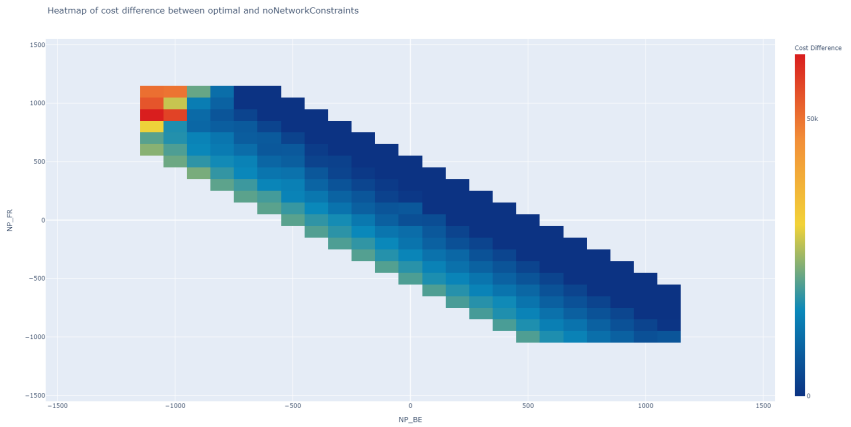

Figure 3.34: Difference in Optimal Dispatch Cost at Set Net Positions

Essentially, if the flow-based domain covered only the dark blue area, there would be zero redispatch cost. As the colors lighten, there is an arbitrage between the two costs. This concept will be discussed in more detail in the next chapter.

Chapter 4

The Multi-domain Approach

Nomenclature

Indices	
n	Node
s(k)	Source Node of Branch, k
e(k)	End Node of Branch, k
k	Branch
g	Generator
o	Offer
t	Time
Variables	
q_o^{acc}	Accepted Real Power of an Offer, o
$\lambda_{t,z}$	
p_o	Offer Price
P_g	Real Power Generation at Generator, g
L_n	Real Power Demand at Node, n
F_k	Real Power Flow on Branch, k
V_n	Nodal Voltage Magnitudes
θ_n	Voltage Angles
δ_k	Binary variable representing breaker open/close status
z_k	Binary variable representing branch open/close status
δ_k^{UC}	Binary variable representing the unit commitment variable
Parameters	
q_o^{max},q_o^{min}	Maximum and Minimum Real Power of an Offer, o
C_o^{fix}, C_o^{var}	Fixed and Variable Costs associated with an Offer, o

$Grad_o^{dec}$, $Grad_o^{inc}$	Maximum Gradient decreasing/increasing for an Offer, o
$\overline{F_k^{dir}}$,$\overline{F_k^{inc}}$	Maximum Flow limits on branch, k, (direct/inverse directions)
$q_o^{OpRange}$	Domain representing real operation of Generator, g
M_B	Big-M parameter for controllable breakers
M_K	Big-M parameter for controllable branches
c_g	Generator, g, Marginal Cost
c_w	"Wear-and-tear" cost for topological actions
c_{LS}	Load shedding cost
N_B, N_{CB}	Number of controllable breakers, branches
Sets	
$\mathcal{K}$	Set of Branches
$\mathcal{K}_B$	Set of Controllable Breakers (Modelled as branches with no flow limit)
$\mathcal{K}_{CB}$	Set of Controllable Branches
$\mathcal{K}_{\notin Flex}$	Set of Non-flexible Branches
$\mathcal{N}$	Set of Nodes
$\mathcal{G}$	Set of Generators
$\mathcal{G}_n$	Set of Generators at Node, n
$\mathcal{Z}$	Set of Zones
$\mathcal{C}$	Set of Contingencies
$\mathcal{O}$	Set of Offers

4.1 Introduction

As discussed in previous chapters, the literature on the flow-based method has expanded significantly since it was put in place in the Central Western European (CWE) region in May 2015. Descriptions of the method can be found in (Van den Bergh et al., 2016). A large part of the existing literature examines issues that can arise through the choices of discretionary parameters by TSOs (Marien et al., 2013) (Felten et al., 2021) (Schönheit et al., 2021b). The previous chapter examined in detail the existing method – both theoretically and operationally – and added to this initial body of work.

This next chapter fits into a second body of literature that work to expand the current method, either through the explicit inclusion of HVDC lines (Müller et al., 2017) or transmission switching (Lete and Papavasiliou, 2020). Several gains have been made in these areas in the operational method in parallel with these recent studies.

For one, beginning in 2020, the "Evolved" flow-based method was put into place. Since this update, the set points of the HVDC line ALEGrO ("Aachen Liège Electricity Grid Overlay") are now determined directly in the day ahead market coupling algorithm, EUPHEMIA. This is done through the addition of two virtual bidding zones, representing the injection and withdrawal points of the line. The will be discussed in more detail in Section 4.2.2.1. This method is somewhat similar to the multi-domain method that will be presented in this chapter, the main difference being the representation of topological changes (and the possibility to include a forecast redispatch cost associated with a specific domain of exchanges).

Additionally, as discussed in the previous chapter, a harmonized remedial action optimization phase has replaced the semi-coordinated validation phase originally used in the CWE method for inclusion of remedial actions (amprion, 2020). This explicit remedial action optimization has been added to

the flow-based capacity calculation – although not yet to the capacity allocation phase. Currently, this phase includes PST tap changes and topological actions (see Figure 3.15 in Chapter 3 for the number of remedial actions considered during this phase), but no costly remedial actions. While the current method may not be ideal (see Section 4.2.2.3), this step demonstrates a move towards a more efficient use of the existing transmission network. A report by the Belgian National Regulatory Authority (NRA), CREG, (Commission de Régulation de l'Electricité et du Gaz (CREG), 2019) goes even further and expresses the need to include a best forecast for all remedial actions – including costly remedial actions – in the day ahead market, a concept that will be possible with the multidomain method proposed here.

Indeed, (Poplavskaya et al., 2020) found that integrating forecast redispatch costs into the day ahead flow-based market coupling (on a small 6-node case study) can have several benefits, including a simultaneous increase in day ahead cross-border trade and a reduction in the *ex post* redispatch volume and cost. This covers both facets of the quality of the flow-based domain discussed in the previous chapter. The proposed method relies on the selection of a set of generation units which can be used for *integrated redispatch*. These generators are not included in the GSK calculation (and therefore their impact is not represented by the zonal PTDFs). Instead, their impact on the flow on the critical network elements is taken into account directly using nodal PTDFs.

(Weinhold and Mieth, 2021) propose an uncertainty-aware extension of the method, using a chance-constrained formulation for FRMs. The authors found that "initially, the reduced commercial exchange capacity provides higher system cost but proves more robust against real-time deviations than the deterministic counter part." This result brings us once again back to the arbitrage surrounding the quality of an exchange domain: the chance-constrained FRM reduces the size of the network capacity available to the day ahead market, yet is more robust across the different market phases.

The motivation of the work presented in this chapter falls into this category of literature, aiming to expand the flow-based method that currently exists, specifically in order to better account for uncertainties at two stages of the calculation process: 1) the generation of a forecasted base case, around which the domain is linearized; and 2) the expansion of the domain in a forecasted market direction through the optimization of remedial actions[1]. In the first case, there is a risk that a single flow-based domain might constrain the possible exchanges to too high of a degree. The second aspect revolves around the manner in which the remedial actions are taken into account. For instance, since the current remedial action phase is based on a single potential set of zonal balances, it is possible that the remedial actions chosen at this phase may not represent the best options. In the same vein, a poorly chosen remedial action optimization function, may in fact reduce the size of the domain in the areas with the eventual higher values of market welfare.

The *multi-domain* flow-based approach proposed in this chapter expands the current flow-based method in a novel way through the inclusion of multiple distinct domains, each one associated with a corresponding set of optimal remedial actions, and potentially a cost of activation if costly remedial actions are considered.[2] The union of the alternative flow-based domains is represented in the market clearing algorithm through the use of binary variables combined with big-M optimization in a way that is fully compatible with the functionalities of the existing market clearing algorithm currently used in Europe. Notice that this latter feature also establishes the general feasibility of incorporating any discrete non-convex security domain in the current European market clearing process.

[1]These actions include phase shifting transformer (PST) tap changes and topological changes and can be extended to costly remedial actions as well, used both in a preventive and curative fashion.

[2]In the latter case, it is crucial to have a good forecast of a potential cost in order for the market clearing algorithm to correctly arbitrate between the two aspects.

The aim of this chapter is to present this new method, first theoretically then in several small case studies. The method was tested and validated directly in the European market coupling algorithm, EUPHEMIA. To place the method in the necessary context, we will begin by describing the European energy market (Section 4.2), specifically the existing European market clearing algorithm, EUPHEMIA, in Section 4.2.1, and the recent evolutions (and their respective limitations) of the applied flow-based method in Section 4.2.2. Section 4.3 will first detail the proposed method (Section 4.3.1), then demonstrate its use in a small example (Section 4.3.2). The method was validated directly in EUPHEMIA for several case studies, discussed in Section 4.3.3. Several ideas for generating the multidomains are explored in Section 4.3.4, as well as the takeaways regarding the advantages or disadvantages of each proposed concept. Finally, conclusions can be found in Section 4.4.

4.2 European Context

4.2.1 European Market Clearing Algorithm - EUPHEMIA

Note that some of this description is taken directly from a previously published work:

E. Little, "Examining the Effects of a European Co-optimized Day-Ahead Market Coupling," Masters Thesis, Department of Civil, Geo, and Environmental Engineering, Technische Universität München, Munich, Germany, 2018.

In order to clearly present the proposed methodology, we will begin with a description of EUPHEMIA, the market clearing algorithm used for a large part of European countries. This is important as the method described in the next sections relies on the current definitions inherent in the existing algorithm. In fact, tests of simple examples of the multi-domain method were run directly on EUPHEMIA through the cooperation of EPEX SPOT. Other extended tests were run on ATLAS, a model developed in RTE that is designed to mimic EUPHEMIA. The slight differences between the two will be noted in the description.

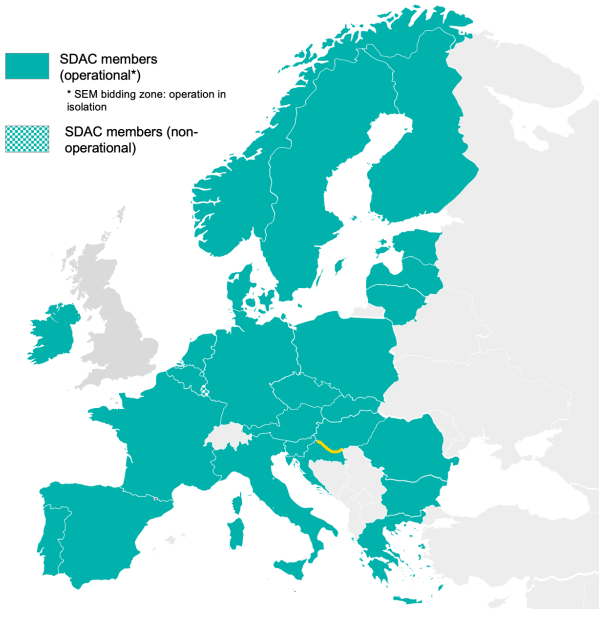

Figure 4.1: PCR Region as of 2021

Currently, Europe is on its way to having an integrated, harmonized market for energy trading. One of the largest steps in this direction came in 2014 with the beginning of the Price Coupling of Regions (PCR). The PCR (newly referred to as SDAC, Single Day Ahead Coupling) established a single market coupling algorithm for North-Western Europe (NWE). This initial region covered the power exchanges EPEX SPOT and Nord Pool Spot and included the following TSOs:

- In Belgium: Elia
- In Denmark: Energinet.dk
- In Finland: Fingrid
- In France: RTE
- In Germany: 50Hertz, Amprion, Tennet GmbH, TransnetBW
- In Luxembourg: Creos
- In Netherlands: Tennet B.V.
- In Norway: Statnett
- In Sweden: Svenska kraftnät
- In UK: National Grid

This region has since expanded across Europe to include 23 countries in Europe (see Figure 4.1), across seven power exchanges – EPEX SPOT, GME, Nord Pool, OMIE, OPCOM, OTE, and TGE.[3][4] This coupling of regions allows for increased market liquidity leading to a higher overall market welfare. It also removed the need for market players to procure separate transmission rights, improving the transparency of the markets (Francisco and Nerves, 2010).

The current list of TSOs and NEMOs[5]: Transmission System Operators (TSOs):

> 50Hertz Transmission, ADMIE, Amprion, APG, AST, ČEPS, Creos, EirGrid, Elering, ELES, ELIA, Energinet, ESO, Fingrid, HOPS, Litgrid, MAVIR, PSE, REE, REN, RTE, SEPS, SONI, Statnett, Svenska Kraftnät, TenneT DE, TenneT NL, Terna, Transelectrica, and TransnetBW

and Nominated Electricity Market Operators (NEMOs):

> BSP, CROPEX, SEMOpx (EirGrid and SONI), EPEX, EXAA, GME, HEnEx, HUPX, IBEX, Nasdaq, Nord Pool, OMIE, OKTE, OPCOM, OTE, and TGE

Since February 2014, a single price coupling algorithm (Single Day Ahead Coupling, SDAC) has been used across Europe known as EUPHEMIA (Pan-European Hybrid Electricity Market Integration Algorithm). EUPHEMIA is currently used across all 23 European countries included in the PCR (see Figure 4.1), enabling an average daily trade of more than EUR 200 million.[6]

It processes the orders from seven power exchanges, deciding which offers are accepted or rejected in order to maximize the market welfare and remain within the physical network constraints. The market coupling model of ATLAS, used for several parts of this thesis work, is a mixed integer linear program based on a slightly simplified version of the EUPHEMIA algorithm.[7]

For the parts of the algorithm considered in this work, the two models function similarly. Each model takes as an input the offers to market from each market area, as well as the market border constraints, whether this is the ATC method or Flow-based Method. From these inputs, the algorithm matches purchase and sale offers to maximize the overall market welfare. It also calculates the market prices and other values and market indicators, including the cross-border capacity flow and the congestion

[3] www.epexspot.com/en/market-coupling/another_step_towards_market_intergration

[4] Note that the UK was at one point a part of this, but since Brexit the UK has split off and no longer remains in the PCR.

[5] Source: https://www.entsoe.eu/network_codes/cacm/implementation/sdac/sdac-geographical-scope-and-extensions

[6] https://www.n-side.com/pcr-euphemia-algorithm-european-power-exchanges-price-coupling-electricity-market/

[7] The type of order is less complex for the model discussed here which allows, for one, the objective function of this model to be linear, rather than quadratic as it is in EUPHEMIA.

rents. The full EUPHEMIA algorithm is described in some detail in Appendix A. However, in the next section, we will discuss specifically the different offer types as they are particularly relevant for the method that will be described later on in the chapter.

4.2.1.1 Offer Types

In order to represent the complex technical constraints of various power plants in the form of bids, there are several types of offers permitted in EUPHEMIA, some of which render the problem much less well-behaved than theoretical models.

The simplest orders are either linear or stepwise, all of which are ultimately aggregated into a single curve, either following Figure 4.2a or Figure 4.2b.

(a) Step Curve (b) Linear Curve

Figure 4.2: Offer Curve Types

In reality, the full aggregated curves are a hybrid combination of these types of offers. Figure 4.3 shows which offers should be accepted (assuming a single market zone).

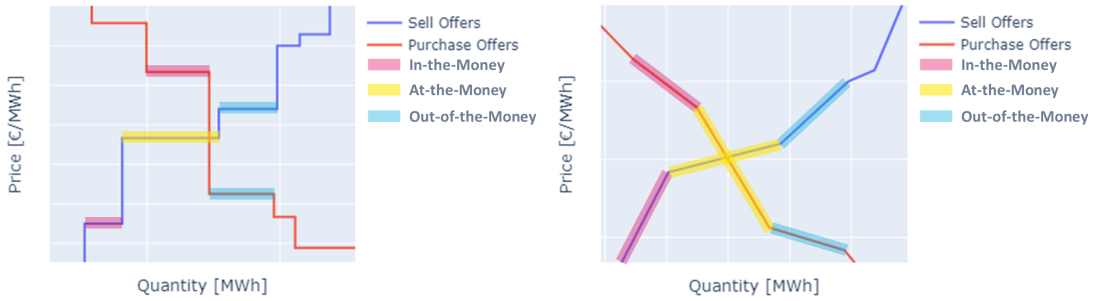

(a) Step Curve (b) Linear Curve

Figure 4.3: Offer Acceptance Status

Since the linear curve offers have a price that depends on the quantity, the resulting objective function will be quadratic. In order to somewhat simplify the problem resolution, for this work, we have ignored this offer type in the ATLAS model and in the studies tested in EUPHEMIA.

Next we have two sets of more complicated order types:

1. Complex Orders
2. Block Orders

Complex Orders are sets of simply hourly piece-wise orders that have an additional constraint applying to the overall set. Currently there are three types of additional constraints permitted:

1) Minimum Income constraints (MIC), 2) Scheduled Stop constraints, and 3) Load Gradient constraints. The first is described as follows:

> *"Generally speaking, the Minimum Income economical constraint means that the amount of money collected by the order in all periods must cover its production costs, which is defined by a fix term (representing the startup cost of a power plant) and a variable term multiplied by the total assigned energy (representing the operation cost per MWh of a power plant)."*[8]

This means that the revenue for the total set of offers must be sufficient to cover fixed and variable costs:

$$\sum_{o,t\in\mathcal{O}_{set}} \lambda_{t,z} q_o^{acc} \geq C_o^{fix} + C_o^{var} \sum_{o\in\mathcal{O}_{set}} q_o^{acc} \tag{4.1}$$

where $\lambda_{t,z}$ is the market price for the zone and time of the offer and q_o^{acc} is the accepted quantity of each offer in the MIC set, respectively. $\mathcal{O}_{set}$ represents the set of offers included in a single Minimum Income Condition. C_o^{fix} and C_o^{var} are the terms of the offer, representing a fixed (start-up) cost and a variable cost. While this type of offer seems quite helpful, it can also increase the risk of rejection. If a single offer price in the set is out-of-the-money, the whole set is rejected. However, this can be avoided in the MIC is combined with a Scheduled Stop constraint. This is generally used if a power plant is already running during the previous day.

Finally, the Load Gradient constraint can be added to a set of offers. This means that the volume that can be accepted in a time, t, is contingent upon the volume accepted in previous time steps. The difference in volume accepted between time steps must respect the increment given, in either direction:

$$Grad^{dec} \leq q_{o,t}^{acc} - q_{o,t-1}^{acc} \leq Grad^{inc} \tag{4.2}$$

Block Orders are unique for two reasons: they are defined over multiple time periods and they have a minimum acceptance ratio (MAR) (a q_{min}, in other words). Because of this, these offers are inherently associated with binary variables. The minimum acceptance ratio of these offers – relative to their given maximum power – can vary between 0.01 and 1 (commonly referred to as a fill-or-kill offer). Additionally, blocks can be *linked*, *flexible* or *exclusive*. Linked offers are sets of parent and child offers whose acceptance adheres to the following principles:

1. *"The acceptance ratio of a parent block is greater than or equal to the highest acceptance ratio of its child blocks (acceptance ratio of a child block can be at most the lowest acceptance ratio among own parent blocks)*
2. *(Possibly partial) acceptance of child blocks can allow the acceptance of the parent block when:*
   a) *the surplus of a family is non-negative*
   b) *leaf blocks (block order without child blocks) do not generate welfare loss*
3. *A parent block which is out-of-the-money can be accepted in case its accepted child blocks provide sufficient surplus to at least compensate the loss of the parent.*
4. *A child block which is out-of-the-money cannot be accepted even if its accepted parent provides sufficient surplus to compensate the loss of the child, unless the child block is in turn parent of other blocks (in which case rule 3 applies)."*[9]

[8](NEMO Committee, 2020)
[9]EUPHEMIA DOC CITATION

Essentially, a parent offer can be accepted even if it is out-of-the-money if the child offer(s) generate enough additional welfare, but not the other way around. A parent offer might represent a start-up cost, for instance. If the hours after the start-up occurs bring about enough surplus, the start-up offer can be accepted. However, the other offers can definitely not be accepted if the start-up offer is rejected.

Next we have flexible offers, which are defined for a single time step (and have a minimum acceptance ratio of 1, i.e. $q_o^{min} = q_o^{max}$), but can be accepted at any point of the day. Exclusive offers are a slightly more complex version of these, where they can be defined across multiple time steps and the sum of the acceptance ratios must be lower than one:

$$\sum_{o \in \mathcal{O}_{block}} \frac{q_o^{acc}}{q_o^{max}} \leq 1 \tag{4.3}$$

If the offers within a certain exclusive block have their own minimum acceptance ratio equal to 1, it means that among the block, only a single offer can be accepted.

For both complex and block offers, if they are out-of-the-money, they must be rejected, even if it leads to a lower market welfare. A block or complex offer that is accepted during the market clearing despite being out-of-the-money is referred to as a *paradoxically accepted* offer. We will discuss these a bit more in Appendix A. There are two additional offer types: Merit Orders and PUN Orders, which we will skip over for the moment as they are not directly relevant to the work presented in this chapter.

As a last note, in order for the solution to be perfectly reproducible, EUPHEMIA has developed criteria to differentiate between identical orders when necessary, first by timestep, then randomly by hash.

For the purposes of the work developed in this chapter, the block offers are particularly important to keep in mind. The full description of the market clearing algorithm can be found in Appendix A.

4.2.2 Recent Modifications of the Flow-based Method

4.2.2.1 Addition of HVDC Lines and PSTs in the Market Coupling

Since November of 2020, the set points of the new HVDC line, ALEGrO, between Germany and Belgium (the only grid asset between the two countries) have been integrated directly into the market coupling algorithm. The line runs from Oberzier in Germany (Amprion) to Lixhe in Belgium (Elia), as shown in Figure 4.4.

(Müller et al., 2017) were one of the first to present the methodology for the direct inclusion of HVDC lines. (Raths et al., 2021) present the particular characteristics of ALEGrO. The line is included through the creation of two virtual bidding zones (referred to as AL-DE and AL-BE in the CORE documentation (TSOs, 2018a)). Since November 2020, we can see the gradual increasing use of ALEGrO in the day ahead market coupling in Figure 4.5. [11]

4.2.2.2 70% Minimum RAM

From ***Regulation (EU) 2019/943 of the European Parliament and of the Council of 5 June 2019 on the internal market for electricity***:

[10] Image source: https://www.amprion.net/Grid-expansion/Our-Projects/ALEGrO/

[11] Note that there are of course other HVDC lines treated in the network capacity constrains. One of the novelties with the modelization of ALEGrO lies with its inclusion "in parallel" to the existing AC network. There are no AC interconnections between Belgium and Germany.

[12] Image source: (Raths et al., 2021)

Figure 4.4: ALEGrO [10]

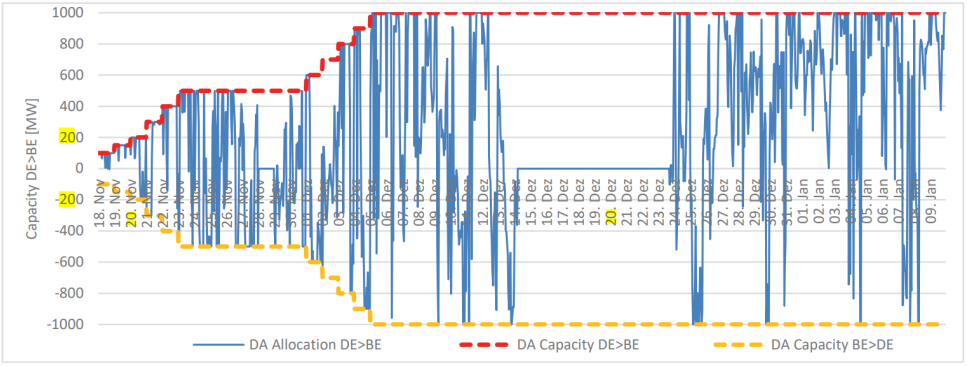

Figure 4.5: ALEGrO Day Ahead Limits and Allocations[12]

"*(27) Uncoordinated curtailments of interconnector capacities increasingly limit the exchange of electricity between Member States and have become a serious obstacle to the development of a functioning internal market for electricity. The maximum level of capacity of interconnectors and the critical network elements should therefore be made available, complying with the safety standards of secure network operation including respecting the security standard for contingencies (N-1). However, there are some limitations to setting the capacity level in a meshed grid. Clear minimum levels of available capacity for cross-zonal trade need to be put in place in order to reduce the effects of loop flows and internal congestions on cross-zonal trade and to give a predictable capacity value for market participants. Where the flow-based approach is used, that minimum capacity should determine the minimum share of the capacity of a cross-zonal or an internal critical network element respecting operational security limits to be used as an input for coordinated capacity calculation under Regulation (EU) 2015/1222, taking into account contingencies. The total remaining share of capacity may be used for reliability margins, loop flows and internal flows. Furthermore, in the case of foreseeable problems for ensuring grid security, derogations should be possible for a limited transitional phase. Such derogations should be accompanied by a methodology and projects providing for a long-term solution.*

...

8. Transmission system operators shall not limit the volume of interconnection capacity to be made available to market participants as a means of solving congestion inside their own bidding zone or as a means of managing flows resulting from transactions internal to bidding zones. Without prejudice to the application of the derogations under paragraphs 3 and 9 of this Article and to the application of Article 15(2), this paragraph shall be considered to be complied with where the following minimum levels of available capacity for cross-zonal trade are reached:

(a) for borders using a coordinated net transmission capacity approach, the minimum capacity shall be 70 % of the transmission capacity respecting operational security limits after deduction of contingencies, as determined in accordance with the capacity allocation and congestion management guideline adopted on the basis of Article 18(5) of Regulation (EC) No 714/2009;

b) for borders using a flow-based approach, the minimum capacity shall be a margin set in the capacity calculation process as available for flows induced by cross-zonal exchange. The margin shall be 70 % of the capacity respecting operational security limits of internal and cross-zonal critical network elements, taking into account contingencies, as determined in accordance with the capacity allocation and congestion management guideline adopted on the basis of Article 18(5) of Regulation (EC) No 714/2009."

As mentioned briefly in Section 3.3.3.4, since 2018 a lower limit on the branch limit margins has been put into place. The value of this lower limit was set at 20% of the F_{max} of each branch in 2019, with the above regulation, this was increased to 70% (although there is a transitional period, so not all TSOs are yet required to already fulfill the 70% rule completely). The physical sense of the value 70% is not specified. Indeed, the rule seems to be a step away from the physical grid constraints. While the flow-based method was put into place originally to better represent the physical limitations of the electricity network, the 70% minimum RAM rule aims to increase European exchanges with little thought to the security limits of the grid. In exploring these new regulations, (Schönheit et al., 2021a) found that – across a variety of tested variations (3 minimum RAM levels: 20%, 45% and 70%, with 3 GSK varieties) – "while the results confirm that the welfare of day-ahead market participants increases with growing minimum trading capacities, this is more than offset by rising congestion management costs in all cases, especially in the summer."

4.2.2.3 Addition of RAO

As described in the previous chapter (more precisely in Section 3.3.3.3), with the new CORE implementation of the flow-based method, an explicit remedial action optimization phase has been added. While this is a big step forward in some ways, it can have some negative impacts depending on the choices made in the definition of this stage. For instance, a global optimization of the remedial actions with an objective function that is poorly chosen will result in less remedial actions used than an operator might otherwise opt for.

For instance, a commonly used objective function would be to maximize the remaining available margin on the network element with the lowest margin:

$$\max \min_i (f_i^{max} - f_i) \tag{4.4}$$

If this objective function is applied carelessly to a geographic scale as large as the CORE region, it is likely to reduce the grid flexibility used. This occurs due to the fact that the grid flexibility options on one side of such a large area will have essentially no impact on network elements on the opposite side.

As the country that already applies easily the largest number of topological actions in Europe, France has the potential to have no remedial actions chosen by the algorithm as the grid is often more congested in areas that are farther away. This will render the flow-based domain smaller in this region of the domain. One potential solution to this problem would be to apply the multi-domain method described in this chapter. This is discussed in more detail in the next section.

4.3 Multidomain Approach

In order to combat some of the specific limits of the existing flow-based method, we propose an extension of the methodology, termed the *multidomain approach*. The method allows for a non-convex domain – the union of several convex flow-based security domains – that remains compatible with the existing market clearing algorithm, described above. In this way, the algorithm of the market clearing can arbitrate between the domains. If there is a high forecast error, a single flow-based domain may have artificially constrained the exchanges (or vice versa, allowed exchanges that are not feasible). It also allows for a choice of the set of remedial actions that best match the bids in the market. Additionally forecasts of redispatch costs can be included, allowing the arbitrage to include a potential redispatch cost. (Poplavskaya et al., 2020) discusses a method to include the effects of redispatch of a subset of plants in the market coupling. The authors found that integrating forecast redispatch costs into the day ahead flow-based market coupling (on a small 6-node case study) can have several benefits, including a simultaneous increase in day ahead cross-border trade and a reduction in the *ex post* redispatch volume and cost. Their proposed method relies on the selection of a set of generation units which can be used for *integrated redispatch*. These generators are not included in the GSK calculation (and are therefore their impact is not represented by the zonal PTDFs). Instead, their impact on the flow on the critical network elements is taken into account directly using nodal PTDFs.[13] The distinctions in the methods will be seen in the next sections.

4.3.1 Method Description

The multi-domain approach proposed in this work is a method to include a set of multiple flow-based domains in the market clearing, each computed with different base case forecasts (topology, generation, etc.) or different sets of respective optimal remedial actions, as demonstrated in Figure 4.6.

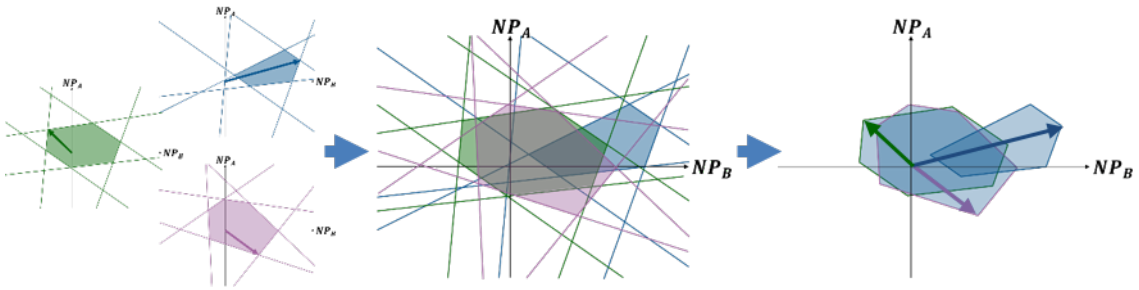

Figure 4.6: Multidomain Representation

The current proposed method for the inclusion of multiple flow-based domains in the market clearing algorithm is designed to function in EUPHEMIA, the existing market clearing algorithm in Europe. It

[13] A full comparison of the proposed multidomain approach and the integrated redispatch proposed in (Poplavskaya et al., 2020) should be performed. It does seem that the integrated redispatch model may have concerns with market power given to the generators that are set apart, although this should be confirmed.

relies on the creation of a set of virtual bidding zones containing block offers, which together perform the effect of a big-M optimization with binary variables. The market clearing algorithm will then choose the set of constraints that lead to the highest market welfare (defined as the sum of the profits of all the market players).

The method relies on the creation of several virtual bidding zones.

We can write the original flow-based constraint set as:

$$[\boldsymbol{PTDF}]_{CNEC\times BZ}\,[\boldsymbol{NP}]_{BZ\times 1} \leq [\boldsymbol{RAM}]_{CNEC\times 1}\,, \tag{4.5}$$

In a case with N^{MD} different flow-based domains, we create N^{VZ} virtual bidding zones (VBZ) (shown in Figure 4.7), such that:

$$card(N^{VZ}) = card(N^{MD}) + 1 \tag{4.6}$$

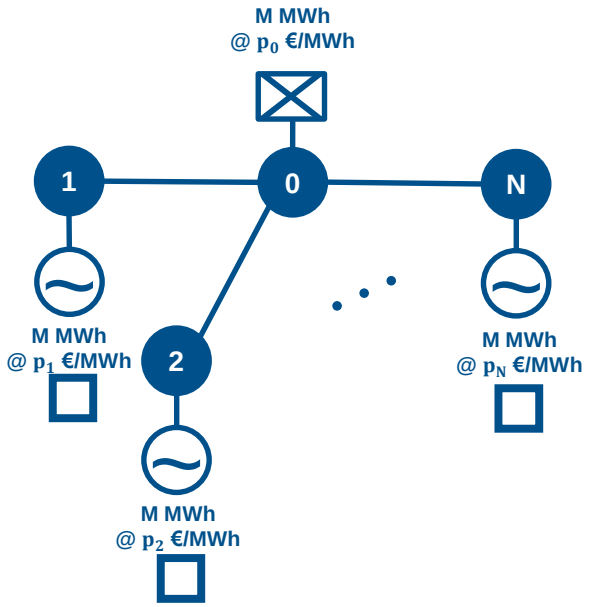

Figure 4.7: Virtual Bidding Zones

The PTDFs for these virtual bidding zones are defined as:

$$\left[\underbrace{\begin{bmatrix}\boldsymbol{PTDF_I}\\ \boldsymbol{PTDF_{II}}\\ \vdots\\ \boldsymbol{PTDF_{N_{md}}}\end{bmatrix}}_{\text{Original BZs}}\underbrace{\begin{bmatrix}0 & -1 & \cdots & -1\\ -1 & 0 & \cdots & -1\\ \vdots & \vdots & \ddots & \vdots\\ -1 & -1 & \cdots & 0\end{bmatrix}}_{\text{Virtual BZs}}\right]\begin{bmatrix}\boldsymbol{NP_{BZ}}\\ \boldsymbol{NP_{VZ}}\end{bmatrix} \leq \begin{bmatrix}\boldsymbol{RAM_I}\\ \boldsymbol{RAM_{II}}\\ \vdots\\ \boldsymbol{RAM_{N_{md}}}\end{bmatrix} \tag{4.7}$$

The new PTDF matrix now has the dimensions $[(CNEC * N^{MD}) \times (N^{BZ} + N^{VZ})]$. While this may seem like it would significantly increase the matrix size, it is important to remember that in practice, a presolve would be performed to each original PTDF matrix prior to aggregation of the PTDF matrices, so while the length may increase, it should not be unreasonably large for the market clearing algorithm.

If each domain is associated with only non-costly remedial actions, prices p_1-p_N would be set to 0. Price p_0 would ideally be set to a positive value to avoid any questions of paradoxically accepted block bids.

If, on the other hand, there is a flow-based domain that includes a forecast redispatch cost, we set the prices of the virtual bidding zones slightly differently to account for the cost arbitrage. The prices for the virtual production offers can be calculated as[14]:

$$p_{VZ} = \frac{c_{RA}}{M} \tag{4.8}$$

while the price for the virtual demand offer must be any number higher than the largest virtual block offer prices.

The following subsection will demonstrate the method for a 3-node, 3-zone system (e.g. no internal zonal networks) and two separate initial topology options. In the demonstration, a different base case topology is considered, but for simplicity, no preventive/curative remedial actions are considered.

4.3.2 Multi-domain Demonstration

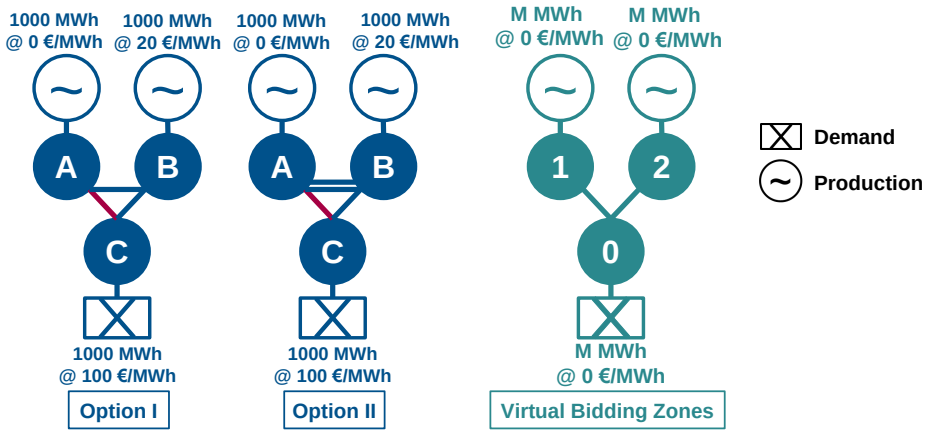

Figure 4.8: Multi-domain Demonstration System

To demonstrate the method, we take a 3-zone, 3-node system, where each node is in its own zone and there is no internal network. Impedances are equal. The zones are A, B, C, with one production offer in A of 1000 MWh at 0 €/MWh, one production offer in B of the same quantity at 20€/MWh and one demand offer in C for the same quantity at 100€/MWh. Therefore, ignoring network constraints, all production would be accepted in A. However, if we assume that the line A-C is constrained, some of the offer in B would be accepted.

Two topology options are considered in this demonstration, denoted as Option I and Option II in Fig. 4.8. If we take the line A-C (solely from A to C), we can write the flow-based constraints in the market clearing for the two topology options:

$$\text{Option I}: \frac{2}{3}NP_A + \frac{1}{3}NP_B \leq RAM^I_{AC} \tag{4.9}$$

$$\text{Option II}: \frac{3}{5}NP_A + \frac{2}{5}NP_B \leq RAM^I_{AC} \tag{4.10}$$

In order to include both constraints in the market clearing, we can employ binary variables multiplied by a value M, much larger than the RAM:

$$\text{Option I}: \frac{2}{3}NP_A + \frac{1}{3}NP_B \leq RAM^I_{AC} + \xi M \tag{4.11}$$

$$\text{Option II}: \frac{3}{5}NP_A + \frac{2}{5}NP_B \leq RAM^I_{AC} + (1-\xi)M \tag{4.12}$$

[14]Note that there are multiple ways to go about setting prices, see Appendix C for others.

In the existing market clearing algorithm, binary variables are associated with block offers—here defined as offers with a minimum power equal to their maximum power (see Section 4.2.1.1). To exploit these variables, we create a system of 3 virtual bidding zones—the number of domains to consider plus one. Two of these zones have block production offers of quantity M and one has a demand offer of the same quantity. We then define some PTDF factors that result in the following constraints:

$$\text{Option I}: \frac{2}{3}NP_A + \frac{1}{3}NP_B - NP_{VZ_2} \leq RAM^I_{AC} \tag{4.13}$$

$$\text{Option II}: \frac{3}{5}NP_A + \frac{2}{5}NP_B - NP_{VZ_1} \leq RAM^I_{AC} \tag{4.14}$$

If the block offer in virtual bidding zone 1 is accepted (implying that the block offer in zone 2 is rejected), the net position of zone 1 will be equal to M and that of zone 2 will be equal to 0, rendering the constraint of Option II non-constraining. As a similar reasoning applies for zone 2, the algorithm will thus include the set of constraints that allow for the highest market welfare.

This system was successfully tested in EUPHEMIA in a feasibility test, with 4 separate topologies and costly remedial actions as well. Costly remedial actions can be included by changing the prices of the offers in the virtual bidding zones. In this case, the market clearing algorithm will arbitrate between an increased market welfare and a potential cost.

4.3.3 Extended Case Studies and Method Validation

Several example cases were run directly in EUPHEMIA[15]. For each case, four topologies were considered, shown in Figure 4.9.

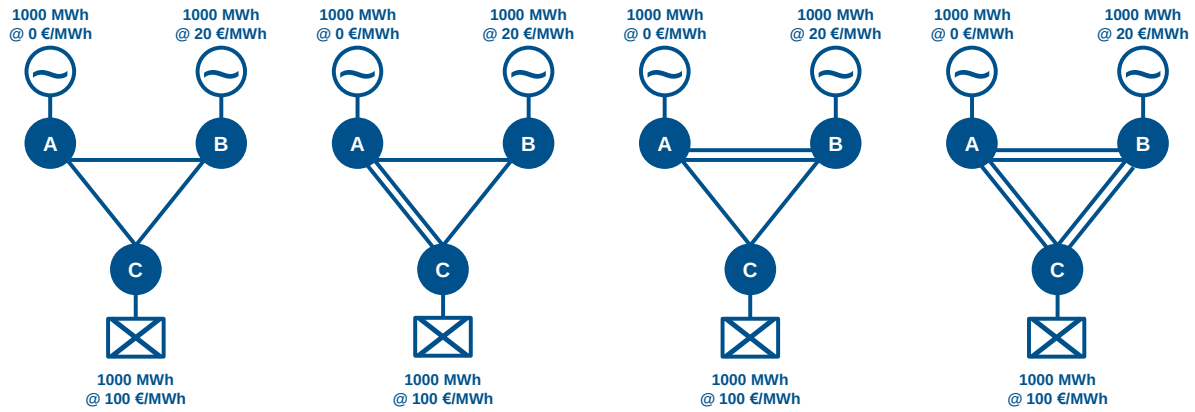

Figure 4.9: Four Topologies used in Method Validation

The first case tested considered no cost for the topological actions. The maximum market welfare of each topology is shown in Figure 4.10.

As described in the previous section, we represent each topology with a virtual bidding zone and a block offer, shown in Figure 4.11.

In the test cases, we consider only branch AC of the A-B-C topology as constraining. The constraints

[15]With the coordination of EPEX SPOT

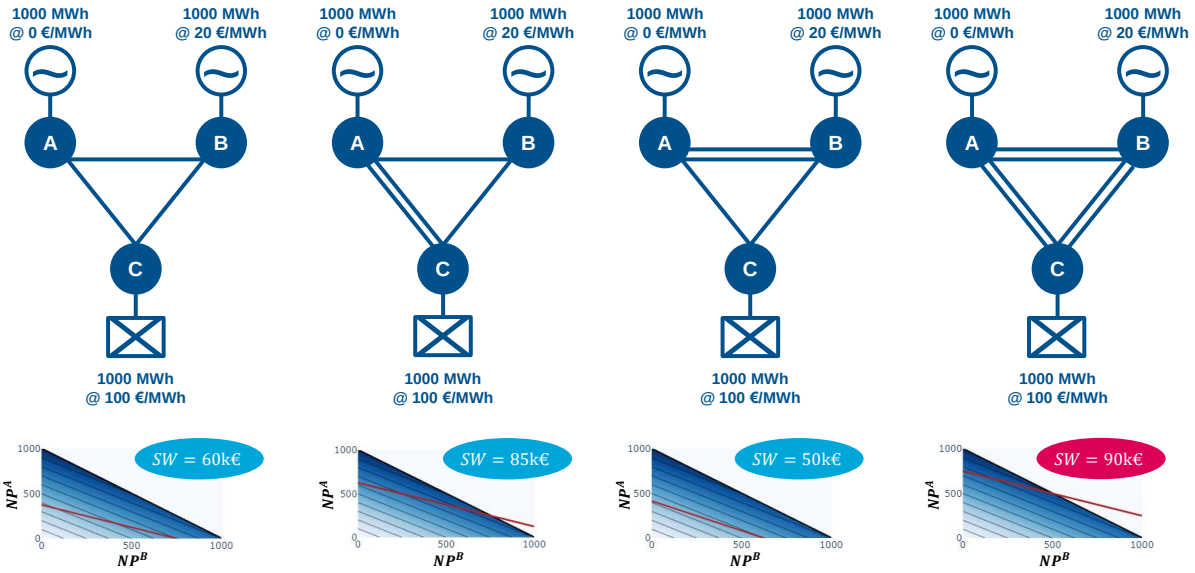

Figure 4.10: Four Topologies with Associated Market Welfare Values

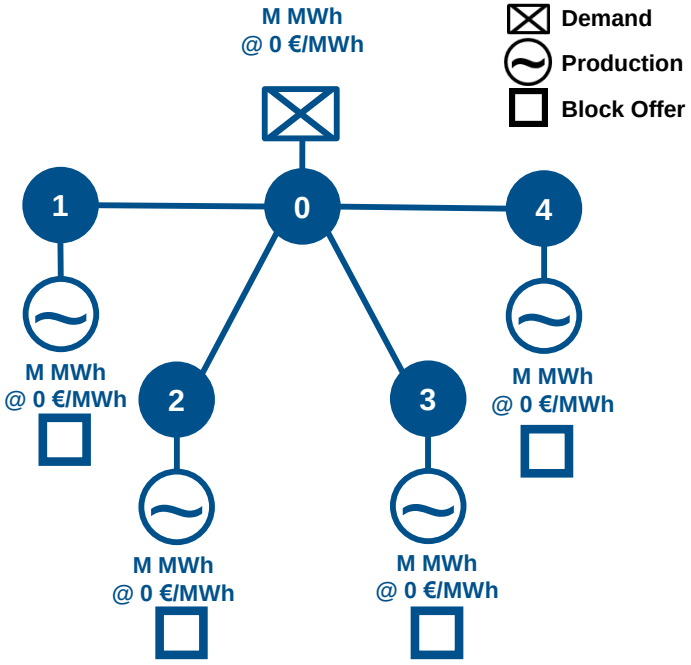

Figure 4.11: Virtual Bidding Zones for Four Topology Case

for this branch are:[16]

$$\text{Option I: } \frac{2}{3}NP^A + \frac{1}{3}NP^B - NP^{VZ_2} - NP^{VZ_3} - NP^{VZ_4} \leq RAM_{AC} \tag{4.15}$$

$$\text{Option II: } \frac{2}{5}NP^A + \frac{1}{5}NP^B - NP^{VZ_1} - NP^{VZ_3} - NP^{VZ_4} \leq RAM_{AC} \tag{4.16}$$

$$\text{Option III: } \frac{3}{5}NP^A + \frac{2}{5}NP^B - NP^{VZ_1} - NP^{VZ_2} - NP^{VZ_4} \leq RAM_{AC} \tag{4.17}$$

$$\text{Option IV: } \frac{1}{3}NP^A + \frac{1}{6}NP^B - NP^{VZ_1} - NP^{VZ_2} - NP^{VZ_3} \leq RAM_{AC} \tag{4.18}$$

[16] Note that there are actually two ways of forming the multidomain constraints. These are explained in Appendix C. While both methods were tested in EUPHEMIA, it remains to be seen if there is a computational benefit of one or the other.

Next, we can designate a representative cost for the action. In reality this could be used to represent a forecast redispatch, as deemed necessary by (Commission de Régulation de l'Electricité et du Gaz (CREG), 2019). For this example, we will continue to use the same four topologies, however this time with a cost associated, as shown in Figure 4.12.

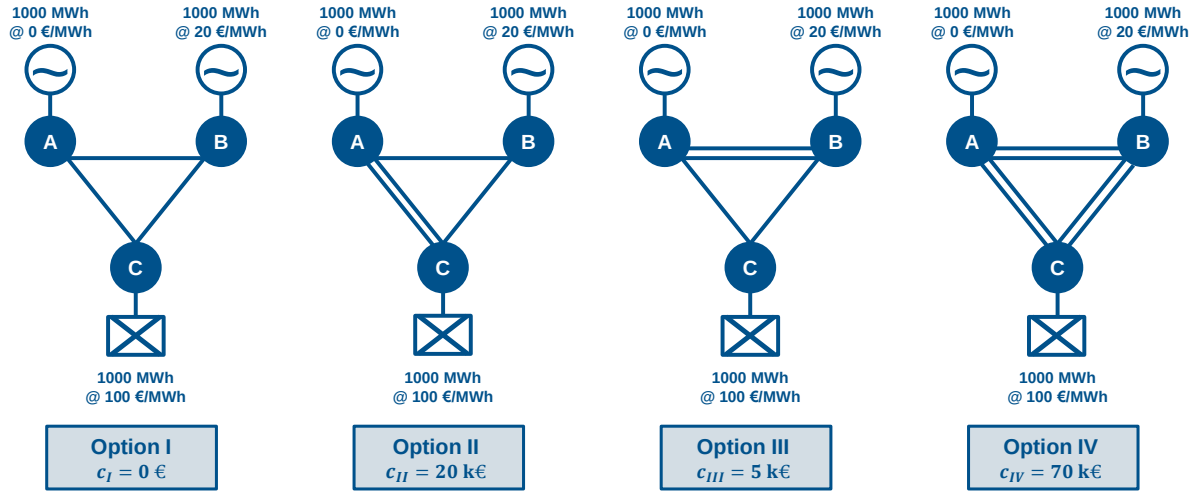

Figure 4.12: Four Topology Case with Associated Costs

We represent the cost of the additional remedial actions in the price of the block offers of the virtual bidding zones.

Four cases were tested in EUPHEMIA, shown in Table 4.2. The prices for the virtual production offers were calculated as:

$$p_{VZ} = \frac{c_{RA}}{M} \tag{4.19}$$

where M was 5000. To avoid paradoxically accepted block offers in the virtual bidding zone set, the virtual demand offer was at a price of 100€/MWh for Cases 2-4 (and 0 €/MWh for Case 1). This value is removed from the market welfare in the *Corrected SW* rows of Table 4.3. In each instance, EUPHEMIA selected the relevant topology (highlighted results in Table 4.3).

		Option 1	Option 2	Option 3	Option 4
Cost of RA [K€]	Case 1	0	0	0	0
	Case 2	0	20	0	70
	Case 3	5	70	0	70
	Case 4	10	35	0	39
Price of VZ Block Offer [€/MWh]	Case 1	0	0	0	0
	Case 2	0	4	0	14
	Case 3	1	14	0	14
	Case 4	2	7	0	7.8

Table 4.2: EUPHEMIA Test Input Data

Table 4.3 shows the market welfare for each case; first the total and then the corrected where the price of the virtual demand block offer multiplied by M is removed.

		Option 1	Option 2	Option 3	Option 4
Original SW (no cost) [k€]		60	85	50	90
Total SW [k€]	Case 1	60	85	50	90
	Case 2	560	565	550	520
	Case 3	555	515	550	520
	Case 4	550	550	550	551
Corrected SW [k€]	Case 1	60	85	50	90
	Case 2	60	65	50	20
	Case 3	55	15	50	20
	Case 4	50	50	50	51

Table 4.3: EUPHEMIA Test Results

4.3.4 Defining Multi-domains

The concept of multi-domains was developed as a solution to two issues: 1) If there is a high forecast error, the flow-based domain may have artificially constrained the exchanges (or vice versa, allowed exchanges that are not feasible) and, 2) Are the "best" group of remedial actions chosen? Could we have allowed a more optimal exchange with a different set of remedial actions (or even a different initial topology)? How to generate these domains is another discussion altogether. Several ideas will be proposed in this section. However, extended testing still needs to be performed on the different methods. Several were tested on the small RTS-GMLC network. Yes the size of the network – among other issues – led to inconclusive results in terms of quantification of the potential gain of the multidomain method.

4.3.4.1 Multiple Base cases

One idea for generating the non-convex flow-based domains – and perhaps the easiest to incorporate into the current calculation process – would be to identify different reference programs, and to generate a valid flow-based domain for each of them, as demonstrated in Figure 4.13. Currently the reference programs are chosen (as discussed in Section 3.3.2.1) based on a recent historical reference day that represents a similar demand profile. In practice, large differences have been seen between the reference program used to generate the flow-based domains and the zonal balances post-Market Clearing, leading to an incoherence in the constraints represented. This method could be expanded to more accurately represent different zonal balance profiles.

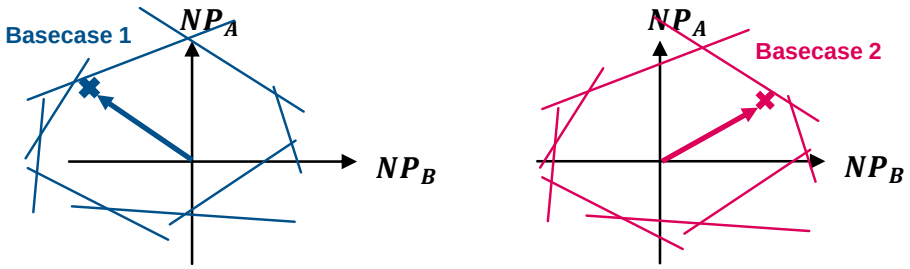

Figure 4.13: Net Position Method

As we saw in Section 3.4.1, it can be difficult to predict the impact a different reference might have on the corresponding flow-based domain. Figure 4.14 shows an example of this method. Each row of the figure corresponds to a different level of renewable penetration – the bottom row has two times the

installed capacity of wind of the top row. Interestingly, the domains are much larger for the same hour, but with more wind capacity. Each column of the image represents a different GSK calculation: first, calculated with respect to the base case generation (TargetP in Table 3.6), second, with respect to the maximum power available (MaxP in Table 3.6), and thirdly with load shift keys (LSK in Table 3.6). The small salmon point that is often outside the set of domains is the maximum social welfare point with no network constraints; in other words, the optimal point that the market clearing algorithm is aiming for. Each base case calculation for these examples was created using a standard DC-OPF, as explained in the previous chapters. However, the objective function was to maximize or minimize the net position of each zone. This represents an extreme application of this method of domain creation, in order to identify some of the possible limits of the method. The reference programs could also be chosen as today, through a set of historical data points with similar load or generation profiles, or using this same method, but setting the point to different percentages of these extreme net positions. For instance, instead of pushing the export and import quantities to the maximum values, it would be possible to calculate a maximum value, and rather run an OPF on a set reference program representing 25, 50 and 75% of the extreme net positions.

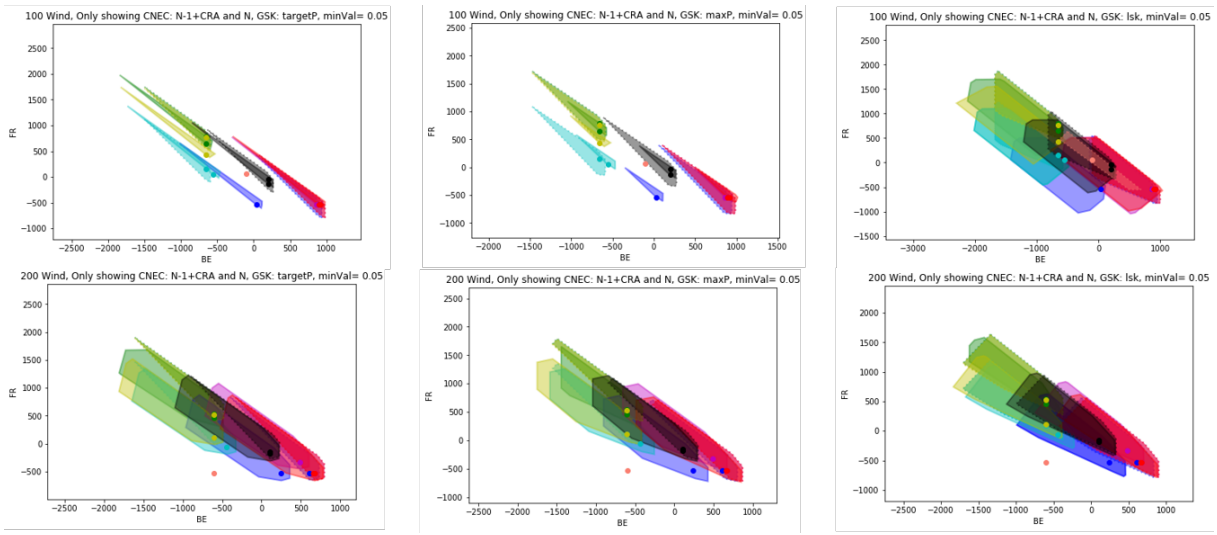

Figure 4.14: Net Position Method - Example

As we can see from the figure, this method can have some clear issues. First off, we can see a problem with the upper left and upper middle plots. This method can potentially lead to disjoint domains. While this is not particularly problematic algorithmically, it is somewhat perplexing. It would be quite difficult to explain to market participants why the points in between are inaccessible. Indeed, in those two plots, the optimal point is actually not included in any domain though we can hypothesize that if we selected not only the most extreme reference programs, but also those lying at different percentages, we would capture the optimal point in a domain.

4.3.4.2 Distributed Remedial Action Optimization

The idea that is perhaps the most promising would be to perform regional remedial action optimizations, each one corresponding to a different final domain. This method corresponds directly to the potential issue posed by the new Remedial Action Optimization stage of the CORE flow-based method. The current objective function may not be well calibrated for the system:

$$\max_i \min(f_i^{max} - f_i) \tag{4.20}$$

This method could be used one of two ways, either maintaining the same objective function but considering a subset of lines that are geographically relevant to each other for each domain or modifying the objective function.

This method could also include a forecast of the cost of remedial actions, potentially using a method similar to that discussed in Section 3.5. We recall that method here.

We can attempt to visualize this arbitrage a bit using the two different DC-OPF models described in the first chapter. The following plot, Figure 4.15 shows the optimal cost at each set of net positions. On the left is the version with all constraints (as well as optimal topology, but no N-1 or complex remedial actions as we have used elsewhere in this chapter) and on the right is the same plot, but this time, using the copper plate model, without network constraints. At each of the points in the graphic, an OPF was run, and the plots show a heat map of the optimal minimum dispatch cost, while forcing the zonal balance to the x and y values. The color scales are identical, with dark blue representing the lowest cost dispatch and red the highest. Finally, Figure 4.16 shows the difference between the two, in the feasible space of the network.

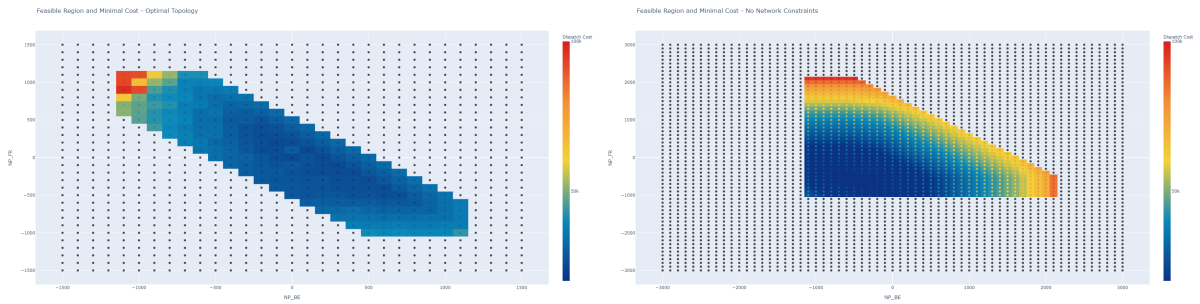

(a) DC-OPF with Optimal Topology Control (b) DC-OPF with No Network Constraints

Figure 4.15: Heatmap of Optimal Dispatch Cost at Set Net Positions

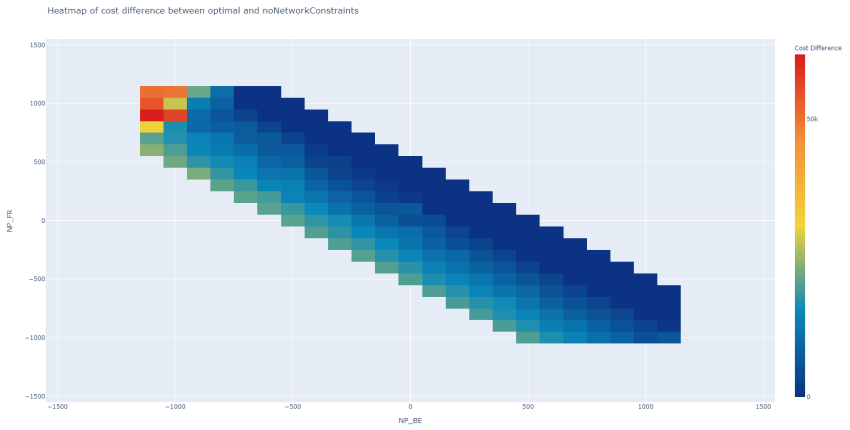

Figure 4.16: Difference in Optimal Dispatch Cost at Set Net Positions

What we see is that at the same set of net positions, we often have a difference in cost that comes from network constraints. Subplot 4.15b represents the social welfare (really the cost minimization, no load price) and shows where the market coupling will go with no network constraints. This means that the reduction of variable space to net positions can incur a cost even with a perfectly represented

flow-based domain, unless we consider a "perfect" flow-based domain as only covering the part of this plot where there is zero cost difference.

Essentially, if the flow-based domain covered only the dark blue area, there would be zero redispatch cost. As the colors lighten, there is an arbitrage between the two costs. This could be a potential way to forecast costly remedial actions. However, this approach must be used with caution. If the redispatch cost forecast is incorrect, the arbitrage will also be incorrect, leading to additional system costs.

4.3.4.3 Statistical Methods

Yet another proposal for defining the domains would be to use a statistical approach. To explore this option, an implementation of a k-medoids clustering[17] on the RTS-GMLC data over a full year in order to identify relevant flow-based domains. The definition of remedial actions for each one of these domains follows the current practice, and relies on the same computational tools presently used in the CORE parallel run.[18]

Following the base case calculation stage, clustering methods were applied to generate the multiple flow-based domains to be used in the flow-based market clearing. This is to ensure that the problem remains tractable by not including too many different flow-based domains. Additionally, this ensures that the set of flow-based domains given to the market clearing remain coherent with seasonal and hourly renewable and load curves.

This restricted set of flow-based domains is computed from a year of historical data which are meant to represent the variety of cases that can be encountered. For this purpose, a standard k-medoid clustering algorithm is used to group all the cases based on their similarity. The distance used to compare two cases is the Euclidean distance in the n-space made by the base case flows on each line of the system. The actual number of clusters is inferred via standard statistical metrics such as the "elbow" and the "average silhouette" methods.

Within each cluster, one can then compute the average distance between each member and all other cluster elements (i.e. the sum of distances divided by the number of elements minus 1). The medoid is by definition the cluster element with the smallest such distance.

Three typical base case hours are then chosen in each cluster: the one corresponding to the case of the medoid as well as those corresponding to the cases of the two elements with the greatest distance to all other elements. Thus for each hour of the year, we will calculate 4 flow-based domains: one corresponding to the current hour, and three resulting from the clustering phase, as shown in Figure 4.17.

For each hour of the year, four flow-based domains are calculated and submitted to the market clearing in the multi-domain (MD) case. The dispatch costs, both during the market coupling and redispatch phases are then calculated and compared to those for the same hour with only the flow-based constraints resulting from the initial hourly forecast. Fig. 4.18 shows a visualization of the 4 flow-based domains included through this approach for the first hour of the year. The figure shows the four original flow-based domains, which correspond to the following:

1. dom0: This is the flow-based domain calculated for the current hour of day ahead data.
2. dom1: This is the flow-based domain associated with the median typical day for the cluster where this hour is found.

[17] See (Zad et al., 2021) for a comparison of clustering techniques applied to flow-based domains.
[18] The documentation for this phase is described here: https://farao-community.github.io/docs/

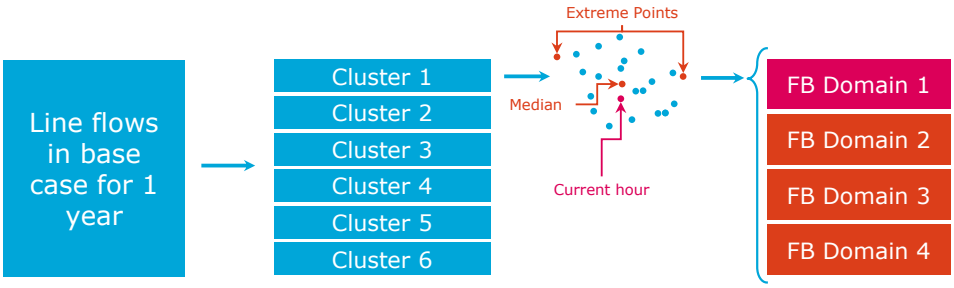

Figure 4.17: Clustering Method

3. dom2 and dom3: These two domains correspond with the hours in the same cluster, but with the largest distance from the medoid. In other words, these represent the extreme cases for a this particular adequacy case.

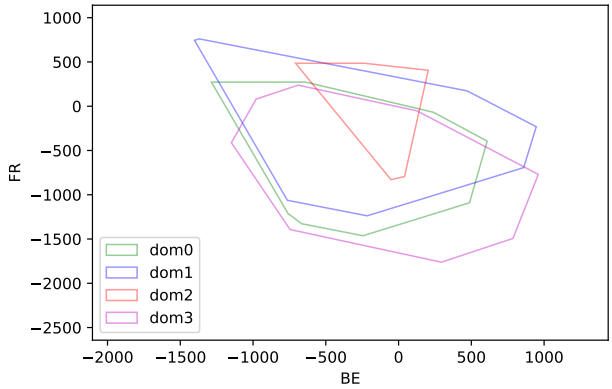

Figure 4.18: Multi-domains for January 1, 2020 at 1:00 AM

We can see that three of these domains are quite similar. There may be little added value to the market welfare depending on how the generation of the different cases is tuned.

4.4 Conclusion

In this chapter, we present a proposal for an updated version of the existing capacity calculation, allowing for improved integration of grid flexibility options and considering the operational complexities and existing market clearing algorithm. The method allows for the incorporation of a non-convex domain – the union of several convex flow-based security domains – that remains compatible with EUPHEMIA. In this way, the algorithm of the market clearing can arbitrate between the domains with different benefits. Three different potential methods for calculating these domains are presented: 1) Multiple Base Cases, 2) Distributed Remedial Action Optimization, or 3) Using a variety of statistical (or even chance-constrained) methods.

The multi-domain method was tested directly in EUPHEMIA and the expected welfare gains were found for several small case studies. The same tests were run through a similar market clearing model, part of the ATLAS project (described in Appendix B), in order to validate the ability of the internal model to correctly take into account block offers in the same manner as EUPHEMIA. Once again, the expected welfare gains were found.

The method proposed in this section allows for increased market welfare. However, the gain depends highly on the method chosen to define the different domains. Attempts were made to quantify the gain on a small test system (the RTS-GMLC). However, many pieces of this method still need to be tested on large-scale systems. For any quantification of the actual gains compared to the European system costs, the calculation of the different domains needs to be tested on real data. We have also found difficulties simulating these methods on test cases, since the base case itself is generated from an OPF. Even with some forecast error, this original base case (if calculated as we hope a base case would be calculated) will generally include the optimal market position. In other words, for a test case, it is difficult to have an original base case that is not already the "best" outcome. The next stage will be to test these on the European data in order to actually quantify the potential gain.

Chapter 5

Conclusion

This PhD work covers a wide view of the capacity calculation, allocation and congestion management topics in the context of the European zonal market. With the energy transition, more variable renewable production will be integrated into the energy system. This will lead to more variable power flows, inciting the need not only for grid infrastructure changes, but also the need to operate closer to the limits of the system.

With that in mind, **Chapter 2** began with a literature review on the impacts of incorporating grid flexibility methods. Next, it presented the relevant network models for this work and several variations that incorporate grid flexibility methods, in particular topology changes. Finally, it presented a case study on a small academic network with increasing variable renewable energy sources. While the benefits of optimal topology control are generally well known in the literature (see Section 2.1 for the literature review on this topic), this study explores how this gain is affected by this increasing variable production. The results, presented in Section 2.5 show that the gains from topological control actions increase significantly with the penetration of variable renewable energies. The study and conclusions in this chapter were performed with a DC-OPF and are therefore not exclusive to the European zonal model.

As variable renewable energies are added, we found an increasing gain from the integration of topological flexibilities (represented by binary control variables), from very little benefit in a system with mainly conventional production to a gain of over 7% of the production cost. While the ideal number of topological actions used increases with the penetration of wind generation, the economic benefit from their use increases along the same axis. In fact, an increase in wind production of a factor of 3 leads to a gain in total system cost by a factor of 3.4 from optimal use of topological controls.

Traditionally, there has been some pushback to market integration of topology optimization especially in nodal markets where switching a line or splitting a bus could render the FTR (Financial Transmission Rights) markets revenue inadequate (Hedman et al., 2011b). These results show that there will be more and more situations where system operators should be incentivized to use these mechanisms, whether for system security or economic reasons. Their development and integration with existing market designs is thus crucial as variable renewable energies become a larger percent of the dispatch.

Chapter 3 therefore goes into more detail regarding the existing European capacity calculation method: the flow-based method. In the first part of Chapter 3, we presented an overarching description of this method, first theoretical and then operational. The particularities and choices of the various European TSOs were explored through analysis of the historical CWE data. Several sources were cross-referenced in order to capture an accurate image of these inputs. Changes to the process since the expansion to

the CORE region were also addressed. The second part of Chapter 3 explored in more detail several of the input parameters of the flow-based method, in particular the type of modelization used for the creation of the base case, the Generation Shift Keys (GSKs), and some discussion on the inclusion of remedial actions at different phases of the process – both in the base case calculation and at the explicit remedial action phase.

This chapter presented a wide perspective around the existing capacity calculation method, beginning with an in-depth look at the operational constraints, specifically at the different applications of the method by the various TSOs. The gains from the integration of the flow-based method as the standard model for the highly-meshed European network are clear, both in the literature and the results from the parallel runs. One of the main focuses of this chapter is to clarify the level of standardization and the reasons for which a lack of harmonization can still be found regarding several of the flow-based parameters. For instance, the use of the external constraints is particular to the network characteristics of the specific TSO, while the most representative GSK may depend not only on the particular installed capacity of each TSO, but also on the hourly balance pattern.

We demonstrate the variety of impacts that can occur to modify the flow-based domain – taking into account more or less network constraints or flexibility, for instance. We show how temporal variations as well as different types of outage modelling in the base case might impact the resulting flow-based domain. More importantly, we show that just knowing the reference program (the set of zonal balances) is nowhere near enough information to try to forecast the similarities between different flow-based domains. Interestingly, in the same small case study network used in Chapter 2, we saw little overall welfare difference between GSK calculation methods when a redispatch phase was included. It will be important to validate these results on a real case study for this result to be fully conclusive.

Finally, in **Chapter 4**, we proposed an evolution of the existing flow-based method, that allows for the inclusion, for example, of non-convex topological changes and that is directly compatible with the existing European zonal flow-based market coupling. This method is referred to as the *multi-domain approach*.

In order to clearly show the context, this chapter began with a brief description of the Single Day Ahead Market Coupling (SDAC) algorithm, EUPHEMIA, presented in Section 4.2.1. This description specifically centered around the types of offers used in the clearing and that are necessary for the proposed methodological modifications. The multi-domain method was then described theoretically and in a small example.

The method allows for the incorporation of a non-convex domain – the union of several convex flow-based security domains – that remains compatible with EUPHEMIA. The method not only allows for the integration of binary topological controls to be integrated into the clearing, but also for costly remedial actions to be included. This allows the market clearing algorithm itself to arbitrate between the day ahead market welfare and a forecast redispatch cost. In this way, the algorithm of the market clearing can arbitrate between the domains with different benefits. Additionally, this method brings forward a potential solution to the issue of the global optimization of grid flexibility actions currently used in CORE (a weak point in the current method). Three different potential methods for calculating these domains were also presented: 1) Multiple Base Cases, 2) Distributed Remedial Action Optimization, or 3) Using a variety of statistical (or even chance-constrained) methods.

The multi-domain method was tested and validated directly in EUPHEMIA and the expected welfare gains were found for several small case studies. The same tests were run through a similar market clearing model, part of the ATLAS project (described in Appendix B), in order to validate the ability of the internal model to correctly take into account block offers in the same manner as EUPHEMIA.

Once again, the expected welfare gains were found. In following work, the gains from the multi-domain approach should be assessed using the three different methods of domain generation on a large-scale system.

5.1 Future Work

The main area of research to follow this body of work is to expand the geographical scale modeled, eventually leading to a parallel run phase that would include a comparison of the multi-domain approach to other similar approaches (for instance the one proposed by (Poplavskaya et al., 2020)). While it is clear that the multi-domain method can bring a certain market welfare gain, this value remains to be quantified at the European scale. In order to properly quantify any gains, these further simulations must include a redispatch phase (including non-costly remedial actions as well) to address any possible trade-offs from having a increased security domain for the day ahead market. While theoretically these domains should maintain the same level of risk as the current method of capacity calculation, this aspect should be tested and validated.

As part of this proposed parallel run, the performance of EUPHEMIA should be monitored to assess the operational feasibility of the method. The current proposed method was developed with the existing algorithm in mind. Looking even further forward, the algorithm of EUPHEMIA itself could be optimized to improve performance regarding the inclusion of the multi-domains.

Aside from the multi-domain method, extended case studies – also on a larger scale (and with a more realistic network) – should be performed to validate the somewhat surprising results found in Chapter 3 regarding the various generation shift key methods.

These extensions of the work presented in this thesis would serve to further advance European electricity system integration in the context of the necessary and impending energy transition.

Appendix A

EUPHEMIA

A.1 Algorithm

EUPHEMIA uses a branch-and-cut approach to solve a mixed integer quadratic program (MIQP). The program itself–shown in Figure A.1–is a single master problem (market welfare maximization, see Section A.1.1) with several sub-problems, two of which serve to generate the relevant cutting planes. The initial point is the solution to the welfare maximization with integer variables relaxed. Then, the problem branches by analyzing the 0/1 values of binary variables linked to violated constraints.

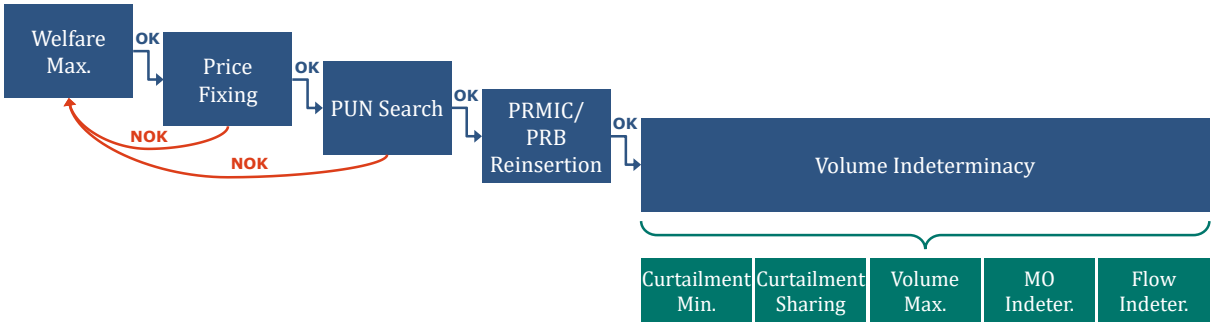

Figure A.1: EUPHEMIA Algorithm

We will not cover the PUN search in this section as it is not directly relevant to this work and requires quite a bit of explanation.[1]

A.1.1 Welfare Maximization

The clearing, or Welfare Maximization, is the classic economic dispatch problem. It has the constraints described above for the different offer types, zonal balance constraints and either the flow-based or ATC flow constraints. The objective function maximizes the total market welfare–the sum of the profits of all market players. It gives as an output the quantity accepted of each offer and the net positions of each bidding zone.

The full objective function, as given by (NEMO Committee, 2020) is:

$$\max f(x) \text{ where:}$$

[1]Note that these offers are specific to Italy.

$$f(x) = -\sum_{o\in\mathcal{O}_{step}} x_o p_o q_o \tag{A.1}$$

$$-\sum_{o\in\mathcal{O}_{lin}} x_o q_o (p_o^{min} + x_o \frac{p_o^{max} - p_o^{min}}{2}) \tag{A.2}$$

$$-\sum_{o\in\{\mathcal{O}_{BO},\mathcal{O}_{CO},\mathcal{O}_{MO}\}} x_o p_o q_o \tag{A.3}$$

$$-\sum_{k\in\mathcal{K}_t} Tariff_k FLOW_k \tag{A.4}$$

$$-M\sum_{o\in\mathcal{O}_{PTD}} |q_o|(1-x_o)^2 \tag{A.5}$$

where x_o ($\in [0,1]$) is the amount of the offered volume, q_o, accepted. The negative sign comes from the fact that q_o is defined as negative for purchase orders and positive for production offers. Parts A.1 and A.2 refer to the market welfare from the step and linear offers, while part A.3 refers to the same for block offers, complex offers and merit orders. We can see that due to part A.2, the objective function is quadratic. Part A.4 is a reduction of market welfare that occurs for certain HVDC lines operated by external companies who implement tariffs relative to the flow on the line. Finally, part A.5 is an additional term that is equivalent to minimizing curtailment in a unit commitment model. It regards $\mathcal{O}_{PTD}$, the set of price-taking demand offers that might be rejected. This term comes back into play later in the Volume Indeterminacy sub-problem.

A.1.2 Price Fixing

In a perfect world, the pricing is the dual of the clearing problem, where the zonal prices are the dual variables associated with the zonal balance constraint (just as nodal prices would be the dual variable associated with the nodal balance constraint). However, certain additional constraints are added to the pricing phase, notably the concrete rejection of paradoxically accepted offers.[2] The objective function is also modified to:

$$\min \sum_{\substack{z\in\mathcal{Z}\\ t\in\mathcal{T}}} \left(\lambda_{z,t} - \frac{p_{z,t}^{UB} + p_{z,t}^{LB}}{2}\right)^2 \tag{A.6}$$

where $p_{z,t}^{UB}$ and $p_{z,t}^{LB}$ are calculated as:

$$p_{z,t}^{UB} := \min(\text{Min. Rejected Sale Price}, \text{Min. Accepted Purchase Price}) \tag{A.7}$$

$$p_{z,t}^{LB} := \max(\text{Max. Accepted Sale Price}, \text{Max. Rejected Purchase Price}) \tag{A.8}$$

The colors here correspond to those offers shown in Figure A.2.

In most cases, the objective function will go to zero, and is not necessary. However, it is crucial for points when the volume offered matches identically, as in Figure A.3; otherwise, the price could theoretically be found at any point along the volume acceptance line.

The price fixing tries to find a market clearing price for each zone that corresponds to the solution found in the welfare maximization stage AND that has no paradoxically accepted offers. If this is infeasible, the algorithm returns to the welfare maximization problem and introduces a cutting plane. The PUN search is similar–if the solution found in the first stage is not feasible with the additional constraints on PUN offers, the algorithm agains returns to the master problem.

[2] See Annex B of (NEMO Committee, 2020) for clarification on the relation of the primal/dual problems.

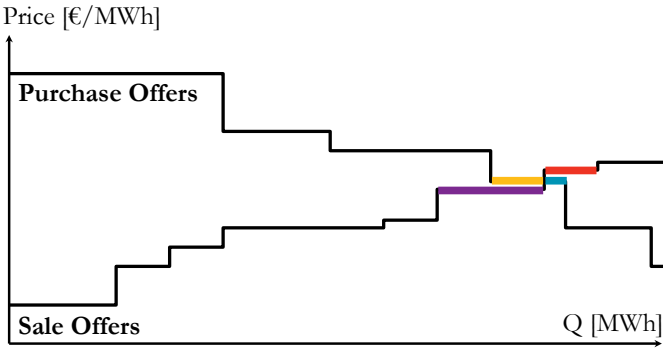

Figure A.2: Upper and Lower Price Bounds

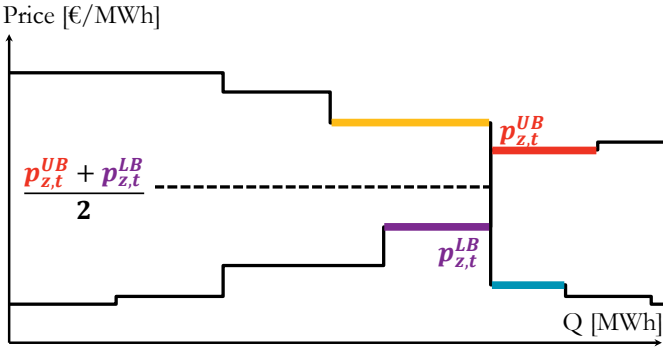

Figure A.3: Reasoning for Pricing Objective Function

A.1.3 PRMIC/PRB Reinsertion

In this phase, EUPHEMIA takes the list of paradoxically rejected minimum income condition offers (PRMIC) and paradoxically rejected block offers (PRB) and iteratively tests them. Each offer is accepted, and the clearing and price fixing modules are rerun. If the market welfare is not reduced and the price fixing is feasible, the offer is accepted. Otherwise, it is rejected.

A.1.4 Volume Indeterminacy

The Volume Indeterminacy module aims to differentiate between solutions that have the same market welfare. It comprises five smaller optimization problems:

1. Curtailment Minimization
2. Curtailment Sharing
3. Volume Maximization
4. Merit Order Indeterminacy
5. Flow Indeterminacy

Curtailment Minimization and **Curtailment Sharing** deal with times when the market clearing price of a zone is set at the maximum (or minimum) permitted price and the offers at this price are not fully accepted. This quantity is first minimized, then, if there remains some volume curtailed, it is shared as equally as possible amongst the bidding zones, while respecting network constraints.

The **Volume Maximization** problem is the next step. As shown in Figure A.4, some marginal offers might not be fully accepted as the acceptance of these offers does not change the market welfare.

The idea here is to maximize the number of offers accepted given the previously-found solution. An example of a case where this is necessary is demonstrated in Figure A.4. This step finds these marginal orders and accepts the available volume at the market price.

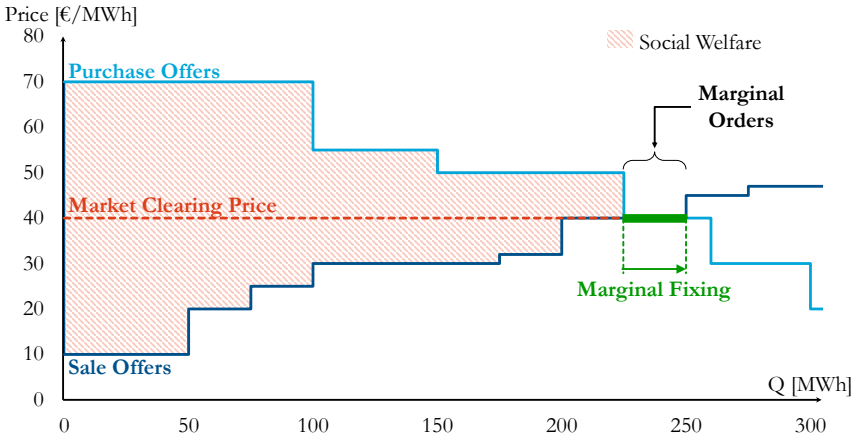

Figure A.4: Marginal Fixing Example

Merit Order Indeterminacy deals with merit order numbers, which are out of the scope of this work.

Finally, the **Flow Indeterminacy** stage occurs. Since the clearing module concentrates on associating sellers and buyers, it may not accurately represent the physical flows through the network. This phase is thus in place to better model these real physical flows. It does this by minimizing the exchanges through the market borders while retaining the solution found by the clearing module. The objective function is laid out in A.9:

$$\min \sum_{\substack{mb_l \in MB \\ t_i \in T}} \alpha \left| \Delta q_{li}^{mb,e} \right| + \beta \left(\Delta q_{li}^{mb,e} \right)^2 \tag{A.9}$$

where $\Delta q_{li}^{mb,e}$ is the exchange on a market border, and α and β are terms parametrizing the linear and quadratic terms. The constraints for this phase are essentially the same as the balance constraints and the cross-border constraints for the welfare maximization module, only now the computed local balances are parameters, rather than variables.

Appendix B

ATLAS Model

ATLAS is a model developed by RTE to simulate different market phases.

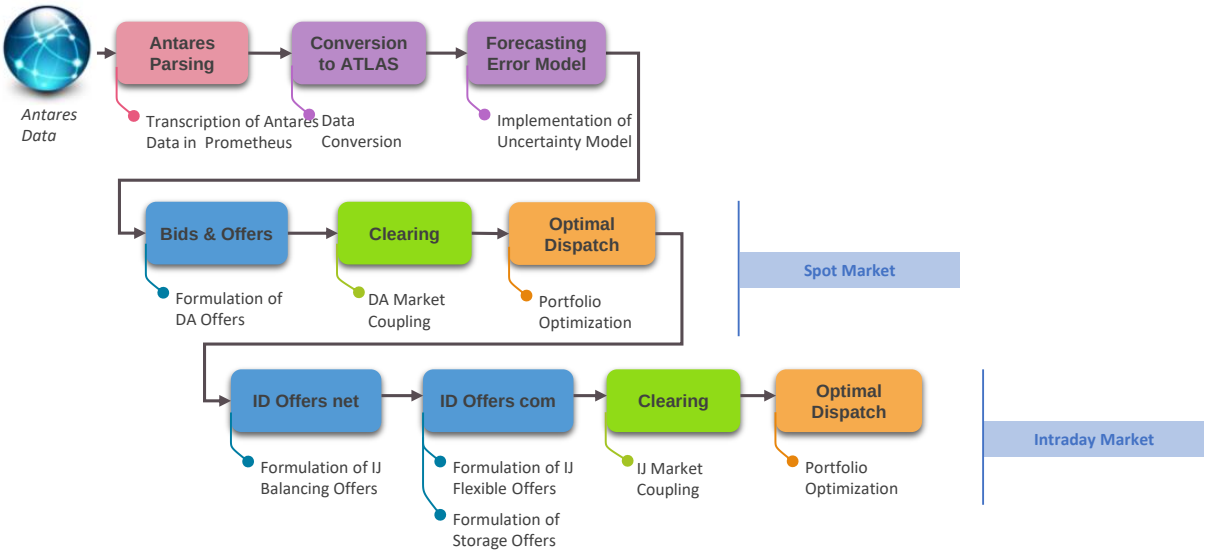

Figure B.1: ATLAS

The only module of this model that was used in these studies was the market clearing algorithm. The differences compared to EUPHEMIA are described in the next section. The data schema for these models in shown in Figure B.4.

B.1 Market Clearing Algorithm

The market clearing algorithm used within ATLAS (Figure B.2) is similar to EUPHEMIA, although some pieces are treated mildly differently. For instance, only some parts of the Volume Indeterminacy module (Section A.1.4) were added. The Exchange Minimization is similar to the Flow Indeterminacy sub-problem, while the Marginal Fixing module of ATLAS corresponds to the Volume Maximization piece of the Volume Indeterminacy module. Additionally, it relies on the use of commercial solvers, rather than the specific branch-and-cut developed in EUPHEMIA. It also does not include linear offers that would render the problem quadratic, and thus solves a MILP.

The Market Clearing model of ATLAS is broken down into four main modules (see Figure B.2): 1)

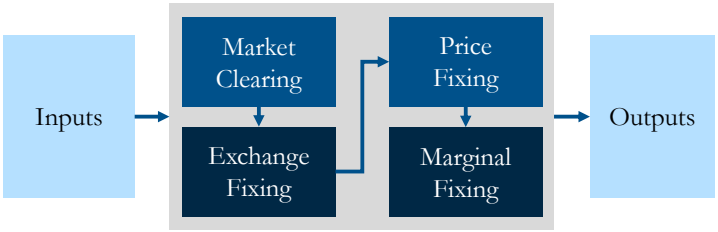

Figure B.2: Model Structure

the Clearing phase, 2) the Exchange Fixing phase, 3) the Price Fixing phase, and 4) the Marginal Fixing phase. The Clearing phase is the primal problem, with the Price Fixing as its dual. The other two modules are sub-problems, used to improve the solution generated by the Clearing module, and representing two pieces of the Volume Indeterminacy sub-problem of EUPHEMIA (Section A.1.4).

B.2 PROMETHEUS Platform

The ATLAS model was developed using an online platform known as PROMETHEUS, an integrated platform developed at RTE for simulating energy systems. It allows for flexible modeling across any time frame and enables the user to create multiple prototypes and processes and link them together to simulate a variety of market designs. Figure B.3 shows an example workflow, demonstrating a sequential market test.

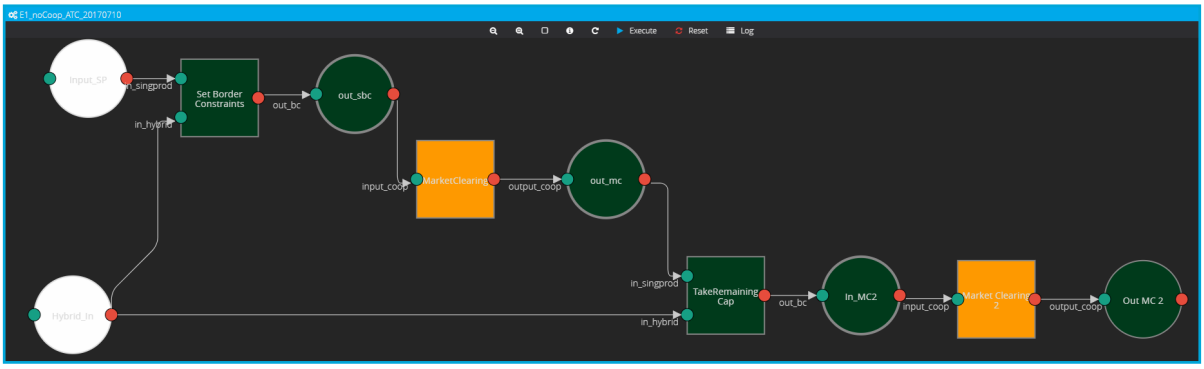

Figure B.3: PROMETHEUS Workflow for Sequential Market Design

Each circle in Figure B.3 represents a packet of data with all or some of the data described in Figure B.4. The data is carried through a variety of different prototypes represented by the square boxes. Each workflow can also integrate different conditions and loops to follow a variety of paths and studies.

Several solvers are integrated with the PROMETHEUS Platform, including (but not limited to):

1. GLPK (GNU Linear Programming Kit)[1]
2. SCIP (Solving Constraint Integer Programs)[2].

[1]For more information on GLPK: https://www.gnu.org/software/glpk/#documentation
[2]For more information on SCIP: https://www.scipopt.org/

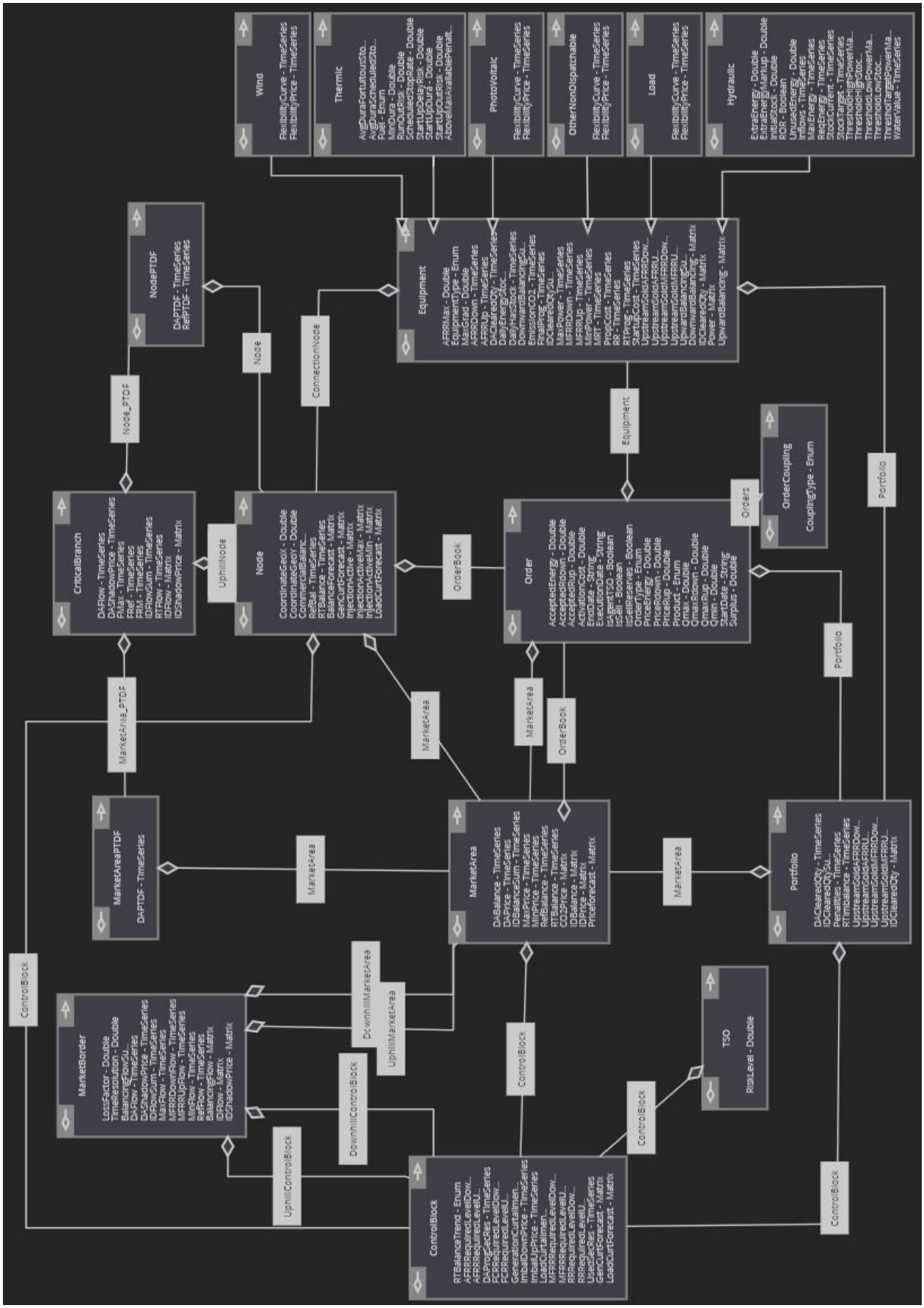

Figure B.4: ATLAS Data Format

Appendix C

Multidomain Calculation

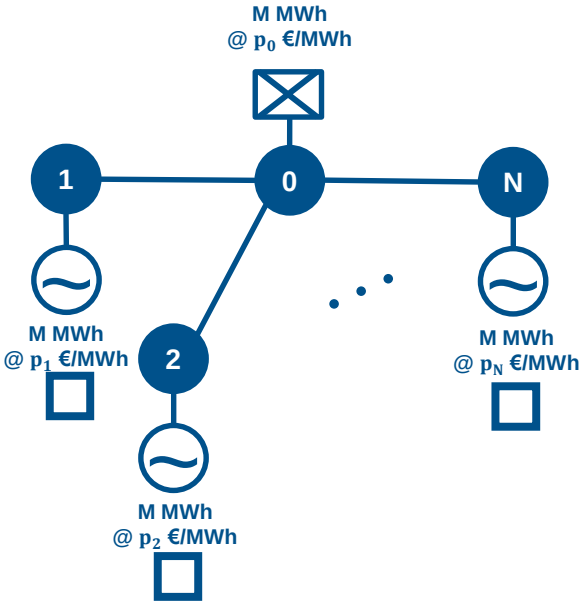

Figure C.1: General Form of Virtual Bidding Zone Structure

C.1 Method I: Virtual production offer accepted represents the chosen topology

$$\text{Option I: } \frac{2}{3}NP^A + \frac{1}{3}NP^B \qquad - NP^{VZ_2} - \ldots - NP^{VZ_N} \leq RAM_{AC} \tag{C.1}$$

$$\text{Option II: } \frac{2}{5}NP^A + \frac{1}{5}NP^B - NP^{VZ_1} \qquad - \ldots - NP^{VZ_N} \leq RAM_{AC} \tag{C.2}$$

$$\vdots \qquad \ddots \qquad \vdots \tag{C.3}$$

$$\text{Option N: } \frac{1}{3}NP^A + \frac{1}{6}NP^B - NP^{VZ_1} - NP^{VZ_2} - \ldots \qquad \leq RAM_{AC} \tag{C.4}$$

$$\left[\underbrace{\begin{bmatrix}\boldsymbol{PTDF_I}\\ \boldsymbol{PTDF_{II}}\\ \vdots\\ \boldsymbol{PTDF_N}\end{bmatrix}}_{\text{Original BZs}}\underbrace{\begin{bmatrix}0 & -1 & \cdots & -1\\ -1 & 0 & \cdots & -1\\ \vdots & \vdots & \ddots & \vdots\\ -1 & -1 & \cdots & 0\end{bmatrix}}_{\text{Virtual BZs}}\right]\begin{bmatrix}\boldsymbol{NP_{BZ}}\\ \boldsymbol{NP_{VZ}}\end{bmatrix}\leq\begin{bmatrix}\boldsymbol{RAM_I}\\ \boldsymbol{RAM_{II}}\\ \vdots\\ \boldsymbol{RAM_N}\end{bmatrix} \tag{C.5}$$

C.1.1 With Costs

$$p_o \geq p_1, p_2, \ldots, p_N \tag{C.6}$$

$$p_i = \frac{c_i}{M} \tag{C.7}$$

C.2 Method II: Virtual production offer rejected represents the chosen topology

$$\text{Option I: } \frac{2}{3}NP^A + \frac{1}{3}NP^B - NP^{VZ_1} \leq RAM_{AC} \tag{C.8}$$

$$\text{Option II: } \frac{2}{5}NP^A + \frac{1}{5}NP^B - NP^{VZ_2} \leq RAM_{AC} \tag{C.9}$$

$$\vdots \qquad \ddots \quad \vdots \tag{C.10}$$

$$\text{Option N: } \frac{1}{3}NP^A + \frac{1}{6}NP^B - NP^{VZ_N} \leq RAM_{AC} \tag{C.11}$$

$$\left[\underbrace{\begin{bmatrix}\boldsymbol{PTDF_I}\\ \boldsymbol{PTDF_{II}}\\ \vdots\\ \boldsymbol{PTDF_N}\end{bmatrix}}_{\text{Original BZs}}\underbrace{\begin{bmatrix}-1 & 0 & \cdots & 0\\ 0 & -1 & \cdots & 0\\ \vdots & \vdots & \ddots & \vdots\\ 0 & 0 & \cdots & -1\end{bmatrix}}_{\text{Virtual BZs}}\right]\begin{bmatrix}\boldsymbol{NP_{BZ}}\\ \boldsymbol{NP_{VZ}}\end{bmatrix}\leq\begin{bmatrix}\boldsymbol{RAM_I}\\ \boldsymbol{RAM_{II}}\\ \vdots\\ \boldsymbol{RAM_N}\end{bmatrix} \tag{C.12}$$

C.2.1 With Costs

$$p_o \geq p_1, p_2, \ldots, p_N \tag{C.13}$$

$$p_i = \frac{1}{M(N-1)}\left(-(N-2)c_i + \sum_{j\in VZ\setminus\{i\}} c_j\right) \tag{C.14}$$

C.3 Comparison

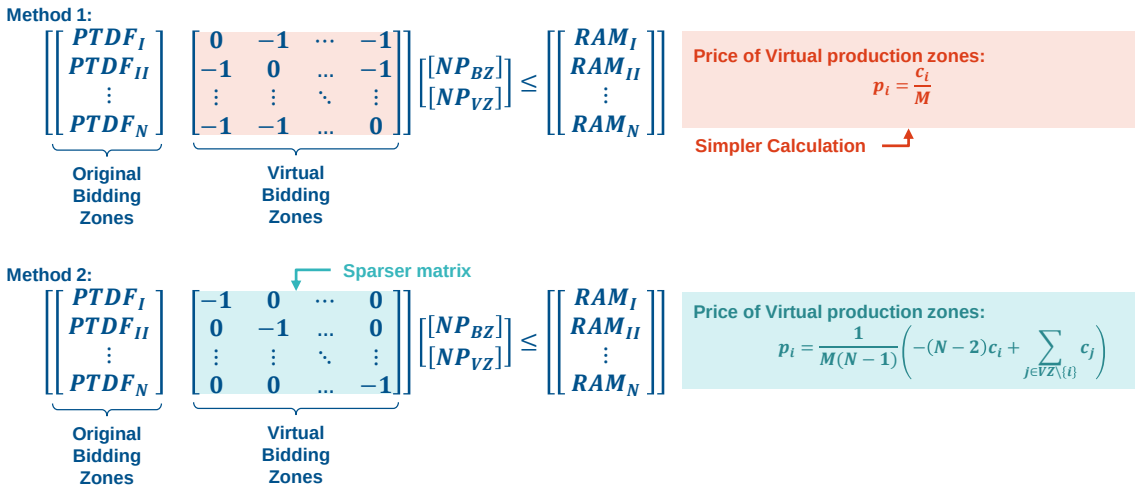

Figure C.2: Comparison of Multi-domain Calculation Methods

Appendix D

TSO Names and Acronyms

From: https://www.entsoe.eu/about/inside-entsoe/members/

	Country	TSO Full Name	TSO Short Name
AT	Austria	Austrian Power Grid AG Vorarlberger Übertragungsnetz GmbH	APG VUEN
AL	Albania	OST sh.a – Albanian Transmission System Operator	OST
BA	Bosnia and Herzegovina	Nezavisni operator sustava u Bosni i Hercegovini	NOS BiH
BE	Belgium	Elia System Operator SA	Elia
BG	Bulgaria	Electroenergien Sistemen Operator EAD	ESO
CH	Switzerland	Swissgrid ag	Swissgrid
CY	Cyprus	Cyprus Transmission System Operator	Cyprus TSO
CZ	Czech Republic	ČEPS a.s.	ČEPS
DE	Germany	TransnetBW GmbH TenneT TSO GmbH Amprion GmbH 50Hertz Transmission GmbH	TransnetBW TenneT DE Amprion 50Hertz
DK	Denmark	Energinet	Energinet.dk
EE	Estonia	Elering AS	Elering AS
ES	Spain	Red Eléctrica de España S.A.	REE
FI	Finland	Fingrid Oyj	Fingrid
FR	France	Réseau de Transport d'Electricité	RTE
GR	Greece	Independent Power Transmission Operator S.A.	IPTO
HR	Croatia	HOPS d.d.	HOPS
HU	Hungary	MAVIR Magyar Villamosenergia-ipari Átviteli Rendszerirányító Zártkörűen Működő Részvénytársaság	MAVIR ZRt.
IE	Ireland	EirGrid plc	EirGrid
IS	Iceland	Landsnet hf	Landsnet
IT	Italy	Terna - Rete Elettrica Nazionale SpA	Terna
LT	Lithuania	Litgrid AB	Litgrid
LU	Luxembourg	Creos Luxembourg S.A.	Creos Luxembourg
LV	Latvia	AS Augstsprieguma tīkls	AST

ME	Montenegro	Crnogorski elektroprenosni sistem AD	Crnogorski elektro-prenosni sistem
NI	Northern Ireland[1]	System Operator for Northern Ireland Ltd	SONI
NL	Netherlands	TenneT TSO B.V.	TenneT NL
NO	Norway	Statnett SF	Statnett
MK	Republic of North Macedonia	Transmission System Operator of the Republic of North Macedonia	MEPSO
PL	Poland	Polskie Sieci Elektroenergetyczne S.A.	PSE S.A.
PT	Portugal	Rede Eléctrica Nacional, S.A.	REN
RO	Romania	C.N. Transelectrica S.A.	Transelectrica
RS	Serbia	Akcionarsko društvo Elektromreža Srbije	EMS
SE	Sweden	Svenska Kraftnät	SVENSKA KRAFTNÄT
SI	Slovenia	ELES, d.o.o.	ELES
SK	Slovak Republic	Slovenská elektrizačná prenosová sústava, a.s.	SEPS
		Observer Member as of April 2022	
UA	Ukraine	National Power Company Ukrenergo	Ukrenergo

[1] In compliance with 12 February 2021 EC Notice to Stakeholders on the Withdrawal of the UK and EU rules in the field of the Internal Energy Market

Appendix E

Additional Figures

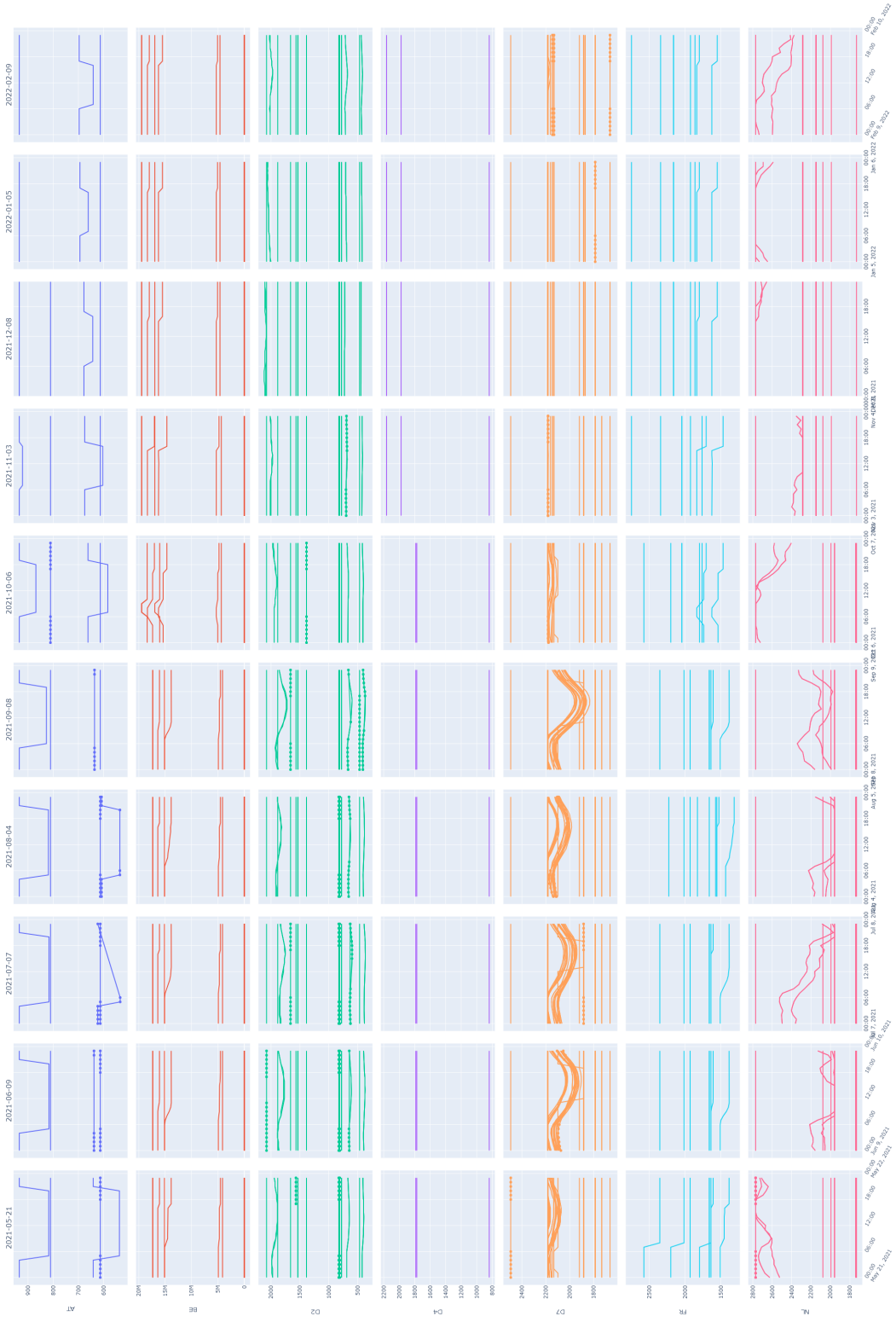

Figure E.1: Fmax by TSO for 10 Sample Dates

Figure E.2: FR-DE Zone-to-Zone PTDFs by TSO for 10 Sample Dates

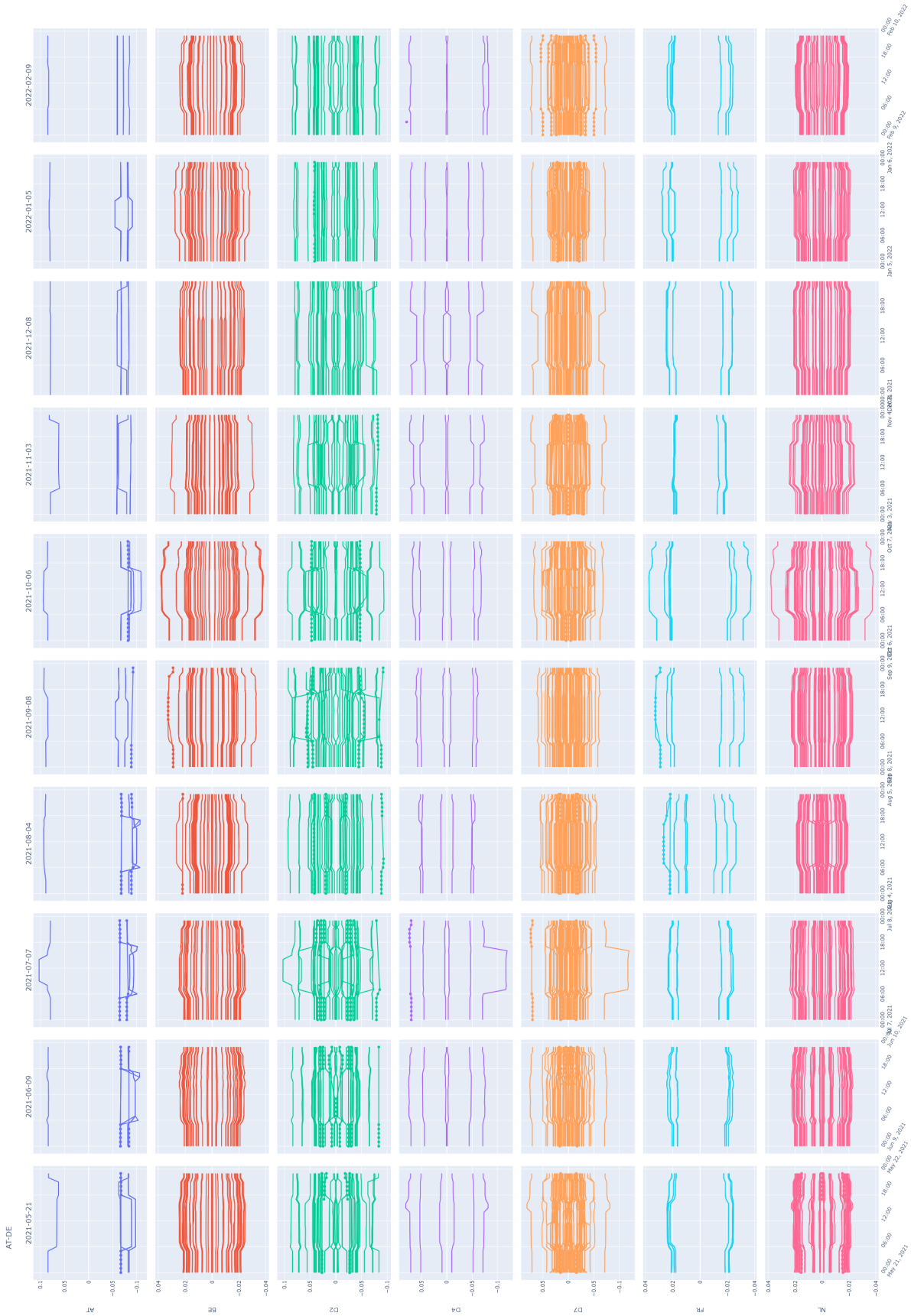

Figure E.3: AT-DE Zone-to-Zone PTDFs by TSO for 10 Sample Dates

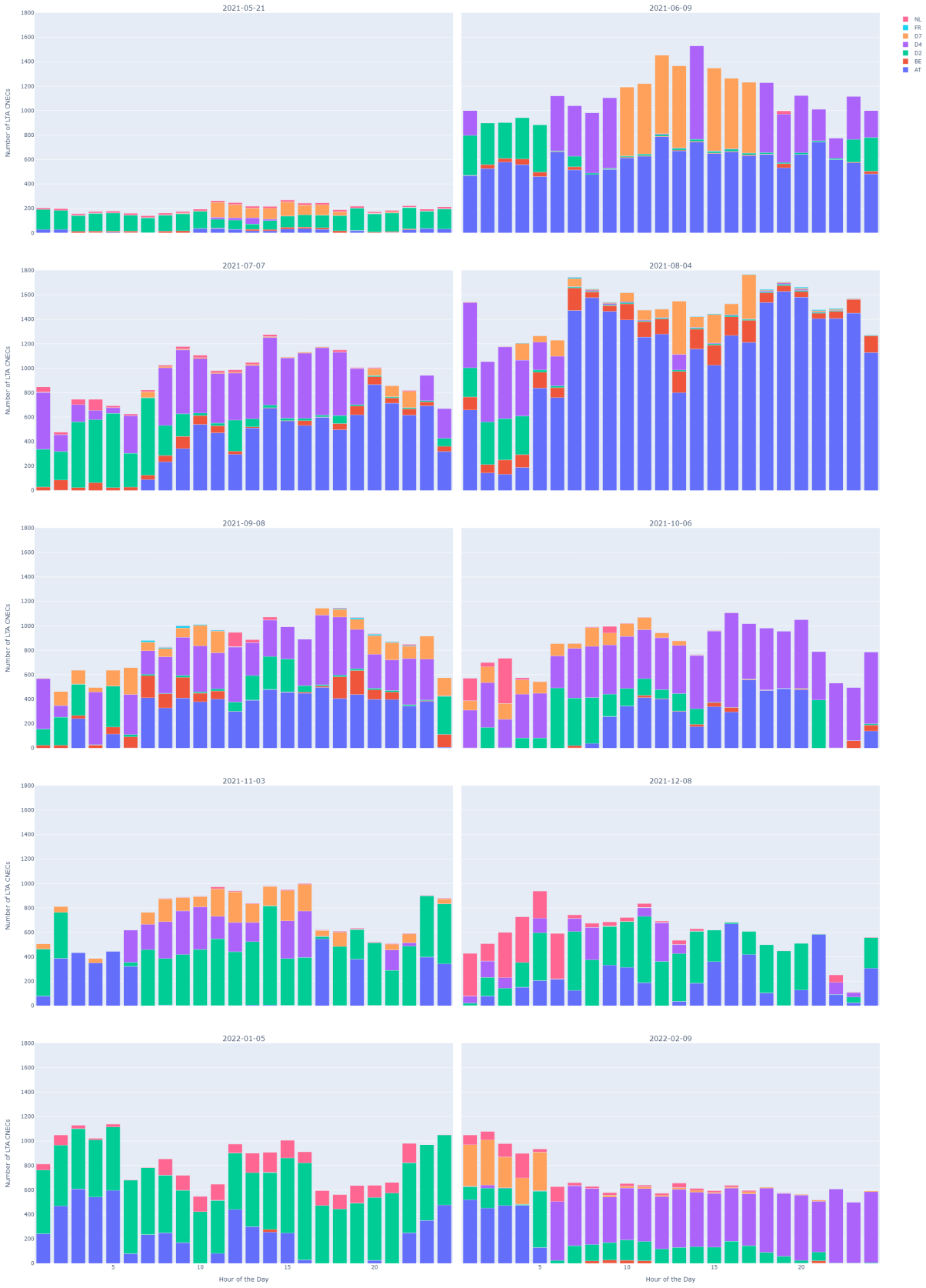

Figure E.4: Number of LTA CNECs for each TSO

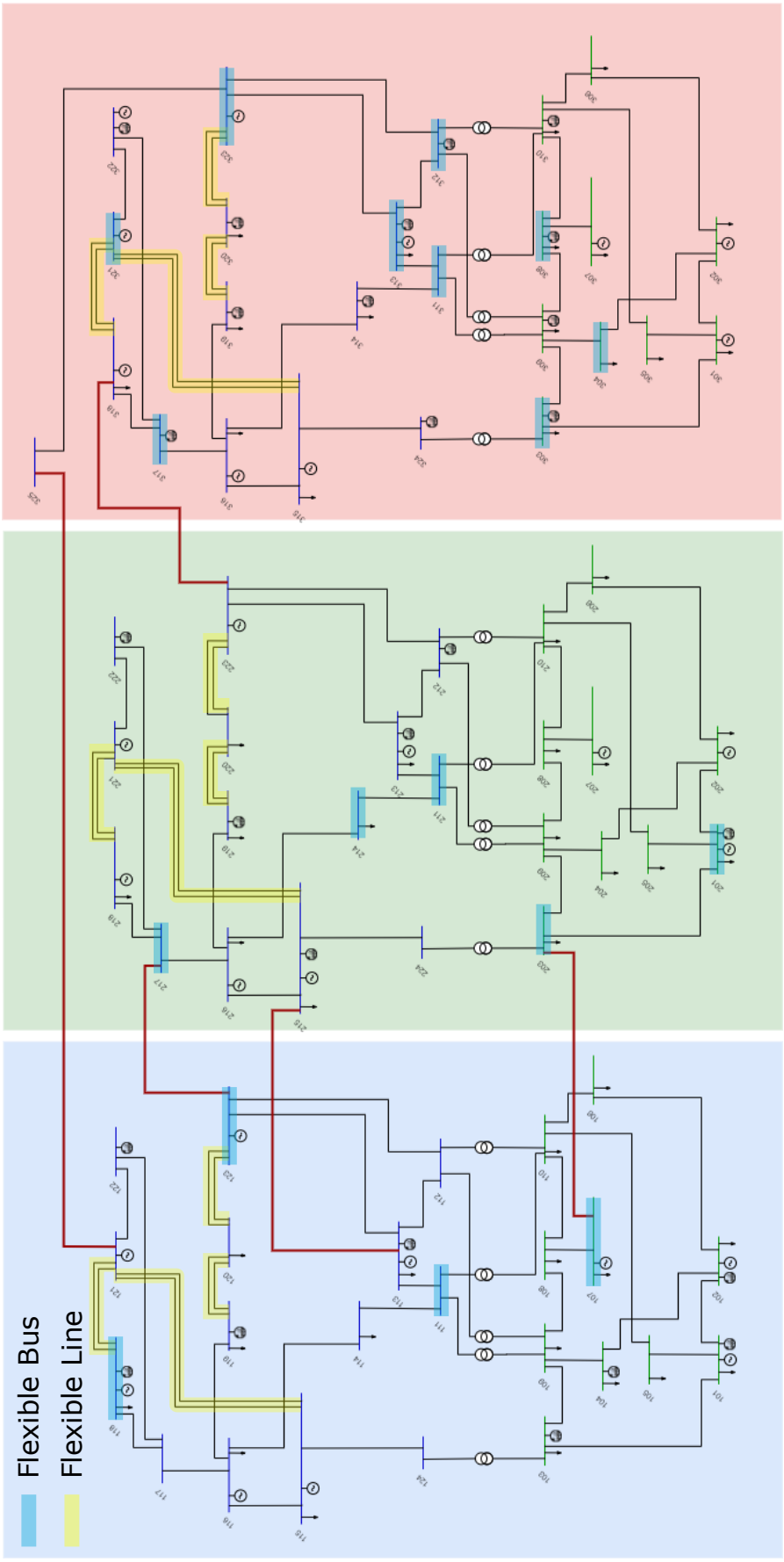

Figure E.5: RTS-GMLC System with Flexible Topology

Appendix F

Comparison of AC vs DC Load Flow with R4CA

F.1 Calculation Details

An initial tool for the flow-based calculation was created by RTE for use by multiple TSOs in 2007 prior to the first parallel run, called R4CA. The load flow at the heart of this tools remains the load flow used in practice for internal studies at RTE (although of course with some evolutions to date). The following pages show five images representing the comparison between AC and DC flows.[1]

The first image, Figure F.1 shows a scatter plot of the flows (in MW), in the AC model on the X-axis and the DC model on the Y-axis, for 3 weeks of the test in 2007. As we can see, the points follow a nice line along y=x.

The next three figures, Figures F.2, F.3 and F.4 show box and violin plots of the absolute error normalized by the Fmax for those same three time periods, this time separated by country (Belgium, Germany, France, the Netherlands and XX representing the border nodes) and by voltage level. For the first time period, there are four hourly timesteps shown and three for the other two. Table F.1 shows the breakdown of the voltage levels by country and by time period. Note that the actual voltage levels for each UCTE level are shown in Table F.2. Finally, Figure F.5 shows the 3 time periods together.

[1]The merging of the national snapshots is done in AC and then the mismatch is spread prorata to the nodal load.

Country	Voltage level	03:00-04:00	10:00-11:00	12:00-13:00	19:00-20:00
BE	380 kV	235	2239	345	241
BE	220 kV	142	1344	217	142
BE	150 kV	2226	21209	3345	2245
DE	380 kV	1519	14531	2297	1541
DE	220 kV	2648	25831	4045	2783
DE	110 kV	78	688	113	74
FR	380 kV	1254	11913	1881	1254
FR	220 kV	4778	45396	7168	4778
NL	380 kV	348	3296	520	348
NL	220 kV	204	1938	306	204
NL	150 kV	1764	16758	2646	1764
NL	110 kV	664	6308	996	664
XX	380 kV	136	1547	240	173
XX	220 kV	68	793	123	89
XX	110 kV	8	76	12	8

Table F.1: Voltage Level by TSO and Time Period

UCTE level	Voltage Reference	cos(phi)	Voltage at Node	Voltage for Fmax
0	750 kV	1	750 kV	750 kV
9	500 kV	1	500 kV	500 kV
1	380 kV	1	399 kV	400 kV
8	330 kV	1	330 kV	330 kV
2	220 kV	1	224,4 kV	225 kV
3	150 kV	1	150 kV	150 kV
4	120 kV	1	120 kV	120 kV
5	110 kV	1	110 kV	110 kV
6	70 kV	1	70 kV	70 kV
7	27 kV	1	27 kV	27 kV

Table F.2: Voltage Levels for UCTE levels

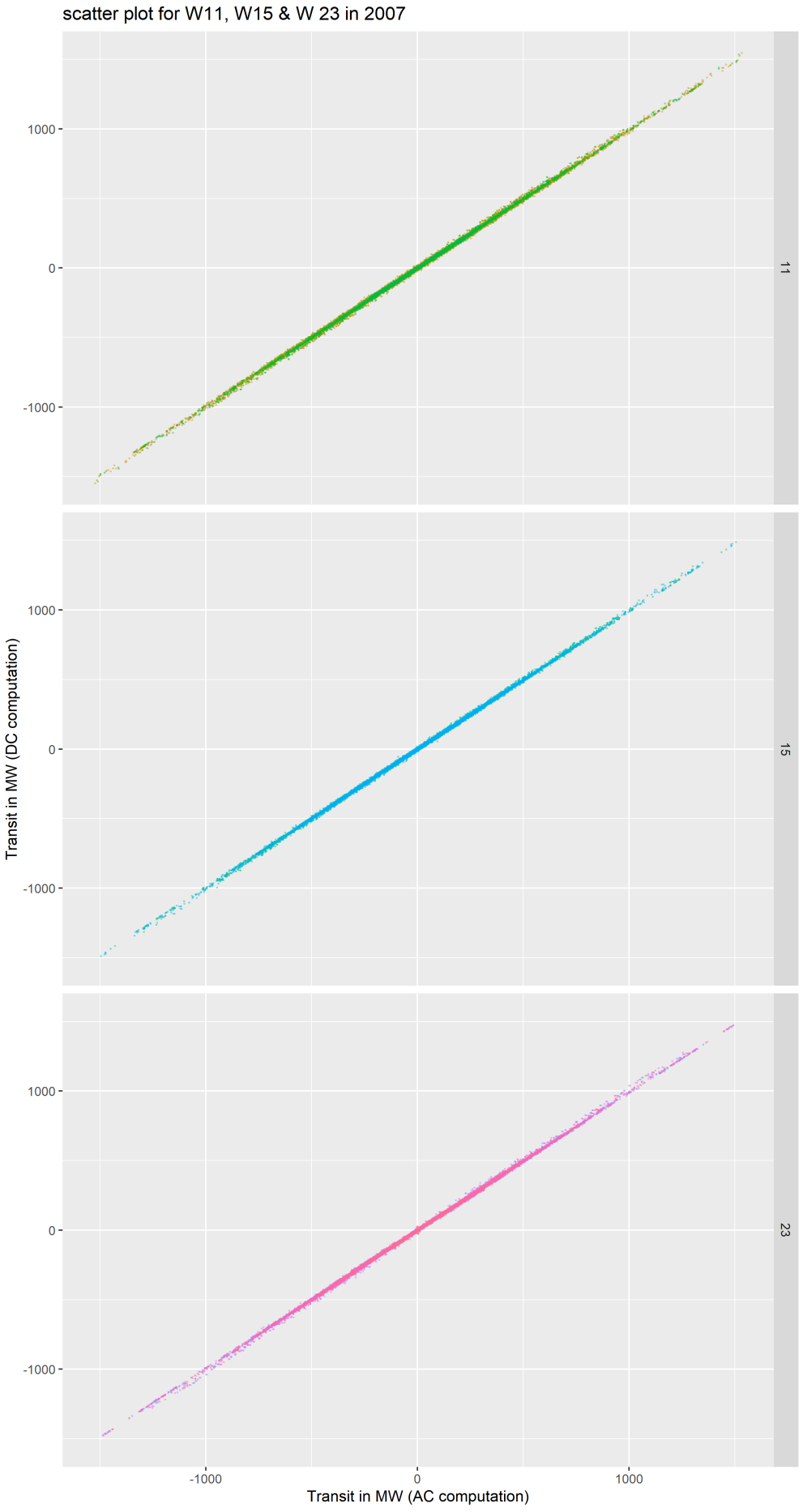

Figure F.1: AC and DC Transit Flows

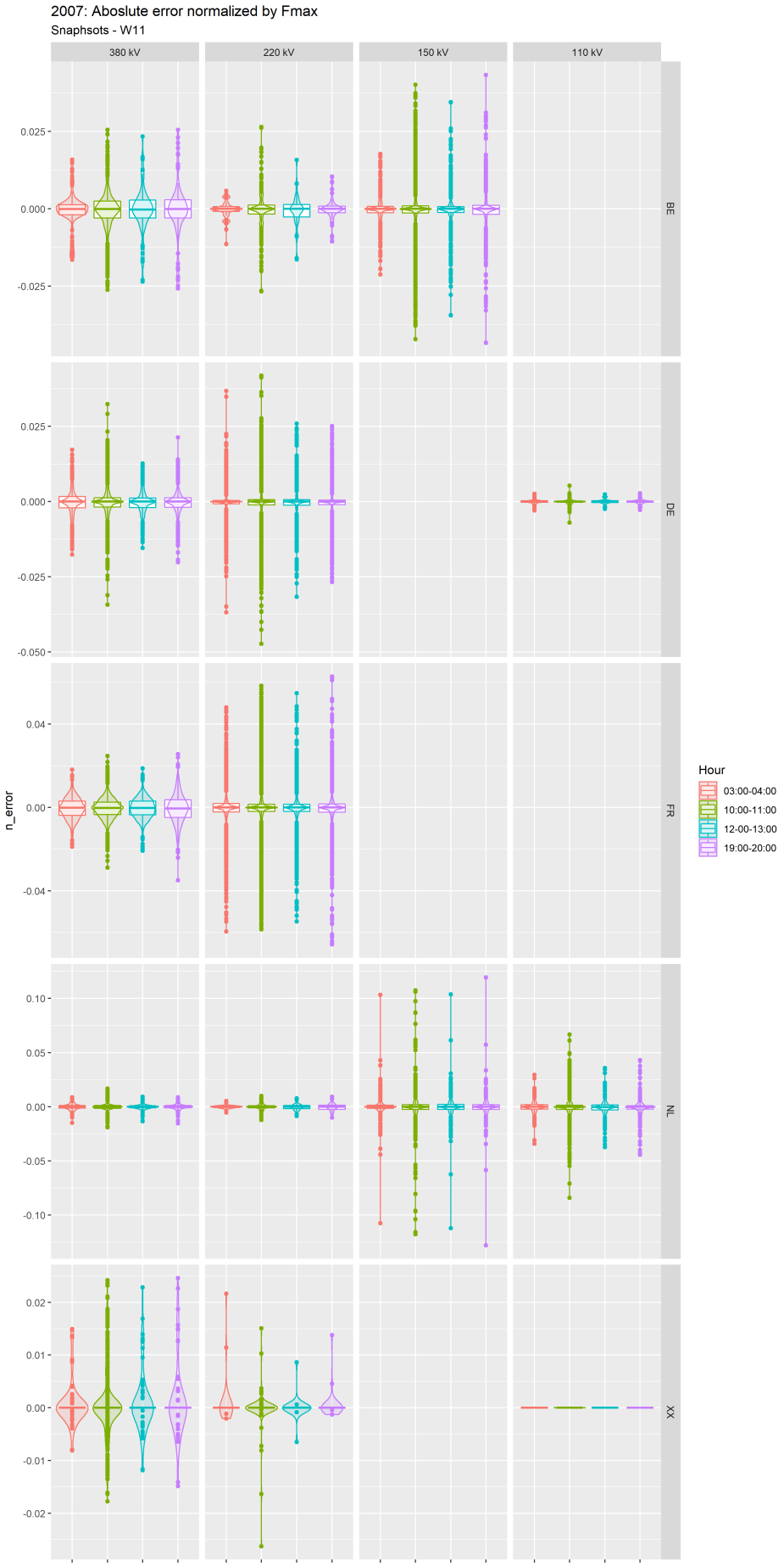

Figure F.2: Absolute Error Normalized by Fmax - Week 11

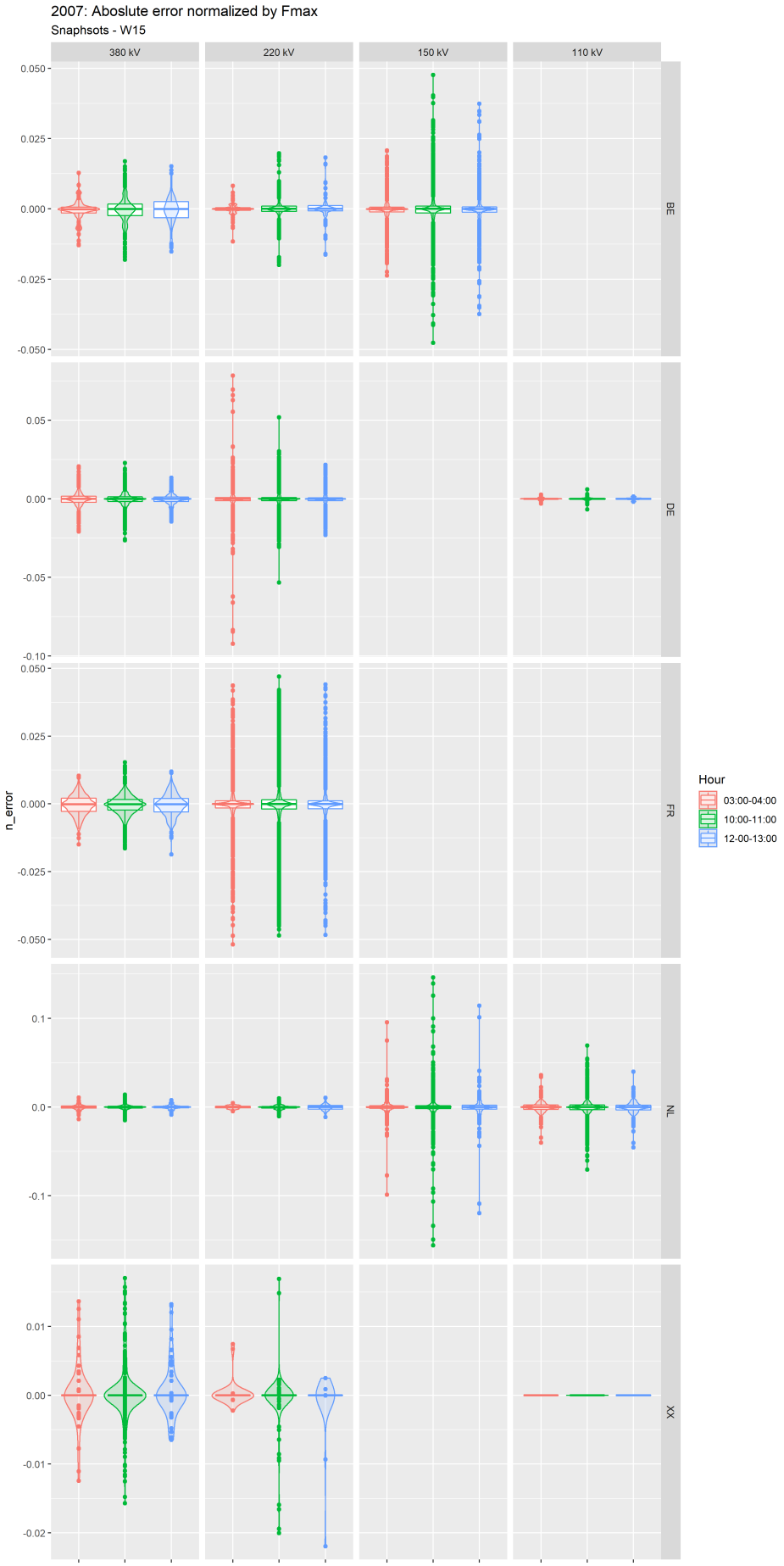

Figure F.3: Absolute Error Normalized by Fmax - Week 15

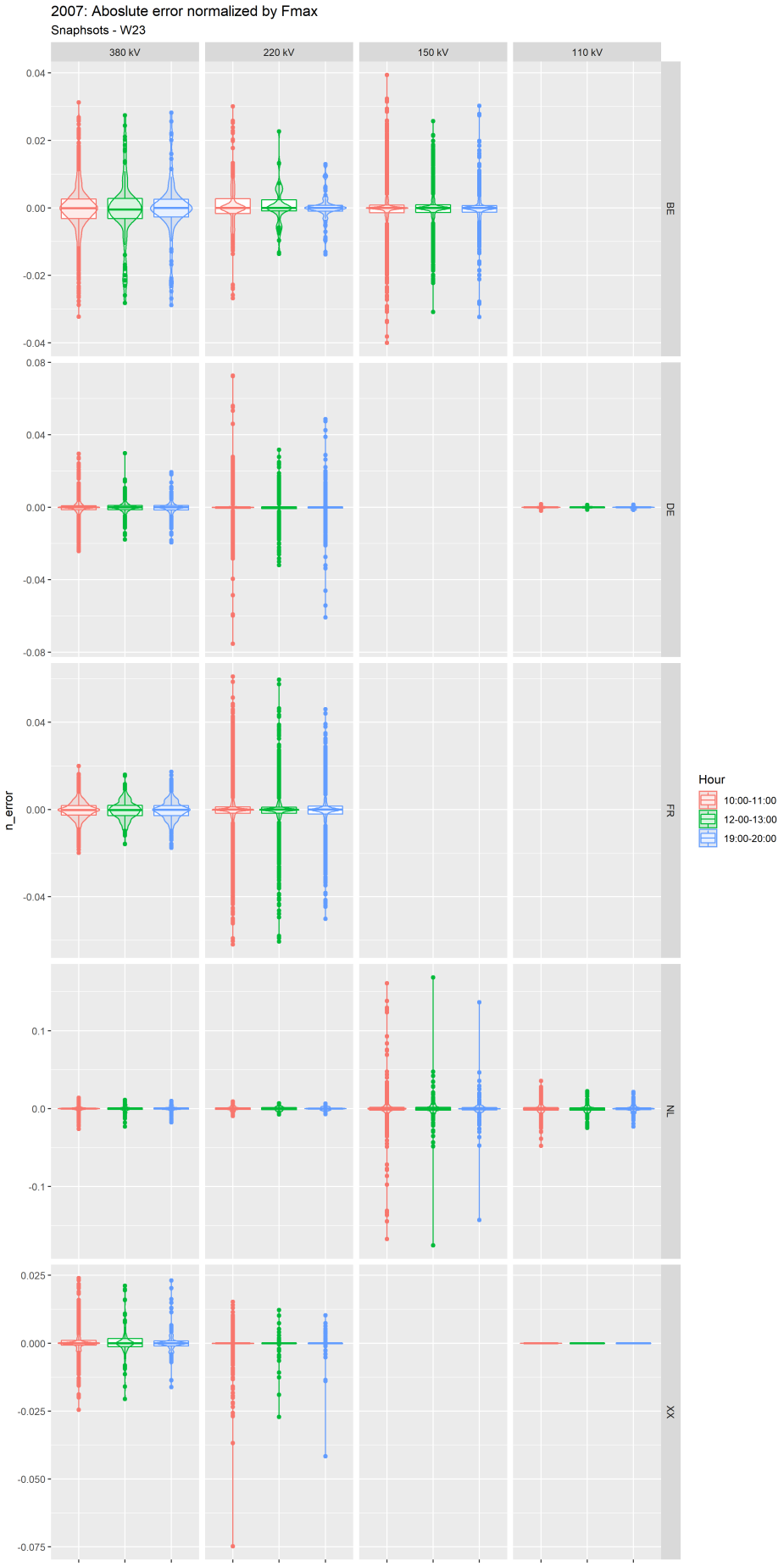

Figure F.4: Absolute Error Normalized by Fmax - Week 23

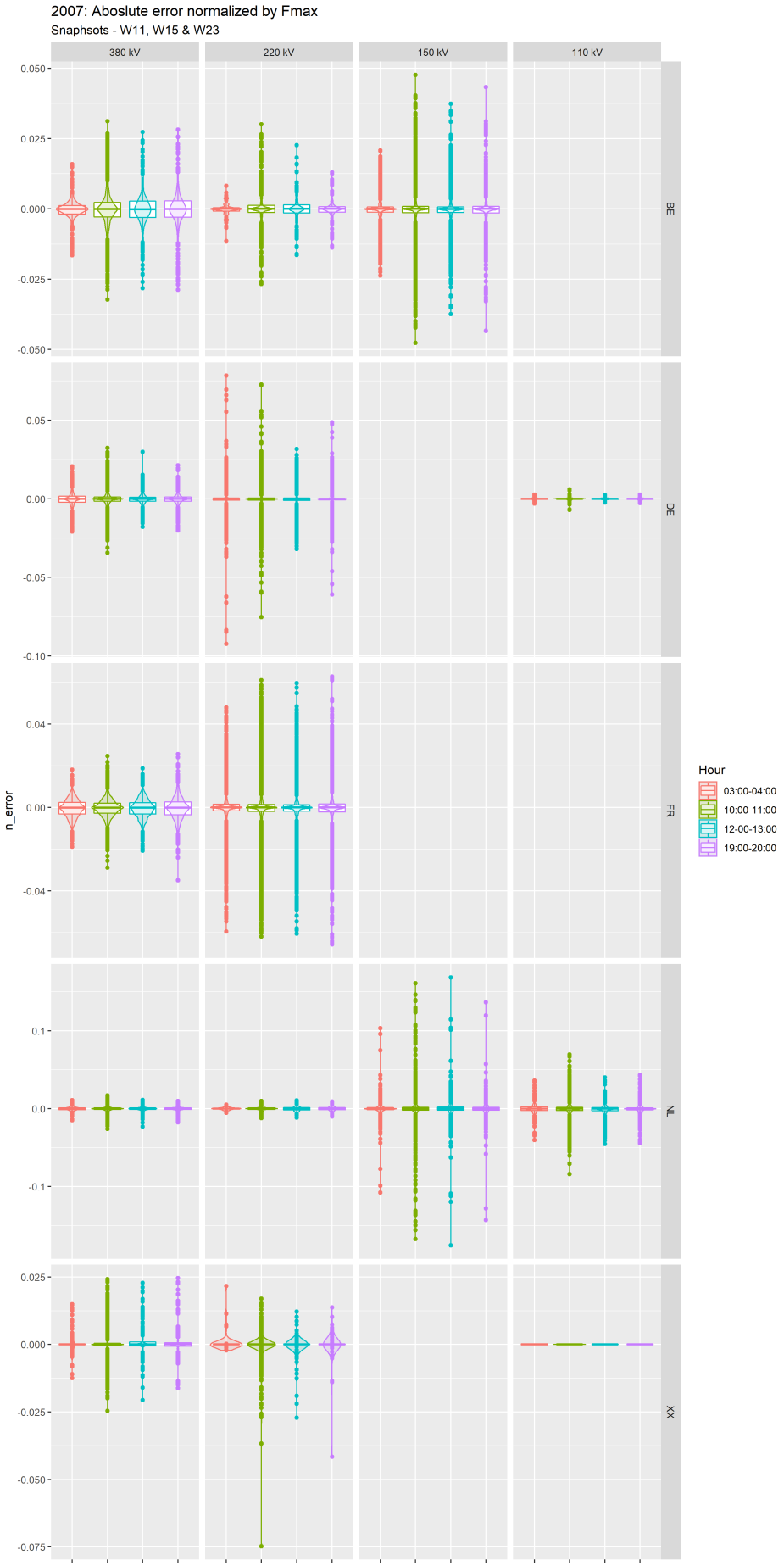

Figure F.5: Absolute Error Normalized by Fmax - All Time Periods

Appendix G

Redispatch Variations

The redispatch models used in this PhD work follow the same general principles as the other DC-OPF models described in Chapters 2 and 3. The main difference comes from the variables used: rather than the generation as the main variable, a change in dispatch compared to the market output was used. The objective function is as follows:

$$\min \alpha \sum_{g \in \mathcal{G}} c_g (\Delta P_g^{up} + \Delta P_g^{down}) + \beta \sum_{g \in \mathcal{G}} (\Delta P_g^{up} - \Delta P_g^{down}) \tag{G.1}$$

where ΔP_g^{up} and ΔP_g^{down} represent the changes of dispatch, up and down respectively ($\Delta P_g^{up} > 0$ and $\Delta P_g^{down} < 0$). In the GSK study in Section 3.4.2, four slight variations were assessed:

1. **DAsec**: Uses the day ahead data and prioritizes the redispatch volume minimization ($\beta >> \alpha$)
2. **RTsec**: Uses the real time data and prioritizes the redispatch volume minimization ($\beta >> \alpha$)
3. **DAopt**: Uses the day ahead data and prioritizes the redispatch cost minimization ($\alpha >> \beta$)
4. **RTopt**: Uses the real time data and prioritizes the redispatch cost minimization ($\alpha >> \beta$)

The first two essentially show how far we are from a secure state while the latter two show how far we are from the optimal state. We can see the different volumes redispatched in each variation in Figure G.1 on the next page. For all the time periods, the RTopt method has of course the highest redispatch volume.

The results presented in the Section 3.4.2 use the so-called "real time" load values and the security assessment method (RTsec). For renewable energies, the minimum value between the real time output and the day ahead market cleared output was used as the dispatch quantity. The maximum allowed capacity for those was updated to the real time values.

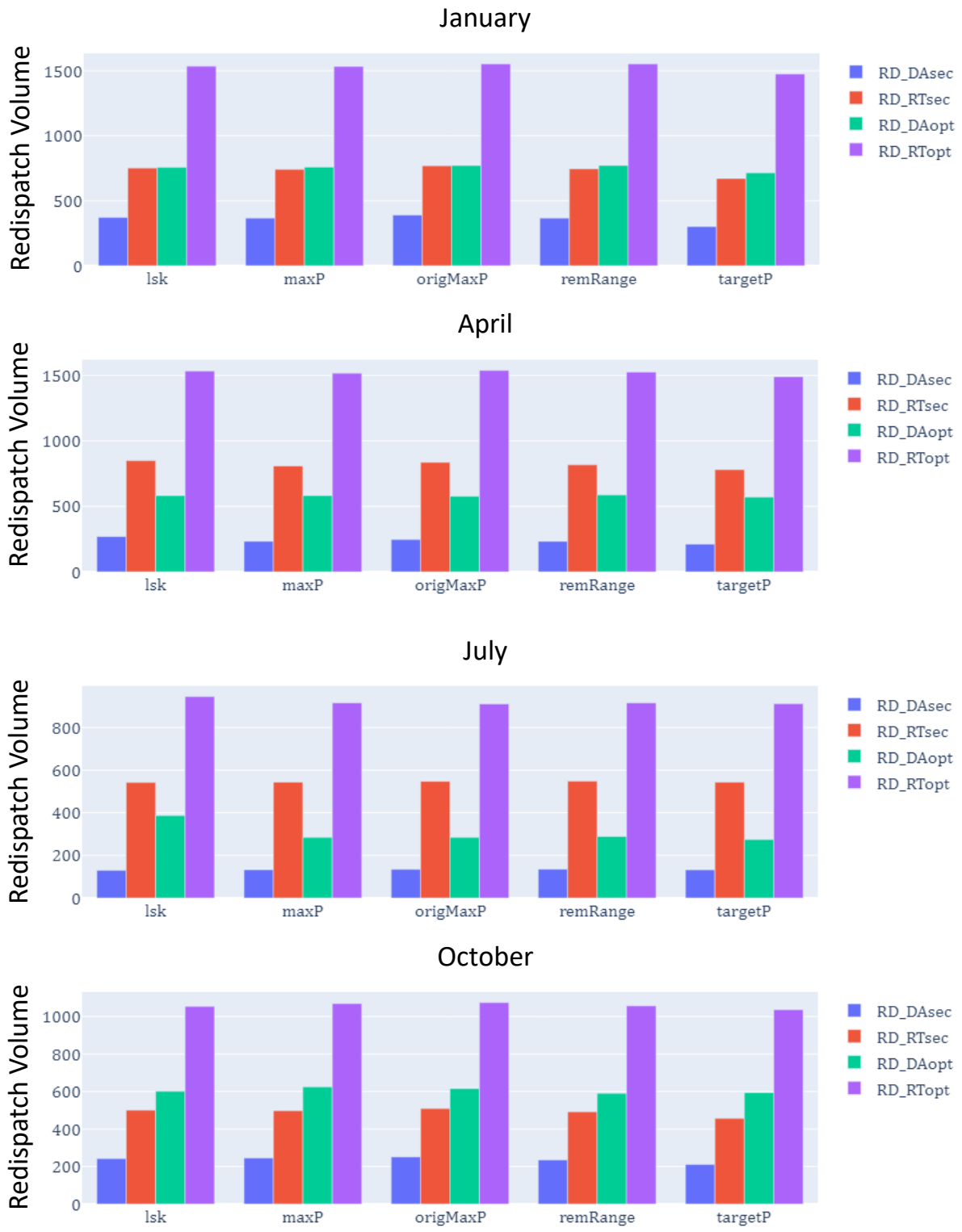

Figure G.1: Redispatch Volumes

Bibliography

(2009). Regulation (EC) no 714/2009 of the european parliament and of the council of 13 july 2009 on conditions for access to the network for cross-border exchanges in electricity and repealing regulation (EC) no 1228/2003. page 21.

ACER (2021). Core long term capacity calculation methodology.

ACER (2022). Report on the result of monitoring the margin available for cross-zonal electricity trade in the EU in 2021.

Ambrosius, M., Egerer, J., Grimm, V., and Weijde, A. v. d. (2020). Uncertain bidding zone configurations: The role of expectations for transmission and generation capacity expansion. 285(1):343–359.

amprion (2020). Documentation of the CWE FB MC solution; july 2020 – version 5.0.

amprion, TenneT Germany, Transnet BW, and APG (2015). Generation shift key (GSK).

Audouin, R. (2002). Coordinated auctioning of cross-border capacity: an implementation. In *Fifth International Conference on Power System Management and Control*, volume 2002, pages 25–30. IEE.

Audouin, R., Chaniotis, D., Tsamasphyrou, P., and Coulondre, J.-M. (2002). Coordinated auctioning of cross-border capacity: A comparison. volume Session 23, Paper 1.

Bacher, R. and Glavitsch, H. (1986). Network Topology Optimization with Security Constraints. *IEEE Transactions on Power Systems*, 1(4):103–111.

Bakirtzis, A. G. and Meliopoulos, A. P. S. (1987). Incorporation of Switching Operations in Power System Corrective Control Computations. *IEEE Transactions on Power Systems*, 2(3):669–675.

Barrows, C., Preston, E., Staid, A., Stephen, G., Watson, J.-P., Bloom, A., Ehlen, A., Ikaheimo, J., Jorgenson, J., Krishnamurthy, D., Lau, J., McBennett, B., and O'Connell, M. (2020). The IEEE Reliability Test System: A Proposed 2019 Update. *IEEE Transactions on Power Systems*, 35(1):119–127.

Bertram, T., Demaree, K., and Dangelmaier, L. (1990). An integrated package for real-time security enhancement. *IEEE Transactions on Power Systems*, 5(2):592–600.

Bjorndal, E., Bjorndal, M. H., and Cai, H. (2018). Flow-based market coupling in the european electricity market – a comparison of efficiency and feasibility.

Boiteux, M. (1956). La vente au coût marginal. page p. 113.

Carpentier, M. J. (1962). Contribution à l'étude du dispatching économique. 8e Série, Tome III(31).

Chao, H.-p., Peck, S., Oren, S., and Wilson, R. (2000). Flow-based transmission rights and congestion management. 13(8):38–58.

Commission de Régulation de l'Electricité et du Gaz (CREG) (2019). Study on the best forecast of remedial actions to mitigate market distortion. Technical report.

CWE TSOs (2015). CWE FB MC project: Parallel run performance report.

CWE TSOs (2022). CWE GSK Monitoring Study.

Dierstein, C. (2017). Impact of generation shift key determination on flow based market coupling. In *2017 14th International Conference on the European Energy Market (EEM)*, pages 1–7. IEEE.

Djelassi, H., Fliscounakis, S., Mitsos, A., and Panciatici, P. (2018). Hierarchical Programming for Worst-Case Analysis of Power Grids. In *2018 Power Systems Computation Conference (PSCC)*, pages 1–7, Dublin, Ireland. IEEE.

Dodu, J., Merlin, A., and David, J. (1981). On the search of optimal switching configurations in power transmission systems studies. In *Power System Computation Conference (PSCC)*, pages 282–292.

Eicke, A. and Schittekatte, T. (2022). Fighting the wrong battle? a critical assessment of arguments against nodal electricity prices in the european debate. 170:113220.

Einhorn, M. A. (1990). Electricity wheeling and incentive regulation. 2(2):173–189.

Energinet, Svenska Kraftnât, Fingrid, and Statnett (2015). Supporting document for the second amendment of the nordic capacity calculation region's proposal for capacity calculation methodology in accordance with article 20(2) of commission regulation (EU) 2015/1222 of 24 july 2015 establishing a guideline on capacity allocation and congestion management.

ENTSO-E (2016). Generation and load shift key implementation guide.

etso (2001). Co-ordinated auctioning: A market-based method for transmission capacity allocation in meshed networks. page 22.

Felten, B., Osinski, P., Felling, T., and Weber, C. (2021). The flow-based market coupling domain - Why we can't get it right. *Utilities Policy*, 70.

Finck, R. (2021). Impact of flow based market coupling on the european electricity markets. 29(2):173–186.

Fisher, E., O'Neill, R., and Ferris, M. (2008). Optimal Transmission Switching. *IEEE Transactions on Power Systems*, 23(3):1346–1355. 38.

Francisco, V. J. E. and Nerves, A. C. (2010). Strategic bidding and scheduling in reserve co-optimized based electricity spot markets. In *TENCON 2010 - 2010 IEEE Region 10 Conference*, pages 592–597.

Freitas e Silva, J. a. O. and Machado, L. J. B. (1993). Switching Lines Selection to Integrate the Network Topology Optimization with the Usual Overload Control Actions of Electric Power Systems. Avignon, France.

Glavitsch, H., Kronig, H., and Bacher, R. (1984). Combined use of linear programming and load flow techniques in determining optimal switching sequences. In *Network Adequacy*, pages 627–636, Helsinki, Finland. Butterworths.

Goldis, E. (2015). Topology control algorithms in power systems.

Goldis, E. A., Ruiz, P. A., Caramanis, M. C., Li, X., Philbrick, C. R., and Rudkevich, A. M. (2017). Shift Factor-Based SCOPF Topology Control MIP Formulations With Substation Configurations. *IEEE Transactions on Power Systems*, 32(2):1179–1190.

Gorenstin, B., Terry, L. A., Pereira, M. V. F., and Pinto, L. M. V. G. (1987). A framework for integration of network topology optimization and generation rescheduling in power system security applications. In *System security and optimization I*, pages 124–130, Cascais, Portugal. Butterworths.

Grigg, C., Wong, P., Albrecht, P., Allan, R., Bhavaraju, M., Billinton, R., Chen, Q., Fong, C., Haddad, S., Kuruganty, S., Li, W., Mukerji, R., Patton, D., Rau, N., Reppen, D., Schneider, A., Shahidehpour, M., and Singh, C. (1999). The IEEE Reliability Test System-1996. A report prepared by the Reliability Test System Task Force of the Application of Probability Methods Subcommittee. *IEEE Transactions on Power Systems*, 14(3):1010–1020.

Hagedorn, C. (2017a). CWE flow factor competition, part II: Quantitative analysis. page 43.

Hagedorn, C. (2017b). CWE flow factor competition study, part i: Qualitative analysis. page 25.

Hagedorn, C. (2017c). CWE flow factor competition study, part III: Fairness assessment. page 83.

Han, J. and Papavasiliou, A. (2016). The Impacts of Transmission Topology Control on the European Electricity Network. *IEEE Transactions on Power Systems*, 31(1):496–507.

Harvey, S. M., Hogan, W. W., and Pope, S. L. (1996). Transmission capacity reservations and transmission congestion contracts. page 105.

Hedman, K. W., O'Neill, R. P., Fisher, E. B., and Oren, S. S. (2008). Optimal Transmission Switching—Sensitivity Analysis and Extensions. *IEEE Transactions on Power Systems*, 23(3):1469–1479.

Hedman, K. W., O'Neill, R. P., Fisher, E. B., and Oren, S. S. (2009). Optimal Transmission Switching With Contingency Analysis. *IEEE Transactions on Power Systems*, 24(3):1577–1586.

Hedman, K. W. and Oren, S. S. (2009). Co-optimization of Generation Unit Commitment and Transmission Switching with N-1 Reliability. page 12.

Hedman, K. W., Oren, S. S., and O'Neill, R. P. (2011a). A review of transmission switching and network topology optimization. In *2011 IEEE Power and Energy Society General Meeting*, pages 1–7, Detroit, MI, USA. IEEE.

Hedman, K. W., Oren, S. S., and O'Neill, R. P. (2011b). Optimal transmission switching: economic efficiency and market implications. *Journal of Regulatory Economics*, 40(2):111–140.

Hogan, W. W. (1992). Contract networks for electric power transmission. page 32.

Joskow, P. L. (2008). Lessons learned from electricity market liberalization. 29(1).

Josz, C. (2022). Application of polynomial optimization to electricity transmission networks.

Koglin, H.-J. and de Medeiros, M. (1985). Corrective Switching Approaching On-Line Application. *IFAC Proceedings Volumes*, 18(7):203–207.

Lehmann, K., Grastien, A., and Van Hentenryck, P. (2014). The Complexity of DC-Switching Problems. *arXiv:1411.4369 [cs, math]*. arXiv: 1411.4369.

Lete, Q. and Papavasiliou, A. (2020). Impacts of transmission switching in zonal electricity markets - part i. *IEEE Transactions on Power Systems*, pages 1–1.

Lin, J. and Magnago, F. H. (2017). *Electricity Markets: Theories and Applications: Theories and Applications*. John Wiley & Sons, Inc.

Makram, E. B., Thornton, K. P., and Brown, H. E. (1989). Selection of Lines to Be Switched to Eliminate Overloaded Lines Using a Z-Matrix Method. *IEEE Power Engineering Review*, 9(5):63–63.

Marien, A., Luickx, P., Tirez, A., and Woitrin, D. (2013). Importance of design parameters on flowbased market coupling implementation. In *2013 10th International Conference on the European Energy Market (EEM)*, pages 1–8, Stockholm, Sweden. IEEE. 8.

Matthes, B., Spieker, C., Klein, D., and Rehtanz, C. (2019). Impact of a minimum remaining available margin adjustment in flow-based market coupling. In *2019 IEEE Milan PowerTech*, pages 1–6.

Mazi, A. A., Wollenberg, B. F., and Hesse, M. H. (1986). Corrective Control of Power System Flows by Line and Bus-Bar Switching. *IEEE Transactions on Power Systems*, 1(3):258–264.

Mekonnen, M. T. and Belmans, R. (2012). The influence of phase shifting transformers on the results of flow-based market coupling. In *2012 9th International Conference on the European Energy Market*, pages 1–7, Florence, Italy. IEEE.

Mekonnen, M. T., De Jonghe, C., Rawn, B., Van Hertem, D., and Belmans, R. (2013). Power flow control and its effect on flow-based transmission cost allocation. In *2013 10th International Conference on the European Energy Market (EEM)*, pages 1–8, Stockholm, Sweden. IEEE.

Müller, C., Hoffrichter, A., Barrios, H., Schwarz, A., and Schnettler, A. (2017). Integration of HVDC-Links into Flow-Based Market Coupling: Standard Hybrid Market Coupling versus Advanced Hybrid Market Coupling.

N-Side (2019). Extended formulation for LTA inclusion. Technical Report Version 1.2, Louvain-La-Neuve, Belgium.

NEMO Committee (2020). Euphemia public description: Single price coupling algorithm. page 69.

Newbery, D., Strbac, G., and Viehoff, I. (2016). The benefits of integrating european electricity markets. 94:253–263.

O'Neill, R., Baldick, R., Helman, U., Rothkopf, M., and Stewart Jr., W. (2005a). Dispatchable Transmission in RTO Markets. *IEEE Transactions on Power Systems*, 20(1):171–179.

O'Neill, R. P., Sotkiewicz, P. M., Hobbs, B. F., Rothkopf, M. H., and Stewart, W. R. (2005b). Efficient market-clearing prices in markets with nonconvexities. *European Journal of Operational Research*, 164(1):269–285.

Pollitt, M. (2004). Electricity reform in chile. lessons for developing countries. 5(3):221–262.

Poplavskaya, K., Totschnig, G., Leimgruber, F., Doorman, G., Etienne, G., and de Vries, L. (2020). Integration of day-ahead market and redispatch to increase cross-border exchanges in the European electricity market. *Applied Energy*, 278:115669.

Raths, D. S., Beck, D., Bongers, D. T., and Sander, I. (2021). ALEGrO – market integration und system operation aspects of the new HVDC link between germany and belgium. page 6.

Ricard, M. J. (1946). La détermination de la répartition economique des charges entre usines génératrices.

Rious, V. (2007). Le développement du réseau de transport dans un système électrique libéralisé, un problème de coordination avec la production.

Rious, V., Glachant, J.-M., Perez, Y., and Dessante, P. (2008). The diversity of design of TSOs. 36(9):3323–3332.

Rolim, J. and Machado, L. (1999). A study of the use of corrective switching in transmission systems. *IEEE Transactions on Power Systems*, 14(1):336–341.

Rolim, J. G., Irving, M. R., and Machado, L. J. B. (1995). SECTE - An Expert System For Voltage Control, Including Topological Changes. *IFAC Proceedings Volumes*, 28(26):177 – 182.

Rosellon, J. and Kristiansen, T. (2013). Financial transmission rights.

Schnyder, G. and Glavitsch, H. (1990). Security enhancement using an optimal switching power flow. *IEEE Transactions on Power Systems*, 5(2):674–681.

Schonheit, D. and Sikora, R. (2018). A statistical approach to generation shift keys. In *2018 15th International Conference on the European Energy Market (EEM)*, pages 1–6. IEEE.

Schönheit, D., Dierstein, C., and Möst, D. (2021a). Do minimum trading capacities for the cross-zonal exchange of electricity lead to welfare losses? 149:112030.

Schönheit, D., Kenis, M., Lorenz, L., Möst, D., Delarue, E., and Bruninx, K. (2021b). Toward a fundamental understanding of flow-based market coupling for cross-border electricity trading. *Advances in Applied Energy*, 2.

Schönheit, D., Weinhold, R., and Dierstein, C. (2020). The impact of different strategies for generation shift keys (GSKs) on the flow-based market coupling domain: A model-based analysis of central western europe. 258:114067.

Sebestyén, M., Divenyi, D., and Sőrés, P. (2018). An enhanced calculation method of generation shift keys in flow based market coupling. In *2018 15th International Conference on the European Energy Market (EEM)*, pages 1–5.

Serra, P. (2022). Chile's electricity markets: Four decades on from their original design. 39:100798.

Sliwak, J. (2021). Résolution de problèmes d'optimisation pour les réseaux de transport d'électricité de grande taille avec des méthodes de programmation semi-définie positive.

Stott, B., Jardim, J., and Alsac, O. (2009). DC power flow revisited. 24(3):1290–1300.

TSOs, C. (2018a). Core CCR TSOs' regional design of the day-ahead common capacity calculation methodology in accordance with Article 20ff. of Commission Regulation (EU) 2015/1222 of 24 July 2015.

TSOs, C. (2018b). Explanatory note on the day-ahead and intraday common capacity calculation methodologies for the Core CCR.

Van Amerongen, R. and Van Meeteren, H. (1980). Security Control by Real Power Rescheduling, Network Switching and Load Shedding. Paris. Cigré.

Van den Bergh, K., Boury, J., and Delarue, E. (2016). The Flow-Based Market Coupling in Central Western Europe: Concepts and definitions. *The Electricity Journal*, 29(1):24–29. 5.

Van den Bergh, K., Delarue, E., and D'haeseleer, W. (2014). Dc power flow in unit commitment models.

van Leeuwen, J. M. (2015). A scenario-based voltage stability analysis for external constraints in flow-based capacity calculation.

Voswinkel, S., Felten, B., Felling, T., and Weber, C. (2019). Flow-based market coupling – what drives welfare in europe's electricity market design?

Weinhold, R. (2021). Evaluating policy implications on the restrictiveness of flow-based market coupling with high shares of intermittent generation: A case study for central western europe. page 23.

Weinhold, R. and Mieth, R. (2021). Uncertainty-aware capacity allocation in flow-based market coupling. page 30.

Wolak, F. A. (2021). Wholesale electricity market design. In *Handbook on Electricity Markets: Part I - Taking Stock: The Legacy*, pages p. 73–110. Edward Elgar Publishing, Inc.

Wu, F., Varaiya, P., Spiller, P., and Oren, S. (1996). Folk theorems on transmission access: Proofs and counterexamples. 10(1):5–23.

Zad, B. B., Vatandoust, B., Toubeau, J.-F., De Grève, Z., and Vallée, F. (2021). Advanced clustering of flow-based domains for adequacy study purposes. In *2021 IEEE Madrid PowerTech*, pages 1–6.

université PARIS-SACLAY | ÉCOLE DOCTORALE Interfaces: matériaux, systèmes, usages

Titre: L'avenir de la gestion de la capacité d'interconnexion transfrontalière en Europe

Mots clés: Flow-based, Réseau, Marché, Interconnections, Electricité

Résumé: L'ouverture du marché européen de l'électricité a renforcé l'enjeu des échanges transfrontaliers. Les méthodes de calcul et allocation de la capacité du réseau sont au coeur de cette question. La méthode flow-based se rapproche de la réalité physique du réseau en intégrant les dépendances de flux entre différentes zones, et offre, à niveau de risque donné, une capacité supérieure à la méthode Net Transfer Capacity utilisée auparavant. Le contexte de la transition énergétique met en lumière de nouveaux problèmes ; par exemple, l'erreur de prévision croissante entre les transactions à long terme, le marché à court terme et la répartition en temps réel. De plus, un modèle de production, plus éloigné des centres de charge et un peu plus largement distribué que les centrales conventionnelles, menace de pousser le réseau existant à ses limites. Si l'investissement dans le réseau est bien sûr un élément important de la solution, il deviendra également encore plus nécessaire d'utiliser le réseau existant aussi efficacement que possible.

Les principales contributions de cette thèse sont de trois types. Tout d'abord, elle montre que l'intérêt économique des flexibilités du réseau croit avec la pénétration des énergies renouvelables intermittentes. Ensuite, elle propose une description minutieuse et actualisée de la méthodologie flow-based opérationelle. Les travaux se distinguent de la littérature existante en donnant une vision plus complète et plus précise des aspects théoriques et opérationnels de cette méthodologie. Enfin, une évolution du flow-based est proposée qui permet de mieux intégrer les flexibilités du réseau dans l'algorithme opérationnel de couplage des marchés.

Title: The Future of Cross-border Capacity Management in Europe

Keywords: Flow-based, Grid, Interconnections, Market, Electricity

Abstract: The liberalization of the European electricity market reinforced the need for efficient, market-driven cross-border congestion management. The methods to calculate and allocate the capacity of transmission networks are at the heart of this discussion. The flow-based method integrates the flow dependencies between market zones to more accurately model the physical constraints of the grid, providing a higher cross-border capacity available to the market without increasing the risk, compared to the Net Transfer Capacity method. The context of the energy transition brings into light new issues; for one, the increasing forecast error between the long term transactions, the day ahead market and the real time dispatch. Additionally, a pattern of generation farther from load centers and more widely distributed than conventional plants threatens to push the existing network to its limits. While network investment is of course a large piece of the solution, it will also become more important to utilize the existing network as efficiently as possible.

The main assets of this thesis are three-fold. First, the increasing value of transmission-level grid flexibility is shown in a system with high levels of variable renewable energy sources. Second, with the ultimate aim of presenting an updated form of the European capacity calculation, the existing flow-based method is presented in detail. This goes beyond the work in the existing literature to provide a comprehensive look at the theoretical and operational aspects in extended detail. Thirdly, an updated version of the existing capacity calculation is proposed, allowing for improved integration of grid flexibility options and considering the operational complexities and existing market clearing algorithm.